Gyroscopic Assistance for Human Balance

Lemus Perez, Daniel

DOI
10.4233/uuid:97f225ec-4a10-4e10-a36e-576876fd3887

Publication date
2019

Document Version
Final published version

Citation (APA)
Lemus Perez, D. (2019). *Gyroscopic Assistance for Human Balance*. [Dissertation (TU Delft), Delft University of Technology]. https://doi.org/10.4233/uuid:97f225ec-4a10-4e10-a36e-576876fd3887

GYROSCOPIC ASSISTANCE FOR HUMAN BALANCE

DANIEL LEMUS

Gyroscopic Assistance for Human Balance

D.S. Lemus

Gyroscopic Assistance for Human Balance

Proefschrift

ter verkrijging van de graad van doctor
aan de Technische Universiteit Delft,
op gezag van de Rector Magnificus prof. dr. ir. T.H.J.J. van der Hagen,
voorzitter van het College voor Promoties,
in het openbaar te verdedigen op dinsdag 18 juni 2019 om 10:00 uur

door

Daniel Santiago LEMUS PÉREZ

Master of Science in Mechanical Engineering,
Universidad de los Andes, Colombia,
geboren te Bogotá, Colombia.

Dit proefschrift is goedgekeurd door de

promotor: prof. dr. F.C.T. van der Helm
promotor: prof. dr. ir. H. Vallery

Samenstelling promotiecommissie:

Rector Magnificus,	voorzitter
Prof. dr. F.C.T. van der Helm,	Technische Universiteit Delft, promotor
Prof. dr. ir. H. Vallery,	Technische Universiteit Delft, promotor
Onafhankelijke leden:	
Dr. E.H.F. van Asseldonk,	University of Twente
Prof. dr. ir. B. Vanderborght,	Vrije Universiteit Brussel, België
Prof. dr. A.C.H. Geurts,	Radboud University Medical Center
Prof. dr. ir. D.A. Abbink,	Technische Universiteit Delft
Prof. dr. ir. J. Harlaar,	Technische Universiteit Delft, reservelid

The work here presented was supported by the U.S. Department of Education, National Institute on Disability and Rehabilitation Research, NIDRR-RERC, Grant No. H133E120010, the Marie-Curie career integration Grant No. PCIG13-GA-2013-618899, and the Innovational Research Incentives Scheme Vidi with Project No. 14865, which is (partly) financed by The Dutch Organization for Scientific Research (NWO).

Keywords: CMG, human balance, stroke rehabilitation, free moments, rehabilitation robotics
Printed by: Gildeprint B.V., Enschede, Nederland
Front & Back: Cover design by Ilse Modder, `http://www.ilsemodder.nl/`

Author's e-mail: `dslemusp@gmail.com`
ISBN 978-94-6384-049-1

An electronic version of this dissertation is available at
`http://repository.tudelft.nl/`.

A la memoria de mi amada abuela Ninfa María,
que me cuida desde el cielo.

To the memory of my beloved grandma
Ninfa María.

Contents

Summary

Over the past few decades, there has been an increasing trend in the development of wearable robotics for rehabilitation and human augmentation. Although most such devices have been envisioned and realized to extend human capabilities, they do not primarily target balance control. For a wide range of physiotherapy recipients, impaired balance, rather than a lack of muscle strength, is the main impediment to functional recovery. Recently I proposed and realized a novel wearable robotic device, *the GyBAR*, that is capable of assisting balance during standing and walking without obstructing the lower extremities; this is achieved by exerting free torques on the upper body with a gyroscopic actuator that is worn like a backpack. This thesis presents a study into the feasibility of control moment gyroscopes (CMGs) as wearable devices for balance assistance in human beings. Here I identify and focus on **sensing**, **actuation** and **control** as the three main components of the GyBAR.

Sensing
Knowledge of stability metrics plays an important role to successfully assist balance in a more transparent way (i.e. without interfering with ADLs). From the many definitions proposed in literature for human locomotion, knowledge of at least the relative position and velocity of the body's center of mass respect to its base of support are required. Knowledge of these variables represent a major challenge for wearable devices due to the limited amount of information that their built-in sensors that can measure given its collocation along the body. These quantities can be complex to sense locally, in particular for upper-body wearable devices, where sensor information of the lower limbs is not available. Pursuant to this, I propose a model-based approach from which the state of balance can be estimated in real-time. Our approach estimates the position and velocity of the CoM by combining local sensor measurements with a simplified dynamic model of the human gait. Here, a bipedal Spring Loaded Inverted Pendulum (SLIP) model with a rigid trunk was implemented along the extrapolated CoM (XCoM) for walking control. Subsequently, an observability analysis is performed over the selected dynamic model using linear acceleration of the CoM and position and angular velocity of the trunk as available measurements. An Additive Unscented Kalman Filter (AUKF) is implemented to estimate the unmeasured states of the system (i.e. CoM position and velocity). Our approach is then validated using experimental data from treadmill walking, where a single upper-body IMU sensor is used along infrared motion capture cameras. It is shown that the CoM position and velocity can be estimated accurately (i.e. with a maximum RMSD of 0.013 m and 0.022 $\mathrm{m\,s^{-1}}$ in CoM position and velocity respectively). It is also shown that the proposed approach exhibited low sensitivity on sensor inaccuracies.

Actuation
Momentum exchange actuators such as CMGs have been widely used in the aerospace industry as attitude-control actuators due their torque amplification and reactionless-torque capabilities. Because of these capabilities, this form of actuation has been re-

cently proposed in literature to be implemented for human balance applications. However, there is a lack of clear guidelines for its synthesis and design given its novel and recent application in human interaction. To this end, I establish design requirements taking into account maximum desired output torque, size and weight. Based on these requirements, parameters for nominal operation and guidelines for structural design and actuator selection are described for both flywheel and gimbal assemblies. Guidelines for flywheel motor selection are described considering aerodynamic drag and bearing friction. Subsequently gimbal motor selection is based on the target output moment and the analysis of undesired dynamics induced by body movements (i.e. *parasitic torques*). The final design is then evaluated in a dedicated test setup consisting of an inverted pendulum where parasitic moments can be induced. Here a simple balance controller emulating a virtual spring is implemented to keep the pendulum upright. Our results showed that the realized CMG successfully keeps the pendulum stable within a -4 to $4°$ range with a maximum output torque of 70 N m.

Control

From the many balance-assisting control paradigms proposed in literature, none have been successfully validated in the context of wearable upper-body CMGs. So far Wojtara *et al.* implemented a discontinuous balance assistive controller for his wearable upper-body RW-based device. Although the reported results showed improve balance on healthy individuals while using the device with the assistive controller, his study failed to show a significant comparison with a baseline condition. It is thus still quite unclear which control strategies could potentially assist balance and whether these strategies would successfully assist balance in individuals with balance disorders. We address these issues in two parts. First, I implemented a set of simple balance-assisting continuous controllers (i.e. including a virtual rotary spring and a virtual rotary damper) which were validated on a first randomized controlled trial (RCT) with healthy individuals. Here subjects were asked to perform a challenging balancing task (i.e. Walking heel-to-toe over a narrow beam with their arms crossed) with and without the GyBAR. Results showed that balance was improved by a median factor of 2 by the best performing controller, the virtual rotary damper. Subsequently, a second RCT was conducted where the virtual rotary damper was tested in a set of clinically-based challenging balancing tasks (i.e. standing or walking with a reduced medio-lateral (ML) base of support (BoS) and standing with a reduced anterior-posterior (AP) BoS) on individuals with chronic stroke. Our results showed that the GyBAR was able to successfully augment balance in the anterior-posterior(AP) balancing task by a median factor of 2.5 on individuals with chronic stroke and 3.1 on healthy individuals.

Conclusion

The results of this thesis show, for the first time, evidence of the feasibility of a CMG-based upper-body actuator as balance assistance device in individuals with balance disorders. Alongside these results three important conclusions are derived. First, continuous damping in the GyBAR can effectively augment balance by median factors of 2-3. Second, and as consequence, only simple trunk angular velocity sensing suffices for its implementation. Finally, a more compact and light version of the GyBAR can be realized as only 32 % of the GyBAR output torque capability was used to assist balance.

1

Introduction

1.1 | Motivation

Over the last few decades, our increasingly aging society has been suffering the consequences of falls, being the leading cause of hospitalization in people aged 65 or older [117, 238]. In addition to environmental hazards [38, 55], factors associated to sensorimotor impairments have been identified as main risk factors of falling in older adults [46]. These include neurological conditions such as stroke and Parkinson's disease [3, 144, 188, 202, 214], neuropsychological factors such as fear of falling, depression and impaired cognition [2, 45], psychosocial and demographic factors such as advanced age, limitation on activities of daily living (ADLs) and history of falls [26, 60, 173].

Currently, early fall risk assessment followed by interventions has proven to be successful reducing risk factors of falls [32, 46, 61, 186, 189, 190, 194]. First, clinically-validated assessment tools are used to systematically and comprehensively identify the factors contributing to an individual's increased risk of falling [12, 37, 46, 200, 226]. Subsequently, and based on the evaluated risks factors, tailored interventions are designed to reduce or prevent falls, with exercise and physical therapy amongst the most recommended interventions in recent evidence-based guidelines for fall prevention [104, 136, 164, 194].

Recently, physical therapy has started to incorporate a wide range of robotic devices as a complementary means for controlled and tailored interventions where custom and repetitive tasks are required, particularly in individuals with neurological impairments [91, 126, 167, 182, 215, 223]. However, most of these robotic devices require either complex fixed structures or bulky mechanical constructions (Fig. 1.1) constraining their use to specialized facilities that are neither practical nor convenient for efficient physical therapy. Therefore, this thesis focuses on the development of a versatile portable robotic device targeting balance assistance and its evaluation on individuals with balance disorders.

1.2 | Overview of current balance-assistive devices

Multiple robotic devices targeting both assistance and rehabilitation have been developed recently. This section gives an overview of the current state of art identifying their benefits and limitations. Here these devices are classified based on the type of actuation they provide to the wearer.

1.2.1 | Externally-applied forces

These devices assist balance by applying forces to the upper-body via fixed or wheeled structures. They typically incorporate a body weight support (BWS) system that can actively unload the individual's weight during overground or treadmill walking yet providing controlled forces in predetermined directions. Although multiple realizations of these devices have been developed, four main groups can be classified: (i) single rail based active overground BWS systems (Fig. 1.1a), (ii) 3D or multidirectional active overground BWS systems (Fig. 1.1b), (iii) BWS treadmill (Fig. 1.1c) and (iv) mobile BWS (Fig. 1.1d).

Active devices based on conventional **single rail BWS** (Fig. 1.1a) such as the Zero-G

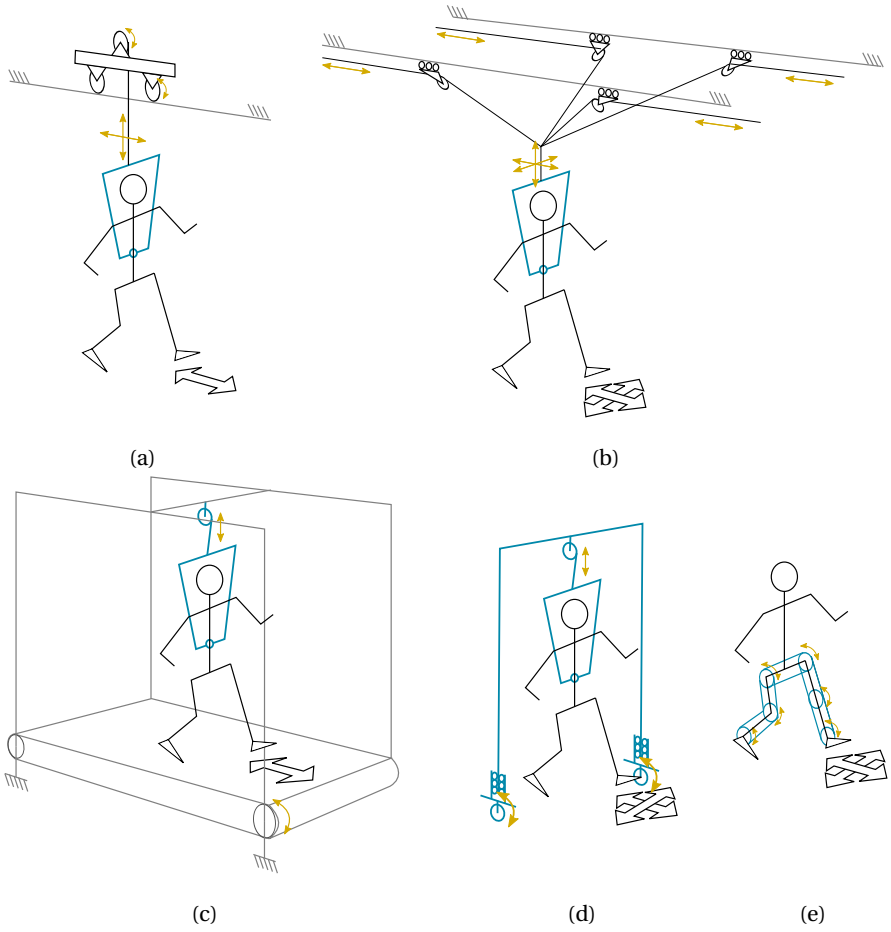

Figure 1.1: Illustration of current balance assistance devices. (a) Single rail, (b) 3D or multi-directional, (c) Treadmill-based and (d) Mobile active Body-Weight support (BWS) systems, and (e) Portable multi-segment exo-structure. White arrows denote directions in which the wearer can move freely.

[80] and the FLOAT Compact (Reha-Stim Medtec) provide support on overground locomotion in a transparent[1] manner along the direction of the rail. This, however, limits movements to a single direction given their single-rail construction, which could potentially induce undesired effects on gait during rehabilitation [153]. This issue, has been addressed by **3D BWS systems**, such as the RYSEN [158] or the FLOAT [205], allowing greater degree of freedom of the user in all directions yet remaining transparent. Unfortunately, having a greater workspace implies much more complex and fixed bulky structures as multiple rails are now needed to provide transparent movements along the extra degree of freedom, which might become a problem in rehabilitation facilities with limited space and impractical in other environments such as nursing houses or residential aged care facilities.

[1] In this context transparent refers to the ability of the device to exhibit zero impedance

BWS treadmills are relatively small compared to single rail and 3D overground BWS systems. As the name suggests, these devices allow controlled weight unloading while performing assisted gait training over a treadmill. Commercially available systems such as KineAssist [152] and the Lokomat ®[95] have been widely used in rehabilitation facilities and multiple scientific studies had been conducted showing its benefits over conventional physical therapy in a number of neurological disorders [79, 126, 167, 182, 215]. However, they are limited to the small treadmill workspace making training for activities of daily living (ADLs) very complex. In contrast, recent **mobile BWS** systems, such as Hocoma's Andago® , try to fill in this gap by providing mobile overground BWS. A mobile BWS generally consists of an active BWS supported by a wheeled structure, which allows the patient to perform 'free' overground walking without being constrained to a single location. Although this type of device is very appealing given its mobility and versatility, it still requires a bulky surrounding structure that makes it impractical for use in regular environments (e.g. climbing stairs or passing through transition strips).

1.2.2 | Internally-applied torques

These robotic devices impart assistance to individual joints through wearable multi-segment exo-structures (hereon referred as *exoskeletons*) enabling portability that does not depend on any surrounding structure. Due the increasing interest on portable wearable robotics over the last few years, many prototypes and commercial exoskeletons systems have been proposed for both upper- and lower-limb assistance and rehabilitation.

Available exoskeletons range from very complex multi-joint systems capable of moving paralyzed legs[62, 74] to simpler systems assisting single joints aiming gait assistance [67, 232]. Despite primarily targeting paraplegics, medical exoskeletons such as The ReWalk (ReWalk Robotics), EksoGT (Ekso Bionics), HAL (Cyberdyne), REX (REX Bionics) and Indego (Parker Hannifin Corp) are being tested as means of rehabilitation in specialized centers. They primarily target patients with severed impaired motor functions such as the sufferers from spinal cord injury (SCI), multiple sclerosis (MS) and stroke [53, 134, 197]. Although these devices can improve balance through reinforcement and training of hip or ankle strategies [108] they do not primarily assist balance and might require the use of crutches or walkers. Thus, target groups with mild or low impaired mobility such as the frail elderly or individuals post-stroke would not effectively benefit from these devices given their inability of assisting balance. Simpler single-joint systems such as the Active Pelvis Orthosis (APO) [67] or the HONDA Stride Management Assist system (SMA) [232] are thus more appealing devices for these target groups. Given that they primarily aim to assist gait impairments, these devices are characterized for their low weight and simplicity. Recently, feasibility studies have been conducted to evaluate improvement in gait parameters in elderly and post-stroke individuals showing positive results [25, 30, 149].

Although promising in gait rehabilitation, these devices could exhibit limitation in balance assistance applications due to their type of actuation. Joint torques create opposite reaction torques in the subsequent body segments which might be detrimental for balance assistance. Suppose for example, that while tripping forward (in the anterior direction) a large hip extension torque is applied to assist foot placement to avoid a fall. Here, given the opposite reaction torque, the forward movement of the trunk would be

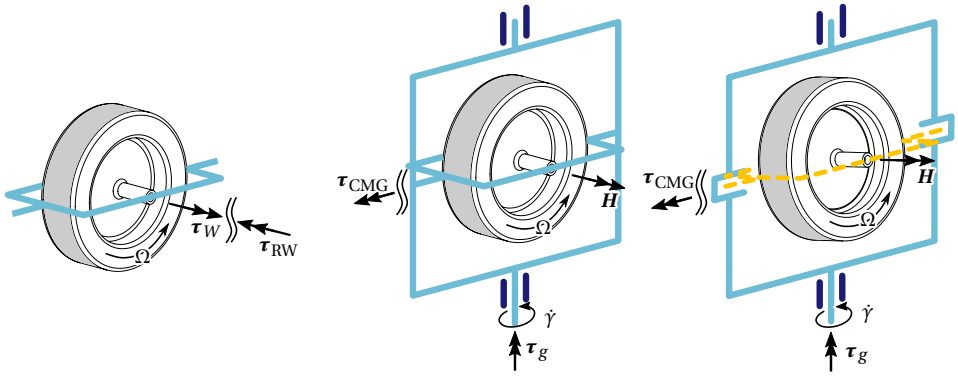

(a) (b) (c)

Figure 1.2: Momentum exchange devices. (a) Reaction Wheel. (b) Single-gimbal Control Moment Gyroscope. (c) Dual-gimbal Control Moment Gyroscope

reinforced which could potentially lead to a fall.

1.2.3 | Free torques

These devices (also known as momentum exchange devices) can produce effective free torques [2] on a body without the need of a coupled inertial frame or multi-segment structures, exploiting conservation of angular momentum. Given their unique actuation capabilities, these actuators have been widely and primarily used in the aerospace industry for attitude control of small and large spacecrafts (e.g satellites, International Space Station, etc.) and in very few terrestrial applications such as vehicle stabilizers (e.g. the Brennans' Monorail [20], 1913 Shilovsky's gyro car, 1961 Ford's Gyron and Lit Motor's C-1), boat stabilizers (e.g. SeaKeeper gyro) and autonomous underwater vehicles [198, 199].

They are typically divided into two types: Reaction-wheels (RWs) and Control Moment Gyroscopes(CMGs). RWs devices generate torques by accelerating or decelerating a fast spinning wheel (hereon referred to as *flywheel*) about its own rotating axis by the input flywheel motor (Fig. 1.2a). Although simple to construct and control, the amount of torque that can be generated directly depends on the flywheel motor ($\boldsymbol{\tau}_{\mathrm{RW}}$). Unfortunately, this makes RWs impractical for torques higher than 1 N m due to high power requirements or impractical wheel mass and size [115]. Despite of this, RWs are typically used in small satellites (e.g. U-class satellites) when output torque requirements are low [115, 179, 212, 235].

When higher torques are required, CMGs are more appealing solutions. Unlike RWs, CMGs output torque does not depend directly on the flywheel motor torque. Here a second input motor rotates a structure containing a flywheel (hereon referred to as *gimbal*) about an orthogonal axis (Fig. 1.2b). While doing this, a free torque ($\boldsymbol{\tau}_{\mathrm{CMG}}$) is generated along a mutually orthogonal axis to its flywheel and gimbal spin axes (Fig. 1.2b). Its mag-

[2] Free torques or moments are those that do not create opposite and equal reactions in subsequent connected segments

nitude and direction are thus dictated by the flywheel's angular momentum ($\boldsymbol{H}$) and the rate at which its surrounding structure is gimbaled ($\dot{\boldsymbol{\gamma}}$).

Because of its unique torque generation, CMGs exhibit important features such as 'torque amplification' and variable output-torque direction. 'torque amplification' is achieved given that the input gimbal torque (τ_g) required to accelerate the gimbaled structure is much smaller than the output torque generated by the CMG [115, 179]. This allows the realization of high-torque CMGs with less powerful motors compared to RWs with similar performance, despite the need of two separate actuators (i.e. Flywheel and Gimbal motors). Concerning the variable output-torque direction, it is defined by the variable position of the flywheel being dictated by the gimbal motion. It thus allows versatility in the predefined desired output-torque direction, although off-axis components are inherently present if only a single CMG is used. This is typically solved by using a second CMG in a 'scissored pair' manner allowing a combined single direction output [21, 35].

Despite their torque amplification and variable output-torque direction, CMGs exhibit certain actuation limitations. CMGs can only generate torque in a given direction for a very short time. This is due to the proneness of CMGs to geometric singular configurations[3] where torque cannot be longer produced in the desired direction. In addition to several control steering laws [13, 203, 217], more elaborated momentum exchange devices such as double gimbal CMGs (DG-CMGs) or variable speed CMGs (VS-CMGs) have been proposed in literature to avoid or better deal with these configurations. DG-CMGs consists of an additional passive or active structure added to the CMG which allows the flywheel to be oriented in any direction. Although this helps to avoid the occurrence of singular configurations, output torque amplification is reduced due to the potential non-orthogonality of the flywheel and actuated gimbal axes. Moreover, DG-CMGs are heavier and mechanically more complex than regular CMGs due to the added structure and more difficult to control due to the added degree of freedom and their proneness to 'gimbal lock' configurations[4]. Conversely, VS-CMGs keep the same structure of regular CMGs but include a more powerful flywheel motor in order to generate torque even in singular configurations, combining both CMG and RW principles. Although keeping the simplicity of regular CMGs, VS-CMGs weight and power requirements increase due to the more powerful flywheel motor.

Very recently, a number of minimalistic support devices for human balance assistance based on RWs and CMGs have been proposed. RW-based devices such as the one presented by Wojtara *et al.* [7, 225], first showed the potential of momentum exchange devices for balance assistance. Their pilot study consisted on the use of a single large flywheel embedded in a customized corset where balance assistive and disruptive controllers where tested with healthy individuals. At the same time, Li and Vallery [116] proposed a minimalistic CMG-based concept consisting on cluster of 3 CMGs enclosed in a backpack-like structure incorporating a cooperative balance assistance controller. This study was later elaborated by *Chiu and Goswami* [35], who realized the first CMG-based human balancing prototype which consisted of a symmetric (scissored) CMG pair. This prototype, however, was not evaluated as balance assistance device and the results

[3] Here the flywheel and desired output axes happen to be aligned
[4] Here the flywheel and gimbal axes are aligned

presented were limited to tests over a fixed test bench.

Given its potential compactness and its unique type of actuation, CMGs are very good candidates as wearable technology for balance assistance. Unfortunately no studies have reported evidence of their feasibility in balance assistance or their evaluation on human beings.

1.3 | Problem Statement

In the context of portable balance-assistance devices, three major issues need to be addressed in order to evaluate CMG actuation in human beings. First, the challenge of real-time **sensing** of stability metrics of a moving human based on upper-body inertial measurement units. Given the limited measurements of these type of sensors, it is unclear how highly specific fall-predictors such as linear velocity can be estimated. Secondly, the challenge that pose the design of a CMG **actuation** unit. Due to its application, this challenge introduces a compromise of actuation capabilities and portability. Inherently a light and small CMG will have a very limited output torque, while a high output torque CMG will must certainly be heavy, bulky or both. And thirdly, the type of **control** and the magnitude of actuation that the CMG device should apply. It is unclear how human beings would react to assistive free torques, and moreover, how much assisting torque is required and how it should be applied to successfully assist balance.

1.4 | Goal

The goal of this thesis is to assess the feasibility of a CMG-based actuator as balance assistance device in individuals with balance disorders. To this end the following questions need to be addressed:

1. *How can stability metrics be assessed in real time using minimum upper-body sensing?*
2. *How can an upper-body CMG-based balance assistive actuator be designed?*
3. *Are free torques applied onto the human torso suitable for balance assistance or augmentation?*
4. *Is the generated assistance suitable to sufficiently augment balance in individuals with balance impairments?*

1.5 | Thesis Outline

Figure 1.3 depicts an overview of a control scheme for a balance assistive device, showing how the different blocks of the system are addressed in this thesis. The chapters presented in this thesis are independently readable as they were written as manuscripts for scientific journals.

Chapter 2 pertains to sensing. It investigates the feasibility of a model-based algorithm to estimate the state of balance based on a single upper-body sensor. This chapter addresses question 1.

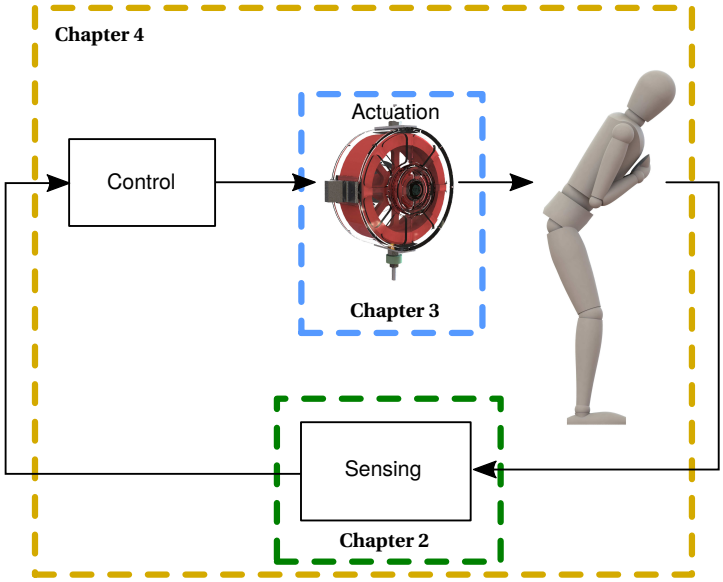

Figure 1.3: Thesis outline illustration. It depicts a generic control scheme for a balance assistive device.

Chapter 3 pertains to actuation design. It presents a detailed design methodology of a single CMG as balance-assistive actuator. This chapter addresses question 2.

Chapter 4 pertains to evaluation of control algorithms and assessment in human beings. It presents a 2 part study where the feasibility of the CMG as balance assistance device in a series of challenging balancing tasks. Part 1 investigates the performance of different types of continuous assistive controllers and their effect on able bodied individuals. Part 2 evaluates the best performing controller on individual post strokes. This chapter addresses question 3 and 4.

The thesis ends with conclusions and future directions in **Chapter 5**

2

Sensing

The content of this chapter have been sligthly modified from the paper:
C. Paiman, **D. Lemus**, D. Short, and H. Vallery, *Observing the State of Balance with a Single Upper-Body Sensor*, Frontiers in Robotics and AI, Volume 3, (2016). [145]

The occurrence of falls is an urgent challenge in our aging society. For wearable devices that actively prevent falls or mitigate their consequences, a critical prerequisite is knowledge on the user's current state of balance. To keep such wearable systems practical and to achieve high acceptance, only very limited sensor instrumentation is possible, often restricted to inertial measurement units at waist level. We propose to augment this limited sensor information by combining it with additional knowledge on human gait, in the form of an observer concept. The observer contains a combination of validated concepts to model human gait: A spring-loaded inverted pendulum model with articulated upper body, where foot placement and stance leg are controlled via the extrapolated center of mass (XCoM) and the virtual pivot point (VPP), respectively. State estimation is performed via an Additive Unscented Kalman Filter (Additive UKF). We investigated sensitivity of the proposed concept to model uncertainties, and we evaluated observer performance with real data from human subjects walking on a treadmill. Data was collected from an Inertial Measurement Unit (IMU) placed near the subject's center of mass (CoM), and observer estimates were compared to the ground truth as obtained via infrared motion capture. We found that the root mean squared deviation did not exceed 13 cm on position, 22 $\mathrm{cm\,s^{-1}}$ on velocity (0.56 to 1.35 $\mathrm{m\,s^{-1}}$), 1.2° on orientation and 17 $\mathrm{°\,s^{-1}}$ on angular velocity.

2.1 | Introduction

Falls pose a major problem, especially in our aging society. Most falls among the elderly occur during forward walking (24 %) and due to incorrect weight shifting (41%) [168]. Balance dysfunction was found to be a considerable risk factor for falls [173].

Wearable robotic devices could play a role in preventing falls, or at least mitigating their consequences, by providing balance assistance in daily life activities. This would result in increased safety and independence of the elderly. Examples for such systems are the balance-assisting gyroscopic backpack [116], the hip orthosis [67] and airbags to reduce fall injuries [196].

Acceptance of such devices is a critical hurdle, and it relies on the technology being unobtrusive, easy to use, and minimalistic. For example, wearable airbags are mostly contained in just a thin waist belt, and the gyroscopic balance-assisting device is contained in a backpack. Both devices need to rely on sensor data that can be acquired by wearable sensors at the upper body, as instrumenting the legs would increase hardware complexity and reduce user comfort in donning and doffing the system.

Standard wearable kinematic sensors are inertial measurement units (IMUs), consisting of accelerometers, gyroscopes, and potentially magnetometers. Such IMUs are commonly used in several fields, not only for real-time fall detection [102, 141], but also for clinical gait analysis [69, 195] or in sport coaching [54]. IMUs are advantageous in terms of weight, size, energy consumption, and cost. A limitation of IMUs is that they do not allow to directly measure one highly specific predictor for imminent falls: linear velocity in vertical direction. This has proven to be a valuable source of information both in literature [18, 228] and in our own experience (with the FLOAT rehabilitation robot of

Vallery et. al. [205]). Despite recent advances in filtering techniques for IMUs [184], they cannot deliver linear velocity information without drift or additional assumptions.

Furthermore, most existing fall detection algorithms are based on data-driven or heuristic approaches [17, 101, 140, 141], where velocity or acceleration thresholds are used to assess loss of balance. Black-box, data-driven approaches intrinsically rely on large amounts of training data to achieve acceptable specificity (low rate of true positives) and sensitivity (low rate of true negatives) in real-world conditions. Such training data is challenging to obtain. Furthermore, the algorithms need to be specifically configured if more insight is desired besides binary classification of movement as fall or non-fall.

Possibly, the performance of such wearable sensor systems could improve considerably if they were combined with knowledge of nominal human balance behavior. To quantify the *state of balance* during bipedal gait, multiple definitions have been proposed in literature, both for human locomotion [48, 78, 82] and bipedal robots [70, 160, 161, 218]. What most definitions have in common is that they require at least the position and velocity of the body's center of mass (CoM) with respect to the center of pressure (CoP), the point of application of the net ground reaction force. These variables are complicated to measure in a wearable application without instrumenting the legs. Moreover, sensors for online measurement usually provide local rather than global information, which is insufficient for fall detection and balance control.

To meet these challenges, we propose to estimate the state of balance by combining local sensor measurements with a simple model of mechanics and control of human gait, in the form of an observer concept.

The choice of model should be as simple as possible, to avoid any unnecessary assumptions. Still, the model needs to contain the main features needed to link the state of balance with available sensor information. Particularly, it has to predict orientation of the upper body (which can be measured by IMUs), as well as the base of support and location and velocity of the CoM with respect to it (critical determinants of balance). Many models focus on foot placement only and reduce the upper body to a point mass, such that sensor information from the upper body (like inclination) cannot be integrated [83, 224]. Also, many models consider double-support phases during gait as instantaneous, which greatly reduces the base of support. This is particularly unrealistic for slow gait of persons with balance impairments, who have extended double-support phases compared to healthy subjects of the same age [10, 123], and also for other postural tasks such as sit-to-stand transitions or standing.

As a first step, we aimed for a sagittal-plane model for forward walking on level ground. First, we formulated a set of requirements for such a model (Section 2.2.1), conducted a small survey on available models and their suitability for the observer concept, and we assembled a model based on this analysis (Section 2.2.1). Using simulations, we evaluated the sensitivity of the implemented observer (Section 2.2.2) to parameter uncertainties (Section 2.2.3). Finally, we evaluated observer performance using real data from experiments with human subjects (Section 2.2.4).

2.2 | Materials & Methods

2.2.1 | Dynamic Model

Definition of Requirements

The purpose of this study was quantification of the state of human balance during walking with limited sensor information and under real-time constraints, by means of a model-based observer concept. The first steps were to choose the sensor and an appropriate model for the observer.

As sensor, we chose a minimalistic setup with only a single Inertial Measurement Unit (IMU) at the upper body, near the waist. This is a convenient location for many wearable applications, such as wearable airbags. Furthermore, previous work suggested that accelerometers worn near the waist are effective for pre-impact fall detection [102], and that placement near the waist is ergonomic and flexible [231].

The model should incorporate the main features of human balance control, while still being observable with the chosen sensor. Three main strategies have been recognized in literature: the *ankle strategy*, which counteracts small disturbances during stance and single support; the *hip strategy*, which utilizes upper-body movement to affect angular momentum in response to slightly larger disturbances; and finally the *stepping strategy* or *foot placement strategy*, which dominates during gait and which copes with disturbances in case ankle and hip strategy do not suffice during stance [90]. Trunk control is particularly relevant, because it has been shown that limited trunk motion results in a higher risk for falls, and elderly, who are more prone to falls, often show limited orientation angles and angular velocities [71]. To represent all these strategies, the model needed to have an articulated upper body, trunk and ankle control, as well as a strategy to place the feet.

We only considered models where experimental evidence existed to confirm their ability to represent human balance strategies.

Finally, the model had to be suitable for a real-time implementation, and it had to include as few parameters as possible, to minimize efforts for calibration or identification.

Choice of Dynamic Model

To choose a dynamic model, human walking models from literature were evaluated against our very specific requirements. An overview of these models is given in Table 2.1. The mechanical models could be categorized in three groups: the linear inverted pendulum (LIP), the spring-loaded inverted pendulum (SLIP) and the multi-body model (MB).

Even though multibody models have shown very valuable to explain human balance strategies [78], the models would not be observable with our chosen extremely limited measurements, and can therefore not be used.

Due to the constraint of an implementation suitable for real-time application, we excluded some other models, even though they might have the ability to model human-like gait accurately, such as the ones based on optimization techniques [6]. We also excluded neuromuscular models, because of the difficulty of determining the many needed muscle-reflex parameters [65].

Category	Reference
Mechanical Models	
Linear Inverted Pendulum (LIP)	
Basic LIP	Kajita *et al.* [99]
Legs with knees	McGeer [127]
Finite-sized foot	Koolen *et al.* [105]
Spring-Loaded Inverted Pendulum (SLIP)	
Basic SLIP	Seipel and Holmes [185]
Accelerated pivot	Jung and Park [98]
Roller foot	Whittington and Thelen [216]
Articulated upper body	Maus *et al.* [124]
Damping	Saranlı *et al.* [175]
Variable impedance	Park [148]
Multi-Body Model (MB)	
System of particles	Chyou *et al.* [36]
Rotational inertia	Lee and Goswami [112]
Musculoskeletal	Geyer and Herr [65]
Control Methods	
Central Pattern Generator	Ogihara and Yamazaki [142]
Finite State Machine	Jo [96]
Optimal Controller	Anderson and Pandy [6]
Artificial Reflexes	Geyer and Herr [65]
Zero Moment Point	Hirai *et al.* [81]
Extrapolated Center of Mass	Hof [83]
Virtual Pivot Point	Maus *et al.* [125]
Angular Momentum	Kajita *et al.* [100]

Table 2.1: Specifications and variations to the three basic mechanical models (Linear Inverted Pendulum, Spring-Loaded Inverted Pendulum and Multi-Body Model) and the two control methods (based on Neural Principle or Mechanical Principle).

Simplified models with spring legs can reproduce the vertical oscillation of the center of mass, and kinetic and gravitational potential energy resemble human gait [66]. Therefore, we chose massless springs as legs.

To represent the upper body in a simple way, we added a single rigid body to the SLIP model, hinged at the hip, as suggested previously by [125] in the context of Virtual Pivot Point (VPP) control. The VPP hypothesis entails that the resultant ground reaction forces at each foot is always pointed toward a virtual point above the center of mass, by means of controlling hip torques. This way, the upper body mimics a physical pendulum, with the virtual point on the trunk as pivot. As opposed to an inverted pendulum, a hanging pendulum is does not require active state feedback control throughout the entire gait cycle. Experimental evidence for this model has been found [125]. Experiments with models based on the VPP, showed high coefficients of determination for predicted ground reaction force direction, and predicted whole-body angular momentum ($R^2 > 97.75\%$ and $R^2 > 96\%$ respectively) for the trunk-attached frame [125].

The feature that remained to be added to the VPP model was a foot placement strategy. To this end, the extrapolated center of mass (XCoM) with *constant offset control* was utilized [82]. Also for this strategy, experimental evidence exists [233], although differences in stability margins seem to exist between healthy young subjects, healthy elderly

subjects, and elderly fallers [118].

Combining this foot placement strategy with VPP control was expected to result not only in stable behavior of the upper body, but also in stable walking behavior. Geometrical definitions of the model are given in Fig. 2.1.

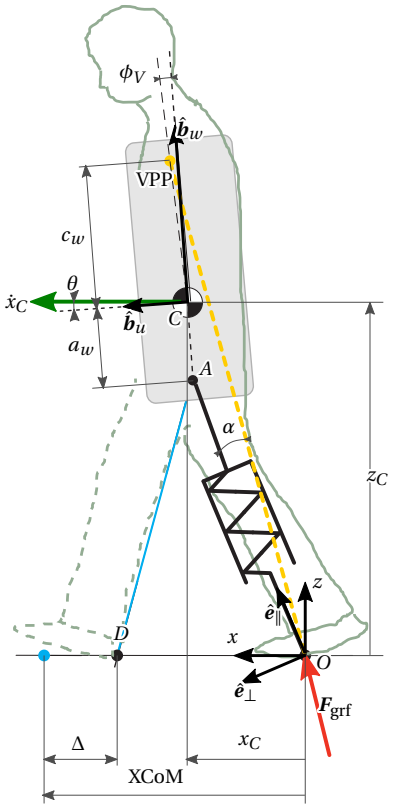

Figure 2.1: Geometrical representation of *Virtual Pendulum Model* with Virtual Pivot Point (VPP) control for the upper body (with ground reaction force $\boldsymbol{F}_{\text{grf}}$) and foot placement with the extrapolated center of mass (XCoM, calculated with i.a. the velocity, v, of the center of mass)

Movement Generation with the Dynamic Model

Assumptions

The equations of motion of the dynamic model were calculated based on the following assumptions:

1. Compliant leg behavior of the human could be modeled with telescopic spring-damper legs; a knee joint did not need to be added to the model.

2. The legs could only be compressed rather than extended, such that the ground reaction force acting on the leg never had a component pointing downwards.

3. Loss of kinetic energy at ground contact was negligible, such that no impact forces occurred and no sudden changes in potential or kinetic energy were present after foot placement; when placing the foot at the ground, the resultant force in direction of the leg equaled zero.

4. Dynamics of the swing leg were negligible; the legs had no mass or inertia, and in swing phase, the legs were at rest length. Accordingly, swing leg dynamics did not appear in the equations of motion.

5. Movement of the center of pressure during single-support phase was negligible; the feet were modeled as point feet, and their positions remained constant throughout stance phase.

Even though the equations of motion of this model could be derived in three dimensions, we neglected the influence of 3D coupling terms and analyzed only a 2D planar model in the sagittal plane.

Equations of Motion

All following calculations used the global reference frame $\mathcal{N}$, the reference frame fixed to the stance foot.

The state vector of the model, $\boldsymbol{q}$, consisted of 6 state variables: components of the center of mass (CoM) position vector ${}^{\mathcal{N}}\boldsymbol{x}_C = (x_C, z_C)^T$ with respect to the origin O and of the CoM velocity vector ${}^{\mathcal{N}}\dot{\boldsymbol{x}}_C = (\dot{x}_C, \dot{z}_C)^T$, upper body angular orientation θ, and upper body angular velocity $\omega = \dot{\theta}$ as

$$\boldsymbol{q} = \begin{pmatrix} x_C & z_C & \theta & \dot{x}_C & \dot{z}_C & \omega \end{pmatrix}^T. \tag{2.1}$$

Transformation of a body vector to the global frame was done with a rotation matrix such as

$${}^{\mathcal{N}}\mathbf{R}_{\mathcal{B}} = \begin{bmatrix} \cos(\theta) & \sin(\theta) \\ -\sin(\theta) & \cos(\theta). \end{bmatrix} \tag{2.2}$$

These state variables described the configuration and movement of a body, floating in space, with forces and moments acting on it. To stabilize the trunk, the ground reaction force of the leg was directed toward the virtual pivot point (VPP). From a biomechanical perspective, this could be explained with a torque on the hip joint. This ground reaction force $\boldsymbol{F}_{\text{grf}}$ consisted of a component $F_{\parallel}$ along the leg (spring and damping forces) with k spring stiffness, d damping coefficient, l_0 rest length of the spring and l current leg length

$$F_{\parallel} = -k\left(l - l_0\right) - d\dot{l}. \tag{2.3}$$

and a component $F_{\perp}$ orthogonal to the leg. Thus, using the unit direction vectors $\boldsymbol{e}_{\parallel}$ and $\boldsymbol{e}_{\perp}$, the angle α between the leg and the direction of $\boldsymbol{F}_{\text{grf}}$, and the position vector $\boldsymbol{x}_{\text{VPP}}$ of the VPP with respect to O, the resultant ground reaction force, $\boldsymbol{F}_{\text{grf}}$, could be expressed as

$$\boldsymbol{F}_{\text{grf}} = F_{\parallel}\boldsymbol{e}_{\parallel} + F_{\perp}\boldsymbol{e}_{\perp} = \frac{F_{\parallel}}{\cos(\alpha)} \frac{\boldsymbol{x}_{\text{VPP}}}{\left\|\boldsymbol{x}_{\text{VPP}}\right\|}. \tag{2.4}$$

Using Newton-Euler, this resulted in the following equations of motion for single-support phase, with mass m of the upper body, graviational acceleration g, gravitational force $\boldsymbol{F}_g = (0, 0, -mg)^T$, and moment of inertia J of the upper body with respect to the CoM (the analysis is restricted to 2D, so the determinant replaces the cross product):

$$\begin{bmatrix} m\ddot{\boldsymbol{x}}_C \\ J\dot{\omega} \end{bmatrix} = \begin{bmatrix} \boldsymbol{F}_{\text{grf}} + \boldsymbol{F}_g \\ \boldsymbol{x}_C \times \boldsymbol{F}_{\text{grf}} \end{bmatrix} \tag{2.5}$$

During double support phase, the system can be described as a trunk segment with two legs, both in contact with the ground. The equations of motion were similar to those of single support, but one additional force, and moments resulting from this, has to be added: the ground reaction force of the front leg. The point of application of this force was located at the position of foot placement, point D. Ground reaction forces of both legs were directed toward the VPP. These forces together defined the location of the center of pressure (point E), which gradually moved from rear to front leg during double support phase.

The non-linear system was described with the state derivative $\dot{\boldsymbol{q}}$ and the measurement function $\boldsymbol{y}$

$$\dot{\boldsymbol{q}} = \boldsymbol{f}_j(\boldsymbol{q}) \quad \text{with} \quad j = 1,2 \tag{2.6}$$

$$\boldsymbol{y} = \boldsymbol{h}(\boldsymbol{q}) \tag{2.7}$$

both functions of the state vector $\boldsymbol{q}$, where the subscript j denoted either single support ($j = 1$) or double support ($j = 2$). These equations could be linearized to get the system matrices $\mathbf{A}_j$ as

$$\mathbf{A}_j = \left.\frac{\partial \boldsymbol{f}_j(\boldsymbol{q})}{\partial \boldsymbol{q}}\right|_{\boldsymbol{q}_k} \tag{2.8}$$

and output matrix $\mathbf{C}$

$$\mathbf{C} = \left.\frac{\partial \boldsymbol{h}(\boldsymbol{q})}{\partial \boldsymbol{q}}\right|_{\boldsymbol{q}_k} \tag{2.9}$$

around a certain state $\boldsymbol{q}_k$ at time instant k.

Hybrid Control of Walking

For movement generation, only straight, forward walking on level ground was considered. A simulation of multiple successive steps consisted of two phases: single-support and double-support phase. These two phases were separated by two events: initial contact, IC, (at heel-strike), when the swing leg touched the ground; and final contact, FC, (at toe-off), when the rear leg left the ground. Both phases were simulated with Heun's numerical integration method (1000Hz).

The event functions were based on the assumption of no change in kinetic energy at ground contact. The distance at which the foot was placed, was based on a constant offset to the XCoM. In literature, this was termed *constant offset control* [83]. It has been stated that a constant spatial margin of stability was a possible objective of human walking [233].

Since the difference between the XCoM of the LIP and the *Virtual Pendulum Model* was assumed to be negligible, the XCoM derived for the LIP by [82] was used. For continuous stable walking, the foot needed to be placed posterior to the XCoM. Therefore, initial contact (IC) occurred as soon as the front foot (denoted by index f) could be placed at a point D at a constant offset Δ from the XCoM such that there were zero spring and damping forces, i.e. $F_{\parallel,f} = 0$ and XCoM $= \Delta + S$, with XCoM computed with:

$$\text{XCoM} = x_C + \dot{x}_C \sqrt{\frac{\|\boldsymbol{x}_C\|}{g}} \tag{2.10}$$

and a constant offset Δ dependent on reference step length $s_{l,\text{ref}}$, reference step duration $T_{s,\text{ref}}$, and the eigenfrequency ω_0 of the pendulum [83]:

$$\Delta = \frac{S_{\text{ref}}}{e^{\omega_0 T_{s,\text{ref}}} + 1} \tag{2.11}$$

Final contact (FC) occurred when the rear leg (denoted by index r), while extending, regained zero spring and damping forces, i.e. $F_{\parallel,r} = 0$ and $\dot{l} \geq 0$.

In double support, the state variables were expressed relative to the foot that first touched the ground (the rear leg). After FC, the origin O was be moved to the position of the stance foot in single support of the next step.

Observability Analysis

The behavior of the model strongly depended on model parameters and constants, which are given in Table 2.2. Both spring stiffness, k, (Section 2.2.1) and damping, d, (Section 2.2.1) were computed from a dimensionless value, K and ζ_d respectively, and other model parameters (mass m, rest length leg l_0 and gravitational constant g):

$$k = \frac{K}{l_0} mg \tag{2.12}$$

$$d = 2\zeta_d \sqrt{km} \tag{2.13}$$

Only angular positions and velocities and linear accelerations were measured; position and velocity of center of mass and leg angle were missing. Only the vertical acceleration $\ddot{z}_C$ was used such that the measurement vector was:

$$\boldsymbol{y} = (\theta \quad \omega \quad \ddot{z}_C)^T \tag{2.14}$$

To estimate of these essential pieces of information, the model needed to be observable. The nonlinear equations required an observability check with Lie derivatives, $L_{\boldsymbol{f}}^i$, which could be calculated with:

$$L_{\boldsymbol{f}}^0 = \frac{\partial}{\partial \boldsymbol{q}} \boldsymbol{h} \tag{2.15}$$

$$L_{\boldsymbol{f}}^i = \frac{\partial}{\partial \boldsymbol{q}} (L_{\boldsymbol{f}}^{i-1} \boldsymbol{f}) \tag{2.16}$$

Parameter/Constant	Symbol	Value	Unit
mass	m	80	kg
leg length	l_0	1.0	m
inertia (η-axis)	J_η	4.58	$\mathrm{kg}\cdot\mathrm{m}^2$
CoM - hip joint (ζ-axis)	a_ζ	−0.10	m
coefficient of restitution	e	0.0	–
dimensionless spring stiffness	K	20	–
dimensionless damping	ζ_d	5×10^{-3}	–
CoM - VPP (ζ-axis)	c_ζ	0.10	m
virtual pivot point angle	ϕ_V	1.35	°
gravitational acceleration	g	9.81	$\mathrm{m\,s}^{-2}$
Reference step length	$s_{l,\mathrm{ref}}$	0.20	m
Reference step duration	$T_{s,\mathrm{ref}}$	0.50	s

Table 2.2: Model parameters and constants.

For local observability, the following holds (with number of states $n = 6$ and $\mathbf{O}$ the observability matrix):

$$\textit{The system is locally observable if: } \mathrm{rank}(\mathbf{O}) = n \text{ with } \quad p < n$$

$$\text{and} \quad \mathbf{O} = \begin{bmatrix} L_{\boldsymbol{f}}^0 \\ L_{\boldsymbol{f}}^1 \\ \vdots \\ L_{\boldsymbol{f}}^p \end{bmatrix}$$

This method showed that the observability condition for the dynamic 2D model was fulfilled, if and only if the following conditions held:

$$\{q_i \,\epsilon\, \mathbb{R} \mid q_i \neq 0\} \quad \text{for} \quad i = 1, 2 \ldots n$$

We assume that the instants were $q_i = 0$ were infinitesimally short.

2.2.2 | Observer Design

Observer Concept

The observer needed to estimate human walking behavior. The *Virtual Pendulum Model* was chosen to approximate this, but it is still, like human walking, nonlinear. A nonlinear state estimation technique was thus required.

Yet, the observer needed to be suitable for daily-life applications, such that the state estimates could be utilized for fall detection algorithms and wearable robot control. Therefore, it needed to be possible to run the observer online. This constrained the allowable degree of complexity of the observer type.

It was chosen to use a stochastic state estimation technique, since human walking behavior is stochastic rather than deterministic. We chose a Kalman filter, which is popular due to its relatively straightforward implementation and moderate computational cost.

A well-known example of a Kalman filter is the Unscented Kalman Filter (UKF). This filter does not require derivatives and proved to outperform the commonly applied Extended Kalman Filter (EKF) in terms of accuracy and consistency, without drastically increasing computation time.

The Additive Unscented Kalman Filter is a simple variation to the UKF, with limited amount of sigma points (minimal set of sample points around the mean). With the need for a proof of principle, this standard observer for nonlinear problems was considered to be appropriate. It should be noted that we do not rule out the possibility of applying other observer types to this method.

Observer Implementation

The observer was implemented offline, but it could also be used online.

The observer was configured to start in single support phase. Therefore, estimation started at the instant when the center of mass just passed the stance foot.

First, sets of Sigma-Points were generated with a probability around the prior state estimates. A foot contact detection algorithm defined whether the phase was single or double support. For the simulation, this instant was detected based on the magnitude of the ground reaction forces (as described in Section 2.2.1). Since for the experiment, this kind of information was not available, an existing algorithm published by [68], based on accelerometer data, was utilized. At initial contact (IC) detection, foot placement was computed with constant offset control and the XCoM (Section 2.2.1), and stored. The process model for double support phase was used for the next time step. At the end of the prediction step, a weighted mean was computed from the predicted Sigma-Points, together with a weighted covariance matrix. The weights were divided equally.

After the prediction step, the predicted state estimates had to be corrected by combining predictions with measurements, with process noise and measurement noise matrices as input. The measurements available were upper body angular orientation, upper body angular velocity and vertical acceleration of the center of mass. The vertical acceleration was integrated to estimate the vertical velocity of the center of mass. A 5-th order, high-pass Butterworth filter (normalized cut-off frequency of 0.5) was applied to correct drift. At final contact (FC), the foot placement location (as calculated after IC) was used to move the reference frame to the stance foot in single-support phase. The process model for single support was used subsequently for the next time step.

To tune the observer, simulation data from multiple successive steps were used (40 steps, approximately 16 s). First, the simulation was manually tuned to find an output that converged to a limit cycle. Noise was added for more realistic measurements. Then, the observer parameters, process noise, covariance matrix, and a parameter determining the spread of the sigma-points (σ_s) were set. The measurement noise covariance matrix was determined from the standard deviation of the added noise. Parameters that were found with the tuning process are given in Table 2.3.

2.2.3 | Sensitivity Analysis

	State variable						
Type of noise	x_C (m)	z_C (m)	θ (rad)	$\dot{x}_C$ (m s^{-1})	$\dot{z}_C$ (m s^{-1})	ω (rad s^{-1})	$\ddot{z}_C$ (m s^{-2})
Process noise	5×10^{-7}	5×10^{-5}	5×10^{-1}	5×10^{-1}	5×10^{-7}	5×10^{-7}	-
Measurement noise	-	-	5×10^{-7}	-	-	5×10^{-5}	1×10^{-5}

Table 2.3: Observer parameters, tuned on simulation data. The square roots of the values given in this table were placed on the diagonal to construct a covariance matrix.

Evaluation Method

First, the assumptions were verified: whether or not leg length did not exceed rest length, the intersection point of the ground reaction forces was the virtual pivot point (VPP), and the preferred step length and step time were tracked.

After this, observer sensitivity was evaluated, by varying initial conditions and parameters. Values were varied separately while keeping all other conditions and parameters perfect. The effect of the magnitude of these errors on various observer parameters gave an indication of the robustness of the observer.

Event detection was set at the time of initial contact (IC) and final foot contact (FC) (with errors ε_{IC} and ε_{FC}). Gait parameters were expected to change depending on type of gait (VPP angle ϕ_{V}, VPP height c_ζ, preferred step length s_l and preferred step duration T_s). All the remaining parameters were model parameters: mass m, leg length l_0, distance from center of mass to hip joint a_ζ, spring stiffness K, damping ζ_d and gravitational acceleration g.

The conditions ranged from perfect values (0 % error) as an input, to values deviating largely from the correct ones (100 % error), in 5 equally divided steps, both added and subtracted from the perfect values, with measurement noise (Table 2.4 shows the values considered to be the 100 % maximum). The sample frequency was set to 500Hz. Errors in event detection were based on the mean and standard deviation of errors found in literature [68].

Outcome Measures

The following outcome measures were investigated: Root Mean Squared Error (RMSE), convergence time, overshoot, coefficient of determination (R^2) and correlation coefficient r.

RMSE of a state variable q_i was calculated with Eq. (2.17) over a total of p time steps. To exclude the effect of convergence speed for this evaluation parameter, the initial index k_0 was set at the sample for which $t = 10$ s, to provide sufficient time to converge. In this equation, $\hat{q}_i$ denotes the estimated, q_i the true state variable.

$$\text{RMSE}_i = \sqrt{\frac{\sum_{k=k_0}^{p}(q_{i,k} - \hat{q}_{i,k})^2}{p}} \tag{2.17}$$

Time of convergence was defined as the time from start to the instant that $\hat{q}_{i,k}$ no longer left the interval $(q_{i,k} - \varepsilon, q_{i,k} + \varepsilon)$, with ε a certain set value for that state variable q_i, based on the range of the state variable and what practically was reasonable. The

State variable	*Symbol*	*Unit*	*True value*	*Maximum error*
anteroposterior position	x_C	m	0.0024	0.30
vertical position	z_C	m	1.08	0.30
angular position	θ	°	1.35	30.0
anteroposterior velocity	$\dot{x}_C$	$\mathrm{m\,s^{-1}}$	1.15	1.00
vertical velocity	$\dot{z}_C$	$\mathrm{m\,s^{-1}}$	0.00	1.00
angular velocity	ω	$^\circ\mathrm{s^{-1}}$	−4.01	50.0
mass	m	kg	80.0	10.0
leg length	l_0	m	1.00	0.15
inertia	J_η	$\mathrm{kg\,m^2}$	4.58	1.00
CoM - hip joint distance	a_ζ	m	−0.10	0.10
dimensionless spring stiffness	K	[−]	20.0	10.0
dimensionless damping	ζ_d	[−]	0.005	0.001
CoM - VPP distance	c_ζ	m	0.10	0.10
virtual pivot point angle	ϕ_V	°	1.35	10.0
desired step length	s_l	m	0.20	0.10
desired step duration	T_s	s	0.50	0.20
gravitational acceleration	g	$\mathrm{m\,s^{-2}}$	9.81	0.05
error initial contact detection	ε_IC	ms	0.00	48.0
error final contact detection	ε_FC	ms	0.00	63.0

Table 2.4: True simulation value and maximum errors on initial conditions, model parameters, gait parameters and event contact detection.

allowed errors were 5cm on positions, 10cm on velocities, 3° on angular position and $5\,^\circ\mathrm{s^{-1}}$ on angular velocity.

Overshoot was defined as the largest difference peak from k=1 to convergence, with index k=k_c (Eq. (2.18))

$$\max_{1\le k\le k_\mathrm{c}} \sqrt{(q_{i,k}-\hat{q}_{i,k})^2} \tag{2.18}$$

R^2, coefficient of determination, could be computed with Eq. (2.19), with $\bar{q}_{i,k}$ the mean value of the data.

$$R^2 = 100\,\%\cdot\left(1-\frac{\sum_{k=k_0}^{p}(\hat{q}_{i,k}-q_{i,k})^2}{\sum_{k=k_0}^{p}(q_{i,k}-\bar{q}_{i,k})^2}\right) \tag{2.19}$$

In case of a bias or a gain difference, the correlation coefficient r indicates if the estimates correlates with the true data (ranging between 0, no correlation, 0.3, weak, 0.5, moderate, 0.7, strong, and 1, perfect correlation) and thereby evaluates on phase of walking rather than absolute magnitudes of state variables.

2.2.4 | Experimental Evaluation

Evaluation Method

The performance of the observer was analyzed by comparing the observer outcomes with experimentally measured data. Ethical approval for the experiment was received from the Human Research Ethics Committee, Delft (March, 2015), and the experiment was carried out in accordance to their recommendations. For this study, the data sets

of 2 young, healthy subjects were analyzed: 1 male (28 year, 56 kg), 1 female (24 years, 71 kg). The subjects gave written informed consent.

The set-up consisted of a treadmill with one belt, of which the speed could be varied manually. The test subjects were asked to perform the following tasks on the treadmill for at least 10 seconds:

1. Low-speed walking ($0.56\,\mathrm{m\,s^{-1}}$) (task LW)
2. Normal-speed walking ($0.97\,\mathrm{m\,s^{-1}}$) (task NW)
3. High-speed walking[1] ($1.35\,\mathrm{m\,s^{-1}}$) (task HW)
4. Normal speed walking with the arms folded in front of the chest ($0.97\,\mathrm{m\,s^{-1}}$) (task AW)

Subjects were instructed to walk normally, with the arms free, unless otherwise indicated. Tasks LW and HW were added to validate whether the same observer, tuned on normal speed walking (task NW) could be utilized for different walking speeds. Task AW was added to evaluate the difference in case inertia of swinging arms was absent, since the model neglected arm movements.

Two measurement systems were used: an Inertial Measurement Unit (IMU) and a Motion Capture (MoCap) system. The IMU was attached to the back of the test subjects, at the waist. The MoCap was a 3D, 5-cameras, Motion Capture system (Qualisys Track Manager) to track the movement of the subject, with reflective markers spread according to the placement in Fig. 2.2.

Movement of the markers, providing global position coordinates of points of interest (center of mass, shoulder joints, hip joints and feet) were tracked with the MoCap system, at 500Hz. Upper-body angular orientation was estimated from the Inertial Measurement Unit (IMU) data with a Kalman Filter, upper-body angular velocity was measured with the gyros and linear center of mass acceleration was measured with the accelerometers (1000Hz, resampled to 500Hz to match the MoCap measurements). The IMU was calibrated with the z-axis pointing in the opposite direction of gravity, and the x and y-axes parallel to the ground, using a right-handed system, such that any axis pointing in a direction orthogonal to the vertical gave zero acceleration as an output.

The IMU was placed at the back of the subject's body in vertical, upright orientation, as close to the position in which the IMU had been calibrated. The alignment was such that the z-axis of the IMU was aligned - as much as possible - with the subject's upright vertical (longitudinal axis), the x-axis with the direction of walking (sagittal axis) and the y-axis pointing to the left (frontal axis). To calibrate the IMU, such that 'zero'-angles represented upright standing, the subject was asked to stand as upright as possible, and the 'initial' angles from the IMU were recorded. Since most subjects were not able to stand perfectly upright for the short period of time, the measured initial angles varied approximately 3°. The Euler angles were found by calculating the corrected rotation matrix with

[1] The treadmill speed indicated at the display was validated with the MoCap data of the foot. For low and normal velocities, the average speed of the foot corresponded to the speed indicated at the treadmill. However, for high velocities, a drift was observed. For tasks HW, instead of 1.4m/s, which was the treadmill input, 1.35m/s was estimated to be the actual velocity according to the processed MoCap data.

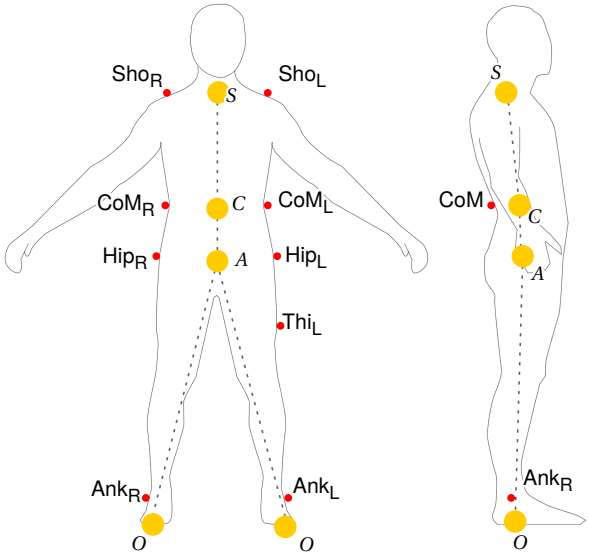

Figure 2.2: Motion capture marker position on the subject, used for data analysis (from left to right: front view, right side view and back view), partially based on guidelines of Carnegie Mellon University. Model shown with dashed line. LThi was used to identify which leg was the left leg. It was assumed the position of the ankle joint (RAnk and LAnk) coincided with the center of pressure. Note that only the x_C positions rather than the y' positions were used.

measured angles (at each time instant) and the (constant) initial angles. A rotation order 1-2-3, from body to global frame, was used (rotating around the body's x-axis with ϕ, about rotated y-axis with θ, around rotated z-axis with ψ). The calculated Euler angle θ obtained from the IMU data was fed into the observer.

During a trial, after IMU data recording had started, the MoCap recordings were started as well, and stopped after approximately 10 s. With the start and the end of the MoCap recordings, a trigger was sent to the computer that recorded IMU data, such that only the IMU data in between the start and end triggers of the MoCap were saved, and IMU and MoCap recordings were synchronized.

Data Processing

Each dataset (of 10 s) was cut in two, such that per task, two datasets of each 5 seconds were obtained (labeled e.g. LW1 for the first 5 s, LW2 for the second 5 s of low-speed walking). The observer was configured to start in single-support phase. Therefore, the start of each dataset was set at the instant when the MoCap recordings of the position of the center of mass just passed the MoCap recording of the position of the stance foot.

After the IMUs were calibrated for upright stance, the instants of initial and final foot contact were estimated with the available data from the IMUs. The use of accelerometers in combination with gyroscopes has been accepted for online gait event detection. An offline approach, which theoretically could be implemented online, was used. It was based on the approach of [68], who showed that initial and final contact events (IC and

FC) could be detected from lower trunk accelerations and heuristics, without false positives or false negatives, with an error of 13 ± 35 ms and 9 ± 54 ms for IC and FC respectively. Although considerable delays were present (117 ± 39 ms for IC and 34 ± 72 ms for FC, it was suggested these could be reduced by applying a different filter, so that further research could lead to an accurate algorithm for real-time gait event detection [68].

The MoCap data, which returned global position coordinates of each marker, needed to be processed to find the state variables as defined in the model: position and velocity of the center of mass with respect to the stance foot in single support, and to the foot of the rear leg in double support. It was assumed the anteroposterior coordinate of the center of pressure always coincided with the marker placed at the ankle joint, of the leg that touched the ground; the vertical coordinate was assumed to be zero. In other words, the foot was assumed to be a point foot.

The markers were labeled in Qualisys Track Manager. In case a marker disappeared, and the gap did not exceed 200 samples (500 Hz), they were gap-filled with a polynomial. Orientation of the upper body for yaw motion, required to extract the anteroposterior coordinates, was based on the direction of the vector from marker LCoM to RCoM or from LSho to RSho, depending on the availability of MoCap data. Anatomical landmarks were used to find points of interest. Hip joint (point A) and shoulder (point S) were defined by the midpoint of the left and right markers of hip and shoulders respectively. The center of mass (point B) was defined to coincide with the midpoint of markers LCoM and RCoM [2]. The inclination angle of the upper body was defined by the orientation of the vector from hip joint to shoulder (point A to S in Fig. 2.2). Linear and angular velocities were calculated from the position vectors with the central difference method and filtered with a Butterworth low-pass filter of 50Hz to filter out noise. For the linear velocity in anteroposterior direction, the central difference method was applied to the absolute position data and the constant velocity of the treadmill was added to the computed velocity.

The initial conditions for each task as input to the observer, were set to the initial conditions found with MoCap and IMU, plus errors that were set to -5 cm for anteroposterior and vertical position, -5 and $5\,\mathrm{cm\,s^{-1}}$ for anteroposterior and vertical velocities respectively, 2.9° for orientation, and $5.7\,^{\circ}\mathrm{s^{-1}}$ for angular velocity.

Model and observer parameters were tuned with data from the first 5 seconds of task NW (normal speed walking), task NW1, with the objective of minimizing the error between estimates and measurements, assuming time instants of IC and FC were known without delay. A first guess of the model parameters was done based on information from the MoCap data, values found in literature for stiffness and damping [236] and the location of the virtual pivot point (VPP) [73]. Measurement noise covariance was found from the standard deviation of constant output IMU data. Remaining observer parameters were manually tuned with trial and error, starting with a similar covariance matrix as found by tuning the observer on simulation data.

The independent variables were treadmill speed and type of gait (arms swinging naturally or arms folded in front of the chest). It was hypothesized that these independent

[2] For some datasets, the RCoM marker was not visible for most of the the time and did therefore not provide sufficient information. In this case, the vector from left to right shoulder was projected to the center of mass plane. The intersection of this vector and the vector orthogonal to it, starting in CoM, defined the center of mass

variables did not affect the parameters that were tuned, except for the VPP angle ϕ_V, desired step length s_l and desired step time T_s. Model and observer parameters from normal speed walking task NW1 were applied to all other tasks, while only tuning ϕ_V for a change in speed and adapting s_l and T_s (LW: 0.20 m and 0.70 s, NW and AW: 0.25 m for subject 1, 0.10 m for subject 2, and 0.55 s, HW: 0.3 m and 0.40 s).

Outcome Measures

Three metrics were defined to evaluate observer performance: the Root Mean Squared Deviation (RMSD) between the two methods, correlation coefficient r and the coefficient of determination R^2 (variance explained). To avoid calculation of metrics before convergence and thereby distort the results, an ample convergence time of 2 s was assumed. The two methods to be compared, were MoCap measurements on the one hand and model-based estimates from the observer, using IMU data, on the other hand.

The results were visualized in a figure, showing mean, 1 standard deviation SD (σ_D) and a 95 % confidence interval (3.182 standard error of the mean SEM (σ_M), $\sigma_M = \frac{\sigma_D}{\sqrt{N}}$ with N the sample size; based on a two-way repeated measures ANOVA with the limited amount of subjects, different types of tasks and different time instants, giving 3 degrees of freedom) and raw data points of RMSD. This type of visualization was chosen because of the limited amount of datapoints. Non-overlapping confidence intervals indicated a significant difference between the separate tasks, with $p < 0.05$.

2.3 | Results

2.3.1 | Sensitivity Results

The minimum and maximum values of the outcome measures, are given in Table 2.5, with an input error of 60 % of the maximum set error. From this table, it could be understood which variables negatively affected which state variables the least and which did this the most. Also, the magnitudes of the metrics gave an indication of the quality of the best and worst estimates.

2.3.2 | Performance Results

The behavior of the tuned observer over time of subjects 1 and 2 is visualized in Figs. 2.3 to 2.4, showing measurements of MoCap and IMU and observer estimates of task NW2, normal speed walking ($0.69 < r < 0.93$, $0.3\% < R^2 < 77\%$ for subject 1, $0.28 < r < 0.98$, $-1\% < R^2 < 67\%$ for subject 2).

A plot showing RMSD, mean, standard deviation and 3.182 standard error of the mean (95% confidence interval) of all trials per task together, is given in Fig. 2.5.

The same was done for r correlation coefficient and R^2 coefficients of determination, for each task and each subject, in Figs. 2.6 and 2.7 respectively.

Each metric (RMSD, R^2 and r), for both subjects, each task and each state variable separately, can be found in Table 2.6.

	State	Evaluation parameter: *RMSE* Min.		*RMSE* Max.		*Convergence time (s)* Min.		*Convergence time (s)* Max.		*Overshoot* Min.		*Overshoot* Max.		R^2 (%) Max.		R^2 (%) Min.		r (-) Max.		r (-) Min.	
Initial Conditions	x_C (cm)	0.02	ω	0.4	$\dot{x}_C$	0.0	ω	4.5	$\dot{x}_C$	0.04	θ	22.0	ω	100.0	ω	99.9	$\dot{x}_C$	1	$\dot{x}_C$	1	z_C
	z_C (cm)	0.03	ω	0.4	$\dot{x}_C$	0.0	ω	6.0	$\dot{x}_C$	0.07	θ	18.0	z_C	100.0	ω	96.4	$\dot{x}_C$	1	x_C	0.99	z_C
	θ (°)	0.007	$\dot{z}_C$	0.009	z_C	0.0	ω	0.03	θ	0.05	z_C	18.0	θ	99.9	$\dot{z}_C$	99.9	z_C	0.99	$\dot{z}_C$	0.99	z_C
	$\dot{x}_C$ (cms^{-1})	0.08	ω	2.4	$\dot{x}_C$	0.0	ω	10.0	$\dot{z}_C$	0.3	θ	67.1	$\dot{x}_C$	100.0	ω	61.3	$\dot{x}_C$	1	$\dot{x}_C$	0.94	z_C
	$\dot{z}_C$ (cms^{-1})	0.1	ω	3.5	$\dot{x}_C$	0.0	ω	12.1	z_C	0.9	θ	251.4	z_C	100.0	ω	96.4	$\dot{x}_C$	1	x_C	0.99	z_C
	ω (°s^{-1})	0.1	ω	0.4	$\dot{z}_C$	0.0	$\dot{z}_C$	3.5	z_C	0.6	$\dot{x}_C$	30.0	ω	99.9	ω	99.8	$\dot{z}_C$	1	ω	0.99	$\dot{z}_C$
Model Parameters	x_C (cm)	0.03	g	1.5	l	0.0	m	3.3	l	0.09	g	10.1	l	100.0	g	98.9	l	1	ζ_d	1	l
	z_C (cm)	0.04	g	9.1	l	0.0	m	∞	l	0.1	g	17.2	l	100.0	g	−1724.6	l	0.99	ζ_d	0.13	K
	θ (°)	0.008	ζ_d	0.05	K	0.0	m	0.0	m	0.03	g	0.4	l	99.9	ζ_d	97.6	K	0.99	g	0.99	K
	$\dot{x}_C$ (cms^{-1})	0.2	g	5.9	l	0.0	m	10.9	l	0.4	g	37.3	l	99.6	g	−128.2	l	1	g	0.87	l
	$\dot{z}_C$ (cms^{-1})	0.3	g	18.4	K	0.0	m	∞	l	0.9	g	131.3	l	100.0	g	−1.5	K	1	g	0.009	K
	ω (°s^{-1})	0.1	ζ_d	2.3	K	0.0	m	2.5	l	0.3	ζ_d	11.0	l	100.0	ζ_d	89.9	K	1	ζ_d	0.98	K
Gait Parameters	x_C (cm)	0.7	c_ζ	5.0	ϕ_V	0.0	c_ζ	∞	ϕ_V	1.2	c_ζ	9.4	ϕ_V	99.8	c_ζ	88.4	ϕ_V	1	s_l	0.99	ϕ_V
	z_C (cm)	0.6	s_l	3.8	ϕ_V	0.0	c_ζ	16.8	ϕ_V	0.7	c_ζ	5.3	ϕ_V	92.9	s_l	−214.8	ϕ_V	0.99	c_ζ	0.95	ϕ_V
	θ (°)	0.02	s_l	0.52	ϕ_V	0.0	c_ζ	0.0	c_ζ	0.05	s_l	0.7	ϕ_V	99.6	s_l	−212.8	ϕ_V	0.99	s_l	0.87	ϕ_V
	$\dot{x}_C$ (cms^{-1})	2.9	s_l	35.6	ϕ_V	0.0	c_ζ	∞	ϕ_V	4.0	s_l	36.9	ϕ_V	44.7	s_l	−8255.8	ϕ_V	99.7	c_ζ	89.5	ϕ_V
	$\dot{z}_C$ (cms^{-1})	4.7	s_l	30.9	ϕ_V	16.8	s_l	∞	c_ζ	10.3	c_ζ	75.3	ϕ_V	93.4	s_l	−184.5	ϕ_V	0.99	c_ζ	0.95	ϕ_V
	ω (°s^{-1})	0.9	s_l	18.8	ϕ_V	0.0	c_ζ	∞	ϕ_V	1.4	s_l	16.5	ϕ_V	98.6	s_l	−554.6	ϕ_V	0.99	s_l	0.67	ϕ_V
Foot Contact	x_C (cm)	2.6	IC	14.4	FC	0.0	IC	∞	IC	4.6	IC	51.0	IC	96.8	IC	3.0	FC	1	FC	0.49	FC
	z_C (cm)	1.3	IC	3.2	FC	0.0	IC	16.8	FC	1.8	IC	4.8	FC	64.5	IC	−130.9	FC	0.99	IC	0.91	IC
	θ (°)	0.02	IC	0.06	IC	0.0	FC	0.0	FC	0.04	IC	0.1	IC	99.7	IC	95.1	IC	0.99	IC	0.99	IC
	$\dot{x}_C$ (cms^{-1})	9.2	IC	28.3	FC	n.a.	n.a.	∞	FC	9.4	IC	33.8	FC	−457.0	IC	−520.1	FC	0.99	IC	0.89	IC
	$\dot{z}_C$ (cms^{-1})	10.7	IC	27.2	FC	n.a.	n.a.	∞	FC	27.0	IC	67.6	FC	65.9	IC	−120.5	FC	0.99	IC	0.90	IC
	ω (°s^{-1})	0.6	IC	2.6	IC	0.0	FC	0.0	FC	1.2	IC	3.6	IC	99.4	IC	87.0	IC	0.99	IC	0.95	IC

Table 2.5: Minimum and maximum values of evaluation parameters, with input errors of 60 % of the maximum set error given in Table 2.4, both subtracted and added from the perfect values. The variables behind minimum and maximum values indicate on which variable the error was introduced. Each row indicates which state variable is affected by the error. Note that larger RMSE, convergence time and overshoot indicate worse performance, while larger R^2 and r^2 indicate better performance. All metrics were rounded to one decimal place or one significant digit (if smaller than 0.1). In case the estimate did not converge to the set error bounds, convergence time was set to ∞.

		Evaluation parameter																	
		RMSD						R^2						r					
State	**Task**	x_C (cm)	z_C (cm)	θ (°)	$\dot{x}_C$ (cm/s)	$\dot{z}_C$ (cm/s)	ω (°s^{-1})	x_C (%)	z_C (%)	θ (%)	$\dot{x}_C$ (%)	$\dot{z}_C$ (%)	ω (%)	x_C (-)	z_C (-)	θ (-)	$\dot{x}_C$ (-)	$\dot{z}_C$ (-)	ω (-)
Subject 1	LW1	2.7	0.5	0.7	6.1	5.1	9.2	94	27	75	35	35	46	0.97	0.77	0.91	0.73	0.69	0.79
	LW2	2.5	0.5	1.0	4.8	5.1	12.9	94	40	56	66	34	18	0.97	0.74	0.88	0.87	0.67	0.62
	NW1[1]	6.5	0.9	0.6	8.0	7.6	9.8	82	32	82	33	56	53	0.95	0.80	0.93	0.60	0.83	0.76
	NW2	7.4	1.0	0.6	7.9	8.7	11.5	77	0.3	79	41	40	42	0.93	0.73	0.91	0.76	0.76	0.69
	HW1	6.9	1.1	0.8	6.5	13.7	14.9	86	41	63	71	45	21	0.97	0.94	0.81	0.89	0.88	0.58
	HW2	17.0	2.7	0.9	45.6	21.3	15.7	16	-212	51	-1248	-26	26	0.67	0.49	0.74	0.14	0.58	0.59
	AW1	3.9	0.8	0.5	7.0	5.3	9.9	94	49	84	43	82	45	0.98	0.95	0.94	0.78	0.91	0.74
	AW2	5.5	0.8	0.5	9.3	8.0	10.1	87	59	88	-22	72	44	0.97	0.91	0.95	0.82	0.86	0.77
Subject 2	LW1	3.0	0.7	0.9	6.0	6.1	7.3	92	-11	32	23	8	7	0.96	0.69	0.71	0.70	0.52	0.51
	LW2	*data not available*						*data not available*						*data not available*					
	NW1[1]	8.7	0.8	1.7	7.6	7.1	11.5	64	13	18	23	51	28	0.97	0.64	0.76	0.79	0.72	0.54
	NW2	8.9	0.6	1.3	6.8	5.7	13.6	62	53	33	46	67	-1	0.98	0.90	0.68	0.86	0.83	0.28
	HW1	10.9	1.7	1.6	16.3	13.1	17.7	56	-118	13	-136	24	-1	0.88	0.45	0.50	0.47	0.61	0.34
	HW2	12.7	2.1	1.5	20.5	15.4	19.1	42	-224	30	-262	1	-8	0.85	0.36	0.56	0.33	0.52	0.29
	AW1	7.4	1.0	1.0	6.1	7.3	9.1	77	13	9	53	59	-12	0.97	0.73	0.75	0.77	0.77	0.39
	AW2	7.7	0.9	1.4	5.2	8.0	9.8	75	30	-240	55	55	-9	0.97	0.77	0.59	0.81	0.75	0.41

[1] Tuned on task NW1.

Table 2.6: Coefficients of determination R^2 and correlation coefficients r of observer estimates of experimental trials, compared to MoCap measurements. LW = Low-speed Walking, NW = Normal-speed Walking, HW = High-speed Walking, AW = Normal-speed Walking with the Arms folded in front of the chest.

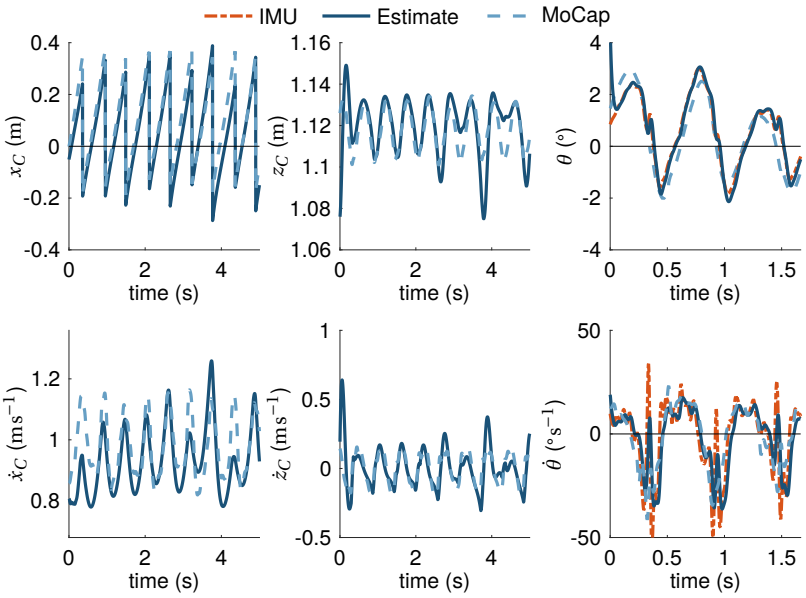

Figure 2.3: Subject 1. Observer estimates against IMU and MoCap data, second trial of normal walking NW (tuned on first trial of normal walking). Error in initial conditions: 5cm on CoM position, 2.9° on upper body orientation, 5 cm s^{-1} on CoM velocity and 5.7 ° s^{-1} on upper body angular velocity. The time window of orientation and angular velocity outcomes was reduced for better visibility.

2.4 | Discussion

2.4.1 | Sensitivity

To verify the working principle of the observer, the dynamic model was simulated to evaluate model behavior, and the sensitivity of the observer was tested with simulation results. It followed that the observer converged when inducing errors on initial conditions. The observer was sensitive to errors in specific model parameters, gait parameters and time of foot contact.

Changing initial conditions did not highly affect the RMSE of the estimates. Maximum errors on CoM position, after 10s, did not exceed 1cm; on linear CoM velocity 7 cm s^{-1}; on upper-body orientation 0.02° and on upper body angular velocity 0.5 ° s^{-1}. R^2 variance explained and r correlation coefficient were hardly affected either, except for anteroposterior CoM velocity ($R^2 = 61.3\,\%$ and $r = 0.94\,\%$ for a 60 % error on anteroposterior CoM velocity). Large errors in initial conditions, did however have an effect on convergence speed and overshoot: CoM velocities needed more than 10s to converge, and overshoot highly increased (up to 2.5 m for $\dot{z}_C$ with a 60 % error on z_C). Overall, mainly errors in upper-body orientation (θ) and upper-body angular velocity (ω) had a minor effect on the performance metrics, while vertical CoM position (z_C) and CoM velocities ($\dot{x}$ and $\dot{z}_C$) had the largest effect. Both θ and ω were hardly affected by errors in

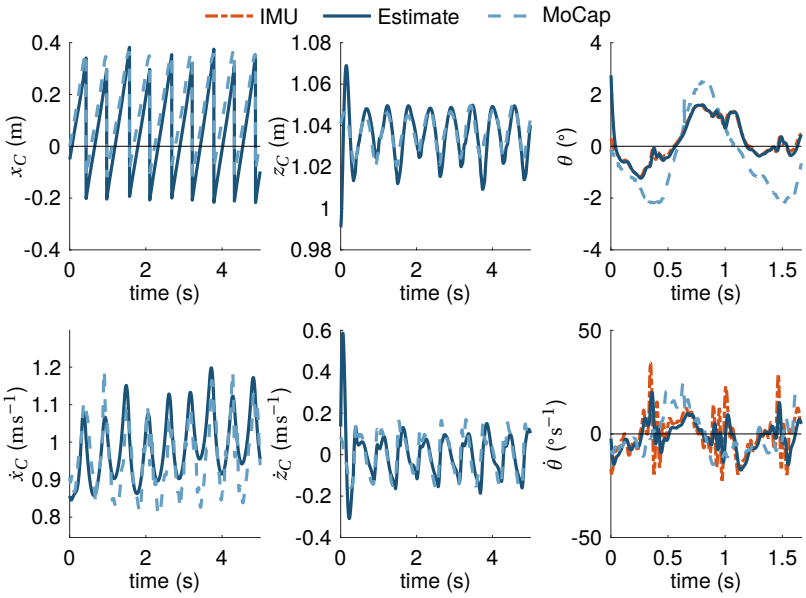

Figure 2.4: Subject 2. Observer estimates against IMU and MoCap data, second trial of normal walking NW (tuned on first trial of normal walking). Error in initial conditions: 5 cm on CoM position, 2.9° on upper body orientation, 5 cms^{-1} on CoM velocity and 5.7 °s^{-1} on upper body angular velocity. The time window of orientation and angular velocity outcomes was reduced for better visibility.

any state variables. This was expected, since these state variables were measured.

The observer was sensitive to various parameter errors. The two model parameters with the largest effects were leg length and spring stiffness. These parameters did not only induce larger RMSE (15cm error on anteroposterior CoM position (x_C) and 18.4cm/s on vertical CoM velocity ($\dot{z}_C$) for 60 % error), longer convergence times and larger overshoot, but also resulted in a bias, such that the estimate did not converge and the coefficient of determination assumed large negative values (-1724.6% and −128.2 % for vertical CoM position (z_C) and anteroposterior CoM velocity ($\dot{x}$) respectively, with a 60 % error). This bias was present in the z_C-coordinate as a result of the hip position parameter. Leg length and hip position were both parameters that could be estimated quite accurately, assuming the center of mass was positioned at the waist. Spring stiffness however proved to be more cumbersome: not only was the spring stiffness of the human leg difficult to estimate, it was also unclear how the actual leg stiffness of the human related to the spring stiffness in the *Virtual Pendulum Model*. The state variables most sensitive to this type of errors, were anteroposterior CoM position x_C and linear, vertical CoM velocity $\dot{z}_C$.

One of the model parameters that depended on type of gait (gait parameters) highly affected the behavior of the observer: the VPP angle ϕ_V, with RMSE errors of 35.6cm/s for anteroposterior CoM velocity ($\dot{x}$), 30.9 cms^{-1} on vertical CoM velocity ($\dot{z}_C$), even 18.8 °s^{-1} on upper body angular velocity (ω) and a mean R^2 of −1555.7 for 60 % error.

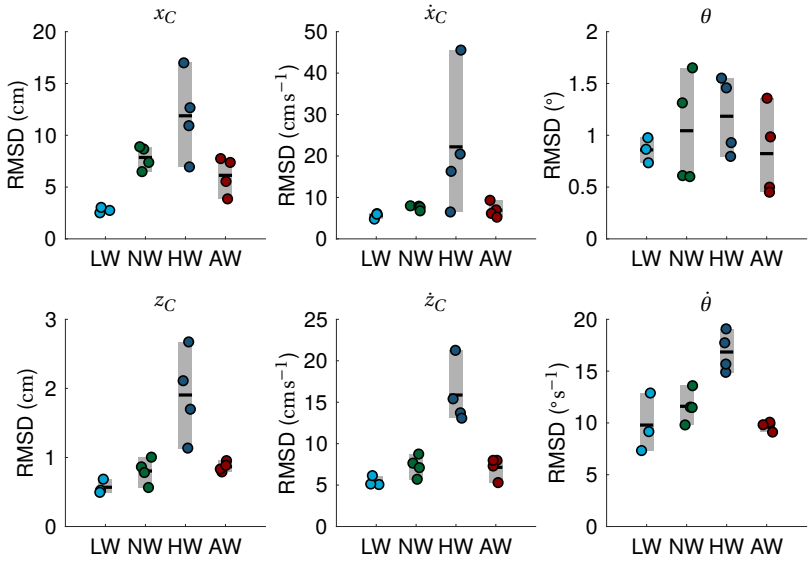

Figure 2.5: RMSD of different speeds (estimates and MoCap data). Raw data, together with means (black bar) shown per task. Note the difference in scale of y-axes.

It was suggested that the VPP angle was related to the speed of walking: a larger positive VPP angle increased the average speed, while zero angle or a small negative VPP angle decreased the speed [103]. Possibly, this parameter should be adapted online, for instance based on heuristics, in order to obtain an observer that could cope with speed changes.

Finally, time of foot contact detection highly influenced the estimates: 14.4cm RMSE on anteroposterior CoM position (x_C), 28.3 cm s^{-1} on anteroposterior CoM velocity $\dot{x}$ and 27.2 cm s^{-1} on vertical CoM velocity $\dot{z}_C$ for 60 % error. In most cases, especially final contact (FC) detection was of importance. Additional sensors on the feet or the event detection algorithm should be robust and accurate to avoid errors in foot contact detection. Also, the delay should be minimized.

Overall, the measurements (upper-body orientation θ and upper-body angular velocity ω), were least influenced by input errors. Anteroposterior CoM position (x_C) was sensitive to errors, especially to time of foot contact. The difficulty of this state variable resided in the fact that it depended on the previous value, which resulted in cumulative errors that kept increasing.

A limitation of this verification method was the dependency on one simulation set. Many limit cycles could be found, of which the one would be more stable than the other [124], and of which the one would correspond better to experimental human walking data than the other.

In case the parameters leg length, hip joint position, (VPP) angle, spring stiffness

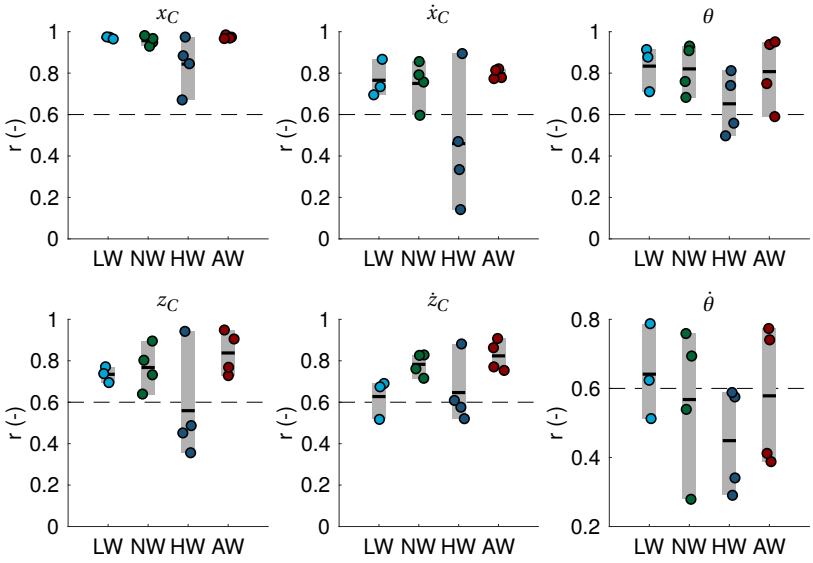

Figure 2.6: Correlation coefficients r of different speeds (estimates and MoCap data). Raw data, together with means (black bar) shown per task. The dashed line indicates $r = 0.60$, a value above which the correlation is preferred.

and time of FC were estimated incorrectly, the estimates became unreliable. Using a less versatile model, such as the LIP, or simply predicting the mean, might in these cases be preferred. The parameters that had little effect on the evaluation parameters were gravitational constant, damping, mass, desired step length and height of VPP. Based on these simulation results, the Additive Unscented Kalman Filter seems a feasible option for estimating the state of balance.

2.4.2 | Performance

A human walking experiment on a treadmill was conducted to validate the hypothesized human walking strategy. This experiment showed that it was possible to predict the state of balance in agreement with Motion Capture (MoCap) measurements, with the proposed *Virtual Pendulum Model* and the *Extrapolated Center of Mass*. Convergence of the estimates of a representative trial is shown in Fig. 2.3.

The quality of the estimates differed per trial: The low-speed walking task LW, and the normal-speed walking tasks NW and AW (arms folded in front of the chest) gave on average lower RMSD values, higher coefficients of determination R^2 and higher correlation coefficients r compared to the high-speed walking task HW. A possible explanation could be the violation of model assumptions with higher velocities: negligible dynamics of the swing leg, negligible movement of the center of pressure or the assumption of no impact forces at foot contact.

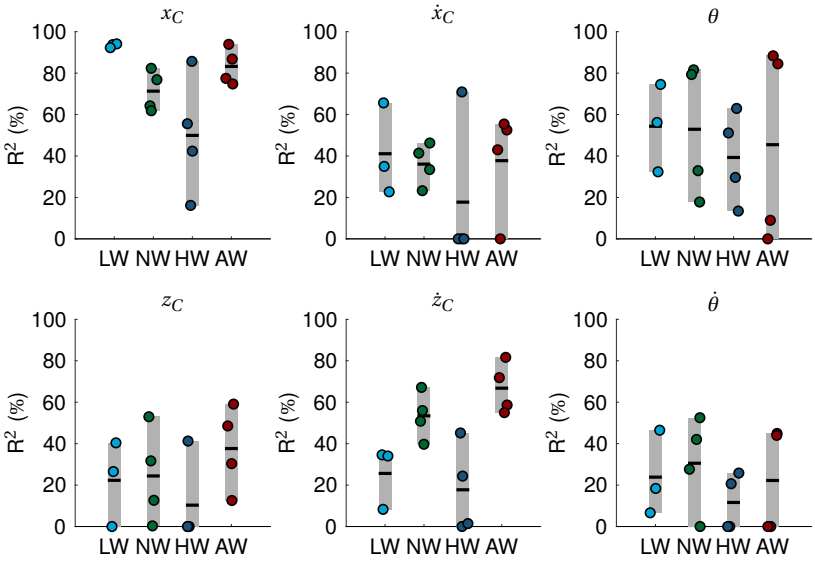

Figure 2.7: Coefficients of determination R^2 of different speeds (estimates and MoCap data). Raw data, together with means (black bar) shown per task. Negative R^2 values are not shown in this plot, to improve visibility of the spread of positive R^2 values. All R^2 values can be found in Table 2.6.

Mean RMSD values did not exceed (approximately) 13 cm for anteroposterior (A-P) CoM position, 2 cm for vertical (V) CoM position, 22 $\mathrm{cm\,s^{-1}}$ for A-P CoM velocity (0.56 to 1.35 $\mathrm{m\,s^{-1}}$), 17 $\mathrm{cm\,s^{-1}}$ for V CoM velocity, 1.2° for upper-body orientation and 17 $\mathrm{°\,s^{-1}}$ for upper-body angular velocity. A trend was observed in Fig. 2.5: RMSD values seemed to increase with increasing velocity. The largest RMSD values were found for HW, even indicating a significant difference for vertical CoM position and velocity, and upper body angular velocity. One of the fall indicators, the vertical velocity of the center of mass, of which the threshold was set at $-1.3\,\mathrm{m\,s^{-1}}$ by [18], showed RMSD values that were considerably lower (0.05 to 0.20 $\mathrm{m\,s^{-1}}$) than the threshold value. The RMSD values found with a 95 % confidence interval of vertical CoM position and upper body orientation were, due to their small magnitude, considered to be practically not important.

The behavior of the human was highly correlated with the behavior of the *Virtual Pendulum Model*: The mean correlation coefficient r was 0.76, 0.77, 0.60 and 0.80 for LW, NW, HW and AW respectively. Especially A-P CoM position x_C and upper-body orientation θ showed high correlation coefficients. Mean r of the LW, NW and AW tasks were above 0.60 for all state variables, except for upper-body angular velocity ω of NW and AW ($r \approx 0.55$), while estimates of HW showed a less strong correlation.

Interestingly, the coefficient of determination R^2 implied a less positive conclusion than implied by correlation coefficient r: mean R^2 was 47, 58, 46 and 54 % for LW, NW, HW and AW respectively. In some cases, especially for vertical CoM position z_C and A-P

CoM velocity $\dot{x}_C$, R^2 assumed negative values, possibly due to little variation in z_C data. Only for x_C and θ, more than, on average, 40 % of the variance in the measurements could be explained with the model.

These findings showed that this controlled mechanical model was, both in theory and in practice, observable with only the limited, local available measurements; local kinematic information of the upper body was sufficient to acquire information on the position of the feet, and on global information of the center of mass. With this proof of principle, the model can be fine-tuned to improve the quality of the estimates, such that it can be applied in wearable robots.

These findings also support the theory of a stabilizing force direction pattern in the sagittal plane. While previous studies validated the existence of the virtual pivot point (VPP) [73, 124, 125], this study focused on exploiting the concept to make enhanced predictions. Herewith, two lines of research were combined: human movement theory [6, 65] and observer application [41, 111, 234]. Moreover, even though the XCoM of a spring legged model not truly coincides with the XCoM of a linear inverted pendulum (LIP) [207], from the limited RMSD in A-P CoM position, it could be concluded the assumption of using LIP XCoM was valid.

It should be noted that the validation measurements of the MoCap data differed from the IMU data, such that the difference between the true error and the estimated deviation was unknown. It was hypothesized that the agreement of MoCap data and IMU for upper-body orientation and upper-body angular velocity was correlated with the agreement of CoM position and velocity estimates with MoCap measurements. However, more data need to be post-processed to draw a significant conclusion.

One limitations of this study concerned assumptions on foot contact. Particularly, the model neglected a moving center of pressure from heelstrike to toe-off, and it assumed zero delay in foot contact detection.

Another limitation concerns manual tuning of gait parameters for different walking tasks, which is disadvantageous for online estimation. The magnitudes of the entries in the process noise covariance matrix were difficult to find. Although a satisfactory result was found, it is very likely that this result was suboptimal. Because of the multitude of parameters, it was expected that optimization techniques would be computationally too expensive and that local minima rather than the global minimum would be found.

A large limitation concerns the type of movements that were investigated. Our experimental trials included walking at three different speeds, but other activities of daily living were not considered. The effect of different activities with a varying rate of angular momentum on the VPP was not investigated, such that no conclusions regarding the performance of the observer in activities other than forward walking could be drawn. Specifically prior to a fall, the rate of change of angular momentum can be large, which could potentially have a negative effect on observer performance. Therefore, for further research, it is suggested to include other activities of daily living and perturbed walking data.

Furthermore, our calibration routine is not practical outside of a laboratory environment and with subjects with balance impairments. In a clinical environment, faster and easier algorithms and protocols should be employed, for example as in [146, 147, 195].

It should be noted that in theory, the same method as presented here could be uti-

lized for frontal-plane evaluation and extended to 3D evaluation. It is suggested to investigate if 3D application is possible for realtime use and significantly better than using two decoupled 2D models (sagittal plane and frontal plane). Also, it would be interesting to explore how the position of the VPP depends on anthropomorphic measures, age or type of daily life activity.

How the human walks and which underlying fundamental principles govern human walking is a comprehensive and complex topic. Further research is required for optimization of the observer based on these concepts, such that it can successfully be applied in wearable robotic controllers. Many other models exist and could be investigated in a similar observer concept.

2.5 | Conclusion

The goal of this study was to quantify balance with measurements on the upper body. It was hypothesized that this could be done with the *Virtual Pendulum Model* as dynamic model, which used the virtual pivot (VPP) concept, combined with the *Extrapolated Center of Mass*, XCoM, and the Additive Unscented Kalman Filter as observer.

First, the observer was tested on simulation data and showed to converge, with varying initial conditions. The observer was especially sensitive to errors in leg length, hip joint position, VPP angle, spring stiffness and time of final contact. Other parameters, such as the gravitational constant, damping coefficient, mass and desired step length, had little effect on the quality of the estimates. A limitation of the observer was the high sensitivity to model parameters and foot contact detection, and the amount of observer parameters that had to be tuned.

Second, the observer was evaluated with experimental data (using a Motion Capture system and an existing foot detection algorithm), showing that, if properly tuned and if instants of foot contact were estimated correctly, the observer gave a satisfactory estimate of human walking. Position of the center of mass could be estimated with an accuracy of less than 13 cm, and congruence of the model with real data was characterized by a coefficient of determination around 50%.

With this study, it was shown that the VPP and the XCoM seem to be valuable principles that can effectively be used in combination with the Additive Unscented Kalman Filter to make predictions on human balance.

Acknowledgments

This research was supported by the U.S. Department of Education, National Institute on Disability and Rehabilitation Research, NIDRR-RERC, Grant Number H133E120010, and by the Marie-Curie career integration grant PCIG13-GA-2013-618899. The authors would like to thank D. van der Pool and M. Wisse for their valuable feedback on the work, and R. di Pace and L. Grande for their support with the experiment.

3

Actuation

The content of this chapter have been modified from the paper:
D. Lemus, J. van Frankenhuyzen, and H. Vallery, *Design and Evaluation of a Balance Assistance Control Moment Gyroscope*, Journal of Mechanisms and Robotics 9, 051007 (2017). [114]

We recently proposed the theoretical idea of a wearable balancing aid, consisting of a set of Control Moment Gyroscopes (CMGs) contained into a backpack-like orthopedic corset. Even though similar solutions have been reported in literature, important considerations in the synthesis and design of the actuators remained to be addressed. These include design requirements such as aerodynamic behavior of the spinning flywheel, induced dynamics by the wearer's motion and stresses in the inner components due to the generated gyroscopic moment. In this paper, we describe the design and evaluation of a single Control Moment Gyroscope, addressing in detail the aforementioned requirements. In addition, given the application of the device in human balance, the design follows the European directives for medical electrical equipment. The developed system was tested in a dedicated balance test bench showing good agreement with the expected flywheel speed, calculated power requirements in the actuators and output gyroscopic moment. The device was capable of producing a peak gyroscopic moment of approximately 70 N m with a total CMG mass of about 10 kg.

3.1 | Introduction

Loss of balance accounts for a significant proportion of injuries among all age groups, but is known to be particularly detrimental among the elderly [46, 117] and those with sensory deficit disorders such as stroke survivors and patients with Parkinson's disease [75, 156]. Several factors associated with balance control have been found to increase the risk of falling, such as impaired stability when leaning and reaching, impaired gait and mobility, impaired ability in standing up and impaired ability with transfers [46].

Multiple hardware solutions for balance assistance are discussed in the literature; currently, advanced wearable actuation technologies [33] and orthotic systems have been developed to assist locomotion, such as the wearable Cyberlegs hip orthosis [149] or exoskeletons such as the MindWalker [213], eLEGS(Ekso Bionics,US) or the ReWalk (Argo Medical Technologies, Israel). So far, these require bulky mechanical constructions attached to multiple segments of the body in order to deliver moments to individual joints of the body. Furthermore, they do not primarily target balance control, sometimes requiring the use of crutches.

Momentum exchange devices such as reaction wheels (RWs) and control moment gyroscopes (CMGs) present an attractive solution for human balance assistance. These devices can produce effective free moments on a body without the need of a coupled inertial frame. RW systems exert moments by accelerating or decelerating the spinning wheel and CMGs exert moments by rapidly changing the orientation of the spinning wheel about an orthogonal gimbal axis [39]. Even though RW systems are much simpler to control and construct, their effective output moment is relatively small if a light and minimalistic construction is desired [179]. In contrast, CMGs present moment amplification capabilities, i.e. given the same wheel actuator as a RW, CMGs can produce higher moments with a relatively small gimbal torque input, making them better candidates for minimalistic assistive devices for human balance. In addition, CMG used

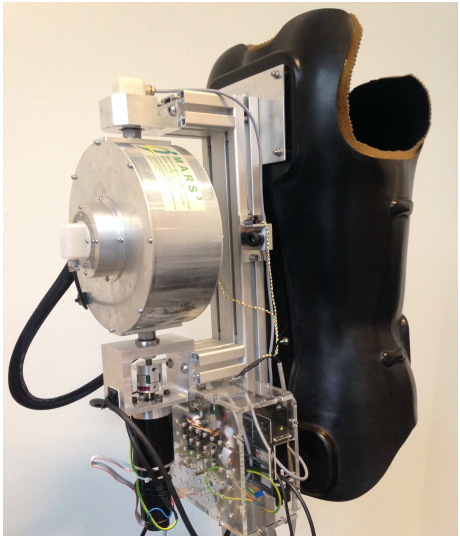

Figure 3.1: Single CMG prototype attached to a wearable corset

in assemblies can exert controlled moments about any direction. Unfortunately, these assemblies are prone to singular configurations in which the desired exerted moment cannot be produced. However, several steering laws have been proposed for spacecraft applications [9, 57, 217], and recently for CMGs as balance assistance devices [13].

In the past several years, a number of minimalistic support devices for human balance assistance based on RWs and CMGs have been proposed. Wojtara et al. constructed a RW-based prototype consisting of a single large flywheel embedded in a corset [7, 225]; although the prototype is specifically designed as balance aid, the assistive torque has to be generated by the flywheel motor, making it bulky if higher moments are required. Theoretical examples of CMG-based devices include gyrostabilizers envisioned in belts or canes [47], or on patient's legs to assist joint motion [137] and haptic devices such as the iTorqU for torque feedback [219] or in intra-vehicular space suits for sensorimotor adaptation[49, 50, 208]. Recently, we proposed an upper body CMG-based wearable device, utilizing multiple control moment gyroscopes (CMGs) to reduce mass and provide balance assistance in any direction [116]. This study was elaborated by Chiu and Goswami [35], who constructed the first CMG-based human balancing prototype which consisted of a symmetric (scissored) pair of CMGs with a mechanical constraint to synchronize gimbal motions; although this gives credence of the use of CMG technology towards gyroscopic human balancing, no experimental data is reported regarding balance capabilities of the device. Moreover, important design specifications such as the dynamic effect induced by the wearers movement, flywheel aerodynamic behavior and internal loads due to gimbal actuation and gyroscopic moment are not addressed. These issues pose an important design challenge as they have great influence on material and actuator selection which in consequence have a direct impact on output assistive moment, power consumption, size and weight.

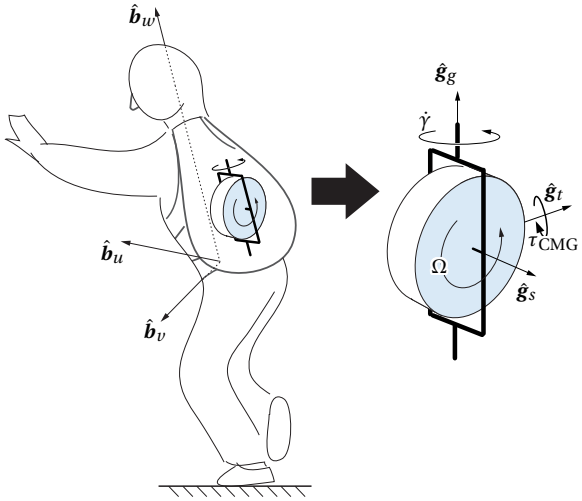

Figure 3.2: Schematic of a worn single-gimbal control moment gyroscope (SG-CMG). The gimbal-fixed frame $\{\hat{\boldsymbol{g}}_s, \hat{\boldsymbol{g}}_t, \hat{\boldsymbol{g}}_g\}$ is oriented such that $\hat{\boldsymbol{g}}_s$ is aligned with the flywheel spin axis and $\hat{\boldsymbol{g}}_g$ is aligned with the body-fixed longitudinal axis $\hat{\boldsymbol{b}}_w$, to constrain the direction of the exerted gyroscopic moment $-\tau_{\mathrm{CMG}}\hat{\boldsymbol{g}}_t$ to the transverse plane. Flywheel and gimbal angular speeds are denoted by Ω and $\dot{\gamma}$, respectively.

3

In contrast to previous reported CMG devices for human balance, we present a detailed design methodology of a single CMG (Fig. 3.1), were the aforementioned design challenges have been addressed. Selection of the actuators was based on the aerodynamic behavior of the flywheel and the influence of the wearer's motion (i.e parasitic moments). In addition, a structural analysis is reported, which is set to comply with the European directives for medical electrical equipment [92], accounting for the loads induced due the gyroscopic moment and centrifugal acceleration. Based on this methodology, a single CMG was built and tested in a dedicated test setup.

3.2 | Control Moment Gyroscope as Actuator

3.2.1 | Modeling

A control moment gyroscope (CMG) is a momentum exchange device which consists of a fast spinning wheel supported by one or more gimbal structures as shown in Fig. 3.2, where the gyroscopic moment τ_{CMG} is given by the rate of change of angular momentum of the spinning wheel [39, 178]. Using Euler's equations of rotational motion, the dynamic equilibrium of a single gimbal CMG (SGCMG) is expressed as [179]

$$\begin{aligned}\dot{\boldsymbol{H}}_{\mathrm{CMG}} = \hat{\boldsymbol{g}}_s &\left(I_s\ddot{\phi}\cos(\gamma) - \left(I_s - I_t + I_g\right)\dot{\gamma}\dot{\phi}\cos(\gamma)\right) \\ + \hat{\boldsymbol{g}}_t &\left(I_t\ddot{\phi}\sin(\gamma) + \left(I_s + I_t - I_g\right)\dot{\gamma}\dot{\phi}\sin(\gamma) + I_{Ws}\dot{\gamma}\Omega\right) \\ + \hat{\boldsymbol{g}}_g &\left(I_g\ddot{\gamma} + \left(I_t - I_s\right)\cos(\gamma)\sin(\gamma)\dot{\phi}^2 - I_{Ws}\Omega\dot{\phi}\cos(\gamma)\right),\end{aligned} \tag{3.1}$$

where I_s, I_t and I_g are the combined moments of inertia of the flywheel and gimbal structure about the flywheel spin axis $\hat{\boldsymbol{g}}_s$, output moment axis $\hat{\boldsymbol{g}}_t$ and gimbal axis $\hat{\boldsymbol{g}}_g$ respectively. The term I_{Ws} denotes the flywheel inertia about the spin axis $\hat{\boldsymbol{g}}_s$. γ, $\dot{\gamma}$ and $\ddot{\gamma}$ are the gimbal angular position, velocity and acceleration respectively, ϕ, $\dot{\phi}$ and $\ddot{\phi}$,are the body angular position, speed and acceleration about the transverse axis $\hat{\boldsymbol{b}}_v$ and Ω is the flywheel angular speed. Note that we constrained our analysis to falls in the sagittal plane (i.e. the $\hat{\boldsymbol{b}}_u - \hat{\boldsymbol{b}}_w$ plane), with body angular velocity $\boldsymbol{\omega} = \dot{\phi}\hat{\boldsymbol{b}}_v$.

To enable easier control design, Eq. (3.1) is conventionally simplified assuming the flywheel angular speed Ω is several orders of magnitude higher than the body angular rate $\dot{\phi}$ and gimbal angular rate $\dot{\gamma}$. Thus, the contribution of the gimbal angular rate in combination with the body angular rate shown as the cross term $\dot{\gamma}\dot{\phi}\sin(\gamma)$ can be neglected as well as the term involving the body angular acceleration $I_t\ddot{\phi}\sin(\gamma)$, as these are typically at least 2 orders of magnitude smaller than the cross term $\dot{\gamma}\Omega$. Hence, Eq. (3.1) can be written as

$$\begin{aligned}\dot{\boldsymbol{H}}_{\text{CMG}} &= \hat{\boldsymbol{g}}_t\tau_{\text{CMG}} + \hat{\boldsymbol{g}}_g\tau_{\text{GM}} \\ &= \hat{\boldsymbol{b}}_u\tau_{\text{CMG}}\sin(\gamma) - \hat{\boldsymbol{b}}_v\tau_{\text{CMG}}\cos(\gamma) + \hat{\boldsymbol{b}}_w\tau_{\text{GM}},\end{aligned} \tag{3.2}$$

with

$$\tau_{\text{CMG}} = I_{Ws}\Omega\dot{\gamma} \tag{3.3}$$

$$\tau_{\text{GM}} = I_g\ddot{\gamma} - I_{Ws}\Omega\dot{\phi}\cos(\gamma). \tag{3.4}$$

Where τ_{CMG} and τ_{GM} are the magnitudes of the gyroscopic moment and the torque exerted by the gimbal actuator respectively. Note that the component about the falling axis (the transverse axis $\hat{\boldsymbol{b}}_v$) of the gyroscopic moment τ_{CMG} depends on how the flywheel is oriented with respect to it, as determined by the gimbal angle γ.

Equation (3.2) provides a starting point for the specification of hardware design requirements, such as flywheel geometry, actuators and gimbal structure. Given the desired gyroscopic moment about the transverse axis $\tau_{\text{IP,ref}}\hat{\boldsymbol{b}}_v$ and flywheel angular momentum, the required gimbal rate can be calculated using Eq. (3.2) as

$$\dot{\gamma} = \frac{\tau_{\text{IP,ref}}}{I_{Ws}\Omega\cos(\gamma)}. \tag{3.5}$$

As the gimbal angle γ increases, a higher gimbal angular rate $\dot{\gamma}$ is necessary to produce the same desired torque. Special care must be taken when $\gamma = \pm\pi/2$. In that case, no gyroscopic moment can be exerted in the transverse axis, as the flywheel spin axis $\hat{\boldsymbol{g}}_s$ is aligned with the transverse axis $\hat{\boldsymbol{b}}_v$. When the gimbal is in such configuration it is said to be in a *singularity*. Thus, the desired gyroscopic moment has to be generated within a range free of singularities, i.e $-\pi/2 < \gamma < \pi/2$.

3.2.2 | Design Requirements

For our design, we based our calculations on the CMG output torque required to counteract the effect of gravity in a fall, when no other balance-recovering actions are applied (e.g. use of crutches, fixed supports or reflexes) and the body is in an out-of-balance state. To obtain quantitative requirements, we simplify a human as an inverted pendu-

lum, where the hip and knee joints are stiff, and no torques are applied about the ankles. It is thus assumed the person falls while pivoting about a horizontal edge. Previously, we estimated that a continuous moment of 280 N m, generated by a set of 3 CMGs, applied for 0.1 s is sufficient to re-orient the human body vertically, based on the same model of a rigidly falling human body with an initial inclination of 10° with respect to the vertical z axis. In that analysis, we assumed a human mass of 70 kg and height of 1.7 m [116].

Based on these findings for an assembly of three CMGs, the design of a single CMG was developed aiming for about a third of the reported gyroscopic moment, i.e 90 N m. It should be noted that even though this first proof of principle is not intended as a full wearable device, size and safety-factor constraints were imposed in the design of the CMG as a first step towards an improved wearable design.

We assume that the CMG should eventually be enclosed in a regular 50 l backpack. Therefore, an outer radius of 200 mm was set as size limit for the device envelope. A safety-factor lower limit of 4 was chosen against structural failure of the rotating components (i.e flywheel and gimbal bearings) as well as the enclosing structure, complying with the European directives for medical electrical equipment [92].

3.3 | Control Moment Gyroscope Hardware Design

3.3.1 | Flywheel Design

In order to store higher angular momentum, the flywheel's moment of inertia was chosen to be as high as possible satisfying the given size constraint and readily available material. A classic disk-with-rim flywheel geometry was chosen as its shape and velocity factors are similar to those of an ideal thin rim [63] and also due to manufacturing practicality. Thus, it is desired that its mass is distributed as far as possible from the spinning axis (i.e at the outer perimeter of the flywheel). Moreover, the width of the flywheel would need to be as large as possible, such that the rim inner radius R_i of the wheel can be as large as possible for a given outer radius R_o. Considering that the wheel needs to rotate also about the gimbal axis, increasing overall volume of the construction, we chose the maximum acceptable rim width $h = 70$ mm and outer radius $R_o = 100$ mm. As material, we chose the readily available aluminum 7075-T6. Moreover, as the device is to be wearable, mass of the wheel was limited to 2.5 kg. This resulted in a rim inner radius of $R_i = 78$ mm, and a moment of inertia of $I_{Ws} = 0.02\,\mathrm{kg\,m^2}$

To couple the rim with the motor, a constant-thickness thin disc was preferred due to manufacturing practicality and weight reduction. A hub was also included such that it could incorporate the motor within the flywheel itself as seen in Fig. 3.3. Further weight reduction was performed by removing material from the thin disk leading to a rim-with-spokes flywheel. However, the presence of these spokes is undesirable in the flywheel geometry due to significant increase of frictional drag while spinning. In order to diminish this effect, thin-plastic discs were placed on each side of the flywheel to cover the spokes after the material was removed.

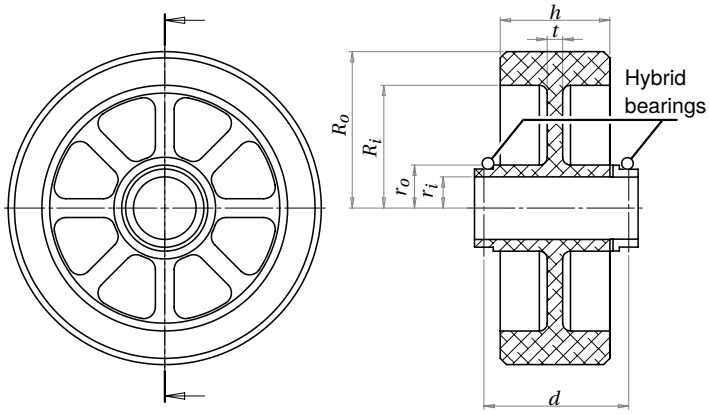

Figure 3.3: Flywheel cross section

Regime	Flow Type Conditions		δ	K_a	K_b	K_c
I	$\mathrm{Re}_a < 3\times10^5$,	$s<\delta$	$5.5\left(\frac{\nu}{\Omega}\right)^{0.5}$	2π	-1	-1
II		$s>\delta$		3.7	0.1	-0.5
III	$\mathrm{Re}_a > 3\times10^5$,	$s<\delta$	$R_o^{\frac{3}{5}}\left(\frac{\nu}{\Omega}\right)^{0.2}$	0.08	$-1/6$	-0.25
IV		$s>\delta$		0.0102	0.1	-0.2

Table 3.1: Axial frictional torque coefficient regimes [42]

3.3.2 | Flywheel Aerodynamics and Actuation

An analysis of the different friction sources was performed to estimate the maximum flywheel speed. The power required to reach a given Ω can be calculated as $P = P_a + P_b$, where P_a and P_b are the power required to overcome aerodynamic drag and bearing friction respectively. The power to overcome aerodynamic drag for a rotating disc can be expressed as [34, 63]

$$P_a = \rho_g \Omega^3 R_o^5 C_{m,a} + \frac{\pi \rho_g \Omega^2 R_o^4 h}{2} C_{m,r} \tag{3.6}$$

where the non-dimensional drag torque coefficients $C_{m,a}$ and $C_{m,r}$ depend on the drag produced by the lateral planar surfaces of the disc and the drag produced by the cylindrical face of the rim respectively.

Estimation of the axial torque coefficient $C_{m,a}$ was based on the relationships determined by Daily and Nece [42] as

$$C_{m,a} = K_a G_a^{K_b} \mathrm{Re}_a^{K_c} \tag{3.7}$$

being a function of the axial rotational Reynolds number Re_a and the axial gap ratio $G_a = \frac{s_a}{R_o}$, with s_a the axial clearance between the flywheel and the casing [34]. K_a, K_b and K_c are constants determined by any of the four flow regimes that can be present [34, 42]

Regime	Conditions	K_u	K_v
Laminar	$\mathrm{Re}_r \leq 64$	10	−1
Transitional Flow	$64 < \mathrm{Re}_r \leq 500$	2	−0.6
Turbulent	$500 < \mathrm{Re}_r \leq 1 \times 10^4$	1.03	−0.5
	$\mathrm{Re}_r > 1 \times 10^4$	0.065	−0.2

Table 3.2: Radial frictional torque coefficient regimes [14, 34]

as shown in Table 3.1. These regimes are categorized depending on the flow type and the nature of the boundary layers [34, 42]. To this end the radial rotational Reynolds number is calculated as

$$\mathrm{Re}_a = \frac{R_o^2 \Omega}{\nu} = \frac{\rho_g R_o^2 \Omega}{\eta} \tag{3.8}$$

where $\rho_g = 1.181\,\mathrm{kg/m^3}$, $R_o = 0.1\,\mathrm{m}$ and $\eta = 1.84 \times 10^{-5}\,\mathrm{Pa\,s}$, are the air density, flywheel's rim outer radius and the air dynamic viscosity, respectively. Subsequently the behavior of the boundary layers (i.e. whether the boundary layers are merged or separate) was determined. Here, the boundary layer thickness δ was compared with the axial clearance s. Table 3.1 summarizes the constants used to estimate the axial frictional moment $C_{m,a}$.

Estimation of the radial torque coefficient $C_{m,r}$ was based on the equations reported by Bilgen and Boulos [14] as

$$C_{m,r} = K_u G_r^{0.3}\, \mathrm{Re}_r^{K_v} \tag{3.9}$$

being a function of the circumferential rotational Reynolds number Re_r and the radial gap ratio $G_r = \frac{s_r}{R_o}$, with s_r the radial clearance between the flywheel and the casing [34]. K_u and K_v are constants determined by any of the four flow regimes that can be present [14, 34] as shown in Table 3.2. These regimes are categorized based on the circumferential rotational Reynolds number

$$\mathrm{Re}_r = \frac{R_o \Omega s_r}{\nu} = \frac{\rho_g R_o \Omega s_r}{\eta}. \tag{3.10}$$

The power required to overcome bearing friction was estimated based on *The SKF model for calculating frictional moment* [191]. This model estimates the bearing frictional moment as

$$P_b = (M_{\mathrm{rr}} + M_{\mathrm{sl}} + M_{\mathrm{seal}} + M_{\mathrm{drag}})\Omega \tag{3.11}$$

where M_{rr} and M_{sl} are rolling and sliding frictional moments, and M_{seal} and M_{drag} are frictional moments caused by the bearing seals and drag due to external lubrication respectively. Given that the formulas used in this model are rather large and complex, we refer the reader to the complete model in [191] for a more detailed description.

Given size constraints in the flywheel's hub, a 120 W Maxon EC 4-pole 22 brushless

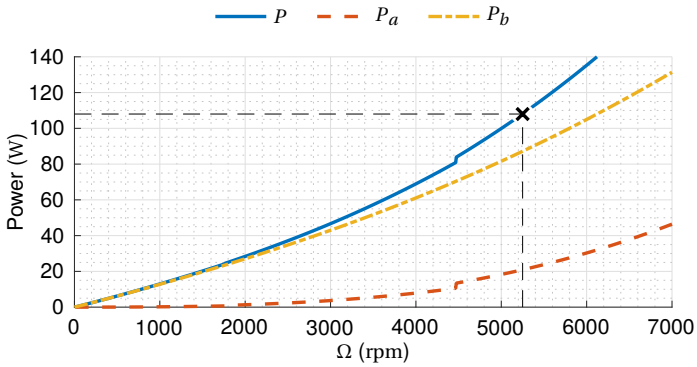

Figure 3.4: Flywheel mechanical power as function of flywheel speed. Here the contributions of both aerodynamic drag and bearing friction are depicted (dashed and dot-dashed lines respectively).

motor and high-precision hybrid angular contact ball bearings (GMN HY KH 61910 TA P4 L 252) were selected as flywheel actuator and suspension respectively. A mechanical power of 108 W was estimated taking into account the losses due to the motor efficiency η_{FM} =90 %. Bearing friction in Eq. (3.11) was estimated using the grease viscosity range reported by the manufacturer (26 mm^2/s @ 40 °C and 6 mm^2/s @ 100 °C for Turmogrease HS L252). Due to the complexity of the expressions to calculate both aerodynamic and bearing friction from Eqs. (3.6) and (3.11), a script was created to estimate the maximum flywheel speed Ω based on total power $P = P_a + P_b$. Figure 3.4 shows the power P required to overcome both aerodynamic drag and bearing friction against flywheel speed Ω, where a maximum flywheel speed of 5250 rpm was estimated for the selected flywheel motor and bearings.

3.3.3 | Flywheel Stress Analysis

To evaluate the mechanical strength of the flywheel under nominal operation, the maximum flywheel angular rate Ω =5250 rpm in addition to the maximum designed gyroscopic moment of 90 Nm were used. Due to the complexity of the flywheel geometry Finite Element Method (FEM) analysis was performed using ANSYS Workbench and its static structural module. As the CMG is not used in reaction wheel mode (i.e the flywheel angular rate remains constant in nominal operation), the imposed condition over the model is constant rotational speed. To validate the FEM results, a simplified model keeping the same overall dimensions but using only centrifugal loads was simulated and compared with analytical results. FEM analysis of the simplified model showed good agreement with the analytic radial and tangential stresses with Root Mean Square Error (RMSE) values of $\sigma_{r,\text{RMSE}}$ =0.07 MPa and $\sigma_{\theta,\text{RMSE}}$ =0.13 MPa.

Using the same simulation parameters and boundary conditions and including the load due to the gyroscopic moment, the flywheel geometry as shown in Fig. 3.3 was used to perform the FEM analysis. Figure 3.5 shows the equivalent (von Mises) stress, where the maximum of 50 MPa is much lower than the yield strength of the flywheel material

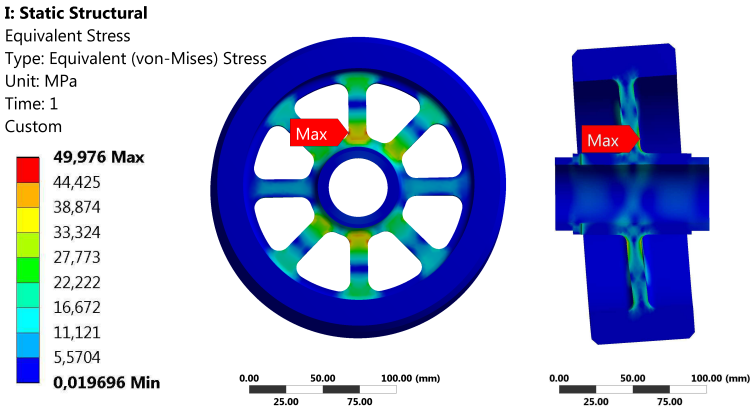

Figure 3.5: FEM equivalent (von Mises) stress for the designed flywheel geometry.

(Aluminum 7075 - T6, $S_y = 503$ MPa), giving a safety factor of 10 against the combined centrifugal and gyroscopic loads.

In addition to the stress analysis, it is necessary to assess the critical speed, since the flywheel can experience several types of vibrations being shaft whirl, lateral and torsional vibrations the most important [139]. This critical speed must be avoided, since the resulting deflections might cause stresses beyond the strength of the material. The ANSYS Workbench modal analysis module was used to perform the critical speed analysis given the complexity of the flywheel geometry. Shaft whirl and lateral vibration effects were neglected as the flywheel was thoroughly balanced after manufacturing and the deflection of the shaft is very small at the flywheel location during bending due to the gyroscopic moment. Thus, Torsional vibrations were analyzed using the same parameters and boundary conditions as the static structural analysis, where the modal analysis results showed a minimum critical speed of 200 778 rpm, giving a margin of 38 when compared with the intended rotational speed ($\Omega = 5250$ rpm).

3.3.4 | Gimbal Structure Design

The gimbal structure consists of a 6 mm thick Al7075-T6 high-strength aluminum case which encloses the whole flywheel. In addition, extra 3 mm thick Al7075-T6 high-strength aluminum plates were placed to reinforce the structure and prevent access to the flywheel from the exterior as shown in Fig. 3.6. The flywheel is supported by a pair of hybrid bearings ensuring low rolling friction and better performance at high speeds than those of conventional materials, allowing higher top speeds and lower power consumption. These bearings are responsible for transfering the gyroscopic moment to the gimbal structure, thus they have to withstand the dynamic loading of the gyroscopic moment. The bearings are symetrically mounted in the flywheel with a distance $d = 92.5$ mm separating them (See Fig. 3.3). Based on the desired gyroscopic moment of 90 N m and the distance between bearings d, the loading in each bearing is thus 973 N. Hybrid bearings were selected with a minimum safety factor of 4, leading to a load rating higher

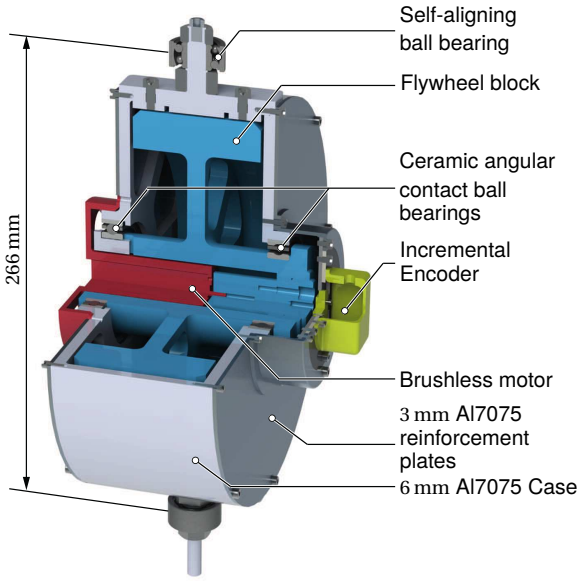

Figure 3.6: A section view of the flywheel prototype. The flywheel block (in blue), includes the rotational parts such as the flywheel itself, coupling to the motor and the housing for the magnet of the absolute-encoder. The motor block (in red) includes the brushless motor and its housing. The gimbal structure (in light gray), includes the Al-7075-T6 case and reinforcement plates. Self-aligning bearings are placed in each end of the gimbal axis (top and bottom).

than 3892 N. The selected bearings (GMN HY-KH 61910) are able to withstand 3900 N of dynamic loading, complying with the designed safety factor against failure for dynamic loading due to the transfer of the gyroscopic moment to the gimbal structure.

The gimbal structure is at the same time supported by a pair of self-aligning bearings (SKF-2200), which are responsible for the transfer of the gyroscopic moment from the gimbal structure to the environment. The self-aligning bearings are mounted apart along the gimbal axis, symetrically at 133 mm from the flywheel spinning axis (i.e. 266 mm from each other) as shown in Fig. 3.6. The dynamic loading withstood by each bearing is hence 349.62 N. Dynamic loading rate for each bearing is reported to be 5530 N, giving a safety factor of 15.8 against dynamic loading produced by the gyroscopic moment.

3.3.5 | Gimbal Actuation and Sensing

To select the gimbal motor, the angular gimbal speed $\dot{\gamma}$ profile can be calculated from Eq. (3.3), given a desired moment profile in the transverse axis. It is important to note that the gimbal motor has to counteract the effect of gyroscopic moments induced by body movements (i.e. *parasitic moments*). To account for this effect the desired gimbal angular acceleration can be computed taking the time derivative of Eq. (3.5) as follows

$$\ddot{\gamma} = \frac{\tau_{\text{IP}} \sin(\gamma)\dot{\gamma}}{I_{Ws}\Omega\cos^2(\gamma)} = \frac{\tau_{\text{IP}}^2 \sin(\gamma)}{I_{Ws}^2\Omega^2\cos^3(\gamma)} \tag{3.12}$$

Body Angular Velocity $\dot{\phi}$ in rad/s	Max Gimbal Mechanical Power P_{GM} in W
0.3	27.68
0.6	55.35
0.9	83.03
1.2	110.7

[1] Calculated to produce a fixed gyroscopic torque of 90 N m in the transverse axis $\hat{\boldsymbol{b}}_v$. Body motion was chosen so it emulates a fall while walking in anterior direction where the maximum body angular velocity corresponds to a fall at normal walking speed.

Table 3.3: Body motion influence ($\dot{\phi}$) in gimbal power (P_{GM}) [1]

combining Eq. (3.12) with Eqs. (3.4) and (3.5), the gimbal motor torque and power can be expressed respectively as,

$$\tau_{\mathrm{GM}} = I_g \frac{\tau_{\mathrm{IP}}^2 \sin(\gamma)}{I_{Ws}^2 \Omega^2 \cos^3(\gamma)} - I_{Ws}\Omega\cos(\gamma)\dot{\phi}, \tag{3.13}$$

$$P_{\mathrm{GM}} = \frac{I_g \tau_{\mathrm{IP}}^2 \sin(\gamma)\dot{\gamma}}{I_{Ws}^2 \Omega^2 \cos^3(\gamma)} - \tau_{\mathrm{IP}}\dot{\phi} \tag{3.14}$$

The second term in Eqs. (3.13) and (3.14) shows the influence of the body motion $\dot{\phi}$ on the gimbal torque and power. This is shown in Table 3.3, where the influence of the body motion considerably affects the required power of the gimbal motor. Based on the required power to exert the desired gyroscopic moment of 90 N m when falling during walking, as shown in Table 3.3, the combination Maxon RE 40 150 W DC motor with a 126:1 planetary gearhead (Maxon GP 52 C) was chosen accounting for a combined mechanical and electrical efficiency of η_{GM} =73.6 % providing a maximum mechanical power of 110.4 W. Both gimbal and flywheel motors are driven each by a Maxon ESCON 50/5 PWM servo controller set in current mode. Renishaw RMB20 enconder modules were placed in the gimbal axis (13-bit absolute RMB20SC) and flywheel axis (9-bit incremental RMB20IC).

3.4 | Evaluation

3.4.1 | Experimental Setup

To evaluate the capabilities of the CMG, an experimental platform consisting of a single-degree-of-freedom inverted pendulum was built, which might emulate a rigid human falling in the sagittal (anterior-posterior) or coronal (medio-lateral) planes. The structure consists of a 1 m long aluminum-profile attached to a hinge joint, in which the CMG and electronics (motor drives and micro-processing unit) are mounted as shown in Fig. 3.7a. In addition to the main aluminum profile, two safety end-stops are coupled to it in order to constrain the tilting angle of the pendulum. Absolute encoders are placed in the pendulum hinge joint and gimbal axis. The CGM was mounted at the top

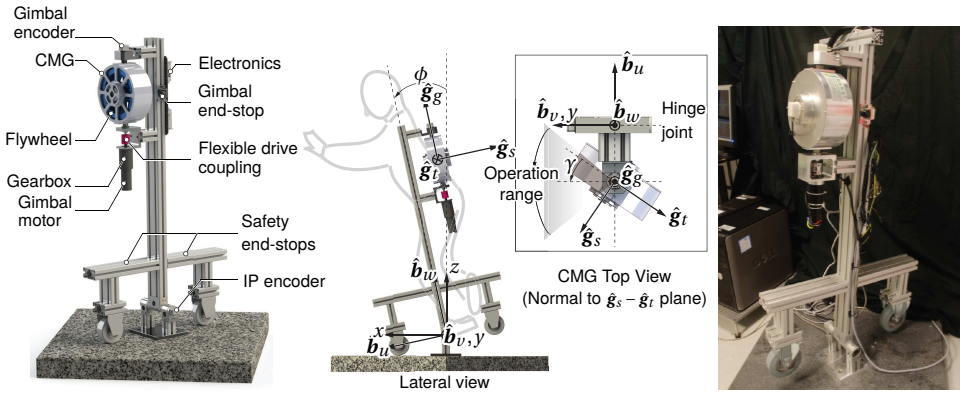

(a) (b) (c)

Figure 3.7: Experimental setup description. (a)) Hardware description. (b)) Lateral and top views of the experimental setup and CMG unit attached to the inverted pendulum (IP), respectively. Note that frames $\{\hat{\boldsymbol{b}}_u, \hat{\boldsymbol{b}}_v, \hat{\boldsymbol{b}}_w\}$ and $\{\hat{\boldsymbol{g}}_s, \hat{\boldsymbol{g}}_t, \hat{\boldsymbol{g}}_g\}$ fulfill the condition $\hat{\boldsymbol{b}}_w \parallel \hat{\boldsymbol{g}}_g$ and $\hat{\boldsymbol{b}}_v \parallel y$. Due to the gyroscopic effect, positive angular rates about the CMG's $\hat{\boldsymbol{g}}_g$ axis (within the operation range) will produce moments on the IP with a positive component τ_{IP} about the $\hat{\boldsymbol{b}}_v$ axis while the flywheel spins in the positive $\hat{\boldsymbol{g}}_s$ direction. (c)) Experimental Setup

of the pendulum as shown in Fig. 3.7b. Note that moments about the $\hat{\boldsymbol{b}}_u$ and $\hat{\boldsymbol{b}}_w$ axis are supported by the hinge joint. These moments were quantified from Eqs. (3.2) and (3.13) giving a maximum of 15.5 N m about the $\hat{\boldsymbol{b}}_w$ axis due to the gimbal motor actuation and 45 N m in $\hat{\boldsymbol{b}}_u$ direction due to the projection of the gyroscopic torque within a gimbal range of operation of $-45° < \gamma < 45°$ to avoid singular configurations. Thus, the combined reaction moment supported by the hinge joint is 47.43 N m which is less of 50% its load capacity of 100 N m against bending moments.

A pair of ESCON 50/5 servo-controllers were used to drive the gimbal and flywheel motors. These servo-controllers are set in current-control mode and receive a reference signal as PWM. A custom-made board (3Mxl) was used to command the PWM reference signals to the servo controllers and read the signal from the encoders. Matlab xPC Target was used as prototyping platform where the target PC is connected to the 3Mxl via RS485 (Quatech Serial Universal PCI Board) as shown in Fig. 3.8. High and low-level controllers were implemented in Matlab Simulink running at a sampling rate of 1000 Hz.

3.4.2 | Control

Figure 3.9 shows the general control scheme of the setup. The high-level controller is responsible for keeping the inverted pendulum balanced. As a proof of concept, a spring-like behavior, similar to the ankle strategy while maintaining balance in quiet stance, was implemented. Thus, the desired gyroscopic moment about the transverse axis is given by $\tau_{\text{IP,ref}} = -k_{\text{IP}}\phi$, where k_{IP} is the desired emulated stiffness.

Once the desired gyroscopic moment is set by the high-level controller, the desired instantaneous gimbal rate $\dot{\gamma}_{\text{ref}}$ is computed from Eq. (3.5). The low-level controller is then responsible for tracking this gimbal rate so the desired gyroscopic moment is gen-

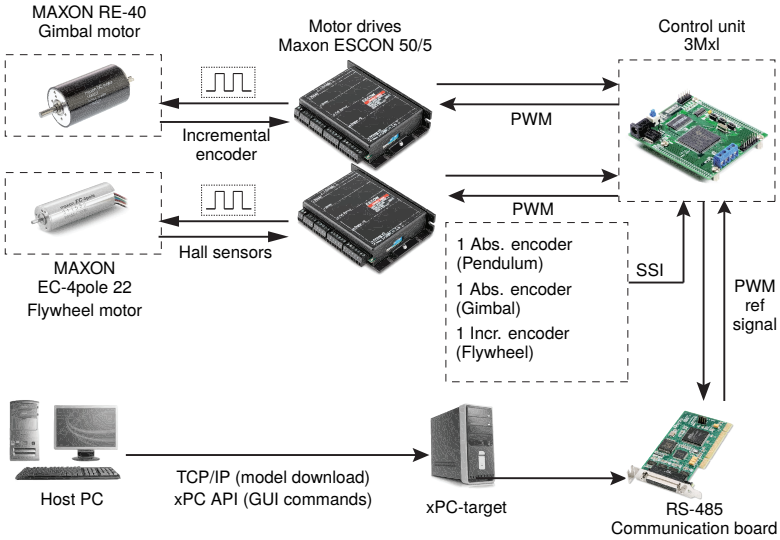

Figure 3.8: Communication flow chart of the experimental setup

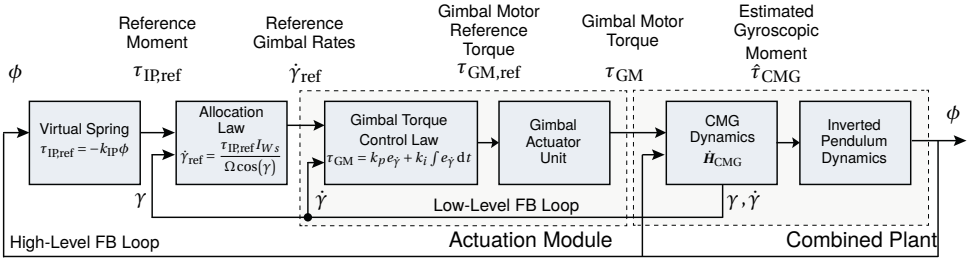

Figure 3.9: Control scheme used in the experimental setup to emulate the spring-like behavior.

erated. A PI controller was implemented to track the commanded gimbal speed. The low level control law is then expressed as $\tau_{\mathrm{GM,ref}} = k_p e_{\dot{\gamma}} + k_i \int e_{\dot{\gamma}}\,\mathrm{d}t$, where $e_{\dot{\gamma}} = \dot{\gamma}_{\mathrm{ref}} - \dot{\gamma}$ is the error between the desired reference gimbal rate $\dot{\gamma}_{\mathrm{ref}}$ minus the actual gimbal rate $\dot{\gamma}$.

To avoid singular configurations, the CMG initial position is set as $\gamma = 0$ (i.e. $\hat{\boldsymbol{g}}_t \parallel \hat{\boldsymbol{b}}_v$), constraining the gimbal to an operation range of $-45° < \gamma < 45°$ as shown in Fig. 3.7b. Once the gimbal has reached the limit of the range, gimbal actuation is overridden and the gimbal stops, acting as a saturation in the gimbal angle γ. Only actuation leading to movement in the direction of the operation range is allowed from the saturated position.

Tests were performed with the inverted pendulum oriented at an inclination angle of $\phi = 0°$ and with different virtual stifnesses implemented (, 600, 800, 1000 and 1200N rad^{-1}). Once the CMG low level controller was enabled, the inverted pendulum was manually perturbed.

3.4.3 | Data Analysis

As outcome measures to quantify performance of the device, we used the achieved maximum speed of the flywheel and the tracking performance of the balancing controller. In addition to the root mean square error (RMSE) of the gyroscopic moment compared to the reference, we estimated the maximum achieved gyroscopic moment in the experiment via $\hat{\tau}_{\mathrm{CMG}} = I_{Ws}\Omega\dot{\gamma}$ from measured flywheel angular speed Ω, gimbal angular position γ and speed $\dot{\gamma}$.

3.5 | Results

A maximum speed of 5400 rpm at 118.56 W was reached in the flywheel. Figure 3.10 shows the tracking results for different virtual stiffnesses, from 600 to 1200 $\mathrm{N\,m\,rad^{-1}}$ which were emulated accurately with a maximum Root-Mean-Squared Error (RMSE) of 0.55 N m. Furthermore, gyroscopic moments up to 70 N m were reached in the $\hat{\boldsymbol{b}}_v$ axis.

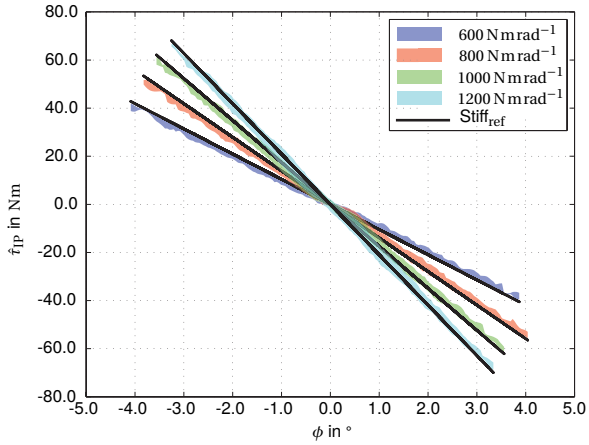

Figure 3.10: Reference (solid line) vs tracked stiffness (colored regions). The estimated transverse moment was computed as $\hat{\tau}_{\mathrm{IP}} = \hat{\tau}_{\mathrm{CMG}}\cos(\gamma)$.

3.6 | Discussion

The implemented controller successfully tracked the reference virtual stiffnesses, while keeping the inverted pendulum within its equilibrium position $\phi = 0$. Even though no damping was emulated in the controller, dry friction was present due to the inherent mechanical construction of the pendulum hinge joint. This resulted in a dead band behavior in the vicinity of the equilibrium point where the pendulum angular velocity was very low. This effect can be seen in Fig. 3.10 where the colored regions showing the tracked stiffness seem to have a slight offset compared to the reference stiffness represented by the solid line. Note that the offset slightly changes as the stiffness tracking passes the equilibrium position showing the effect of the dead band caused by the dry friction in

the hinge joint.

Despite the rather heavy weight of our device, it showed a substantially better gyroscopic torque-to-weight ratio against the only other comparable device reported in literature (7 N m/kg vs. 3.4 N m/kg by Chiu and Goswami [35]), although the target gyroscopic moment of 90 N m was not reached in this specific experiment. To improve the generated gyroscopic moment, we presume that implementation of a partial vacuum flywheel chamber could considerably diminish the effect of the aerodynamic drag as lower air density can be achieved, decreasing even more power consumption and weight, and increasing top speed, thus producing higher angular momentum. Further improvements in weight reduction can be made using different material and geometry selection for the flywheel, where higher moment of inertia can be achieved with a smaller wheel size using materials with higher density (e.g steel, iron, tungsten, etc). This could have a direct impact on the size and weight of the gimbal structure as well as on aerodynamic drag in the flywheel given that it increases rapidly with the peripheral speed. This reduction in aerodynamic drag implies at the same time a reduction in the power requirement for the flywheel motor.

Experimental results showed that our estimations were rather conservative. Measured maximum flywheel speed was higher (Ω =5400 rpm), although in the same oder of magnitude than the estimated maximum speed ($\hat{\Omega}$ = 5250 rpm). This can be explained from (i) the effect of the bearings running-in period and increase of running temperature [191] and (ii) due to assumptions in flywheel geometry and air properties in the aerodynamic drag estimation. First, frictional moment in the bearings could be either similar or lower than the estimated values. Once grease evenly distributes inside the bearing, lubricant temperature can rise over our assumed temperature lowering its viscosity and thus reducing lubricant friction. Second, aerodynamic drag is affected by changes in the air properties. Air density and viscosity were calculated assuming constant temperatures and pressure which can also vary in the closed flywheel chamber.

Although, special care must be taken in the aerodynamic analysis if a more complex flywheel geometry is used, such as variable thickness flywheels with spokes or conical constructions, the estimations presented here could be used as reference for flywheel actuator selection during early design stages. It is recommended that these estimations are validated using CFD or experimentally.

As our prototype was conceived as wearable device, safety requirements were set to comply with directives for medical devices. Thus, pilot tests could be conducted to assess how humans react to transmitted moments in the upper body.

Finally, the setup used to evaluate the capabilities of the CMG as balance assistance device is rather simplistic, as it is based on a overly simple human model. Future research should involve tests with more realistic experimental platforms, for example emulating falls in all directions using a set of 2 or more CMGs in a 2 DoF inverted pendulum.

3.7 | Conclusions

By including the bearing friction and aerodynamic behavior of the spinning wheel and the induced dynamics of the wearer, we demonstrated that, with the proposed design methodology, a CMG-based human balance assistance device can be built to comply

with the designed specifications given a proper selection of the actuators. We showed that our device is capable of producing up to 70 Nm with a total weight of approximately 10 kg.

Acknowledgments

This research was supported by the U.S. Department of Education, National Institute on Disability and Rehabilitation Research, NIDRR-RERC, Grant Number H133E120010, the Marie-Curie career integration grant PCIG13-GA-2013-618899 and the Innovational Research Incentives Scheme Vidi with project number 14865, which is (partly) financed by the Netherlands Organisation for Scientific Research (NWO). The authors would also like to thank Ines Santos for her contribution in the conceptual design of the experimental setup and Guus Liqui Lung, Andries Oort, Nisse Linskens and Simon Toet for technical support.

4

Control

The content of this chapter have been sligthly modified from the paper:
D. Lemus & A. Berry, S. Jabeen, C. Jayaraman, K. Hohl, F. C. T. van der Helm, A. Jayaraman and H. Vallery, *Gyroscopic Actuators on the Upper Body Effectively Assist Human Balance*, Submitted to Nature Scientific Reports.

Gyroscopic actuation is appealing for wearable applications due to its ability to impart free moments on a body without exoskeletal structures on the joints. Even though similar solutions have been previously reported, none have been evaluated with humans. Here we show for the first time that wearable gyroscopic actuation is feasible for augmenting the balance function of healthy adults and individuals with chronic stroke, as demonstrated with our portable device, the GyBAR. Our results show that, for two challenging reduced-base-of-support balancing tasks, simple controllers using only trunk state feedback enabled both groups to improve task performance by, on average, a factor of two to three when compared to the case in which the GyBAR was worn but was inactive. Due to its wearability and versatility of control, the GyBAR could enable new therapy interventions for training and rehabilitation.

4.1 | Introduction

Falling is among the most frequent causes of hospitalization and death among the elderly [183]. More than 1 out of 3 adults over the age of 70 fall in a 12-month period [76]. Compared to their healthy counterparts, individuals post stroke have an even sevenfold higher risk of falling [188, 214].

While it is known that impaired balance is a key risk factor for falls [59], balance training programs for survivors of stroke have not yet been proven an effective means to actually reduce fall risk [209]. This may be due to the fact that there are many possible contributing factors to falls, including sensory deficits such as loss of proprioception, motor deficits such as paresis, or visuo-perceptual and cognitive deficits such as hemineglect.

When provided with *external* forces from overhead support [131], many otherwise non-ambulatory individuals can walk. This often even occurs with very low amounts of assistance, effectively aiding balance and instilling confidence. However, existing devices that could provide such support in a controlled way are bound to treadmills [58, 229, 230], mounted to the ceiling [80, 158, 205], or require large wheeled frames around the user, like the Andago (Hocoma AG, CH) or the original KineAssist [152]. This restricts their use to training inside rehabilitation facilities.

Conventional wearable robotic devices like exoskeletons (e.g. Ekso, ReWalk, HAL, or X1) or exosuits [8], which are are based on the principle of spanning human joints to provide them with actuation, generate only *internal* moments. Such internal moments have no direct net effect on the body's angular momentum, a key measure of bipedal balance [70]. Instead, they can only influence balance indirectly, for example by effecting changes in foot-ground interaction forces, or by stepping. This severely restricts possibilities for exoskeletal systems to target balance, compared to overhead systems. In fact, for all existing exoskeletons, users still need crutches to maintain their balance.

A new type of actuation principle may enable both effective and wearable balance assistance: gyroscopic actuators. Earlier, we suggested that such actuators can be integrated in a backpack, providing *external* balance-assisting torques on a person's body in a finely controlled way, while not even being noticeable as an aid [116]. Such a system

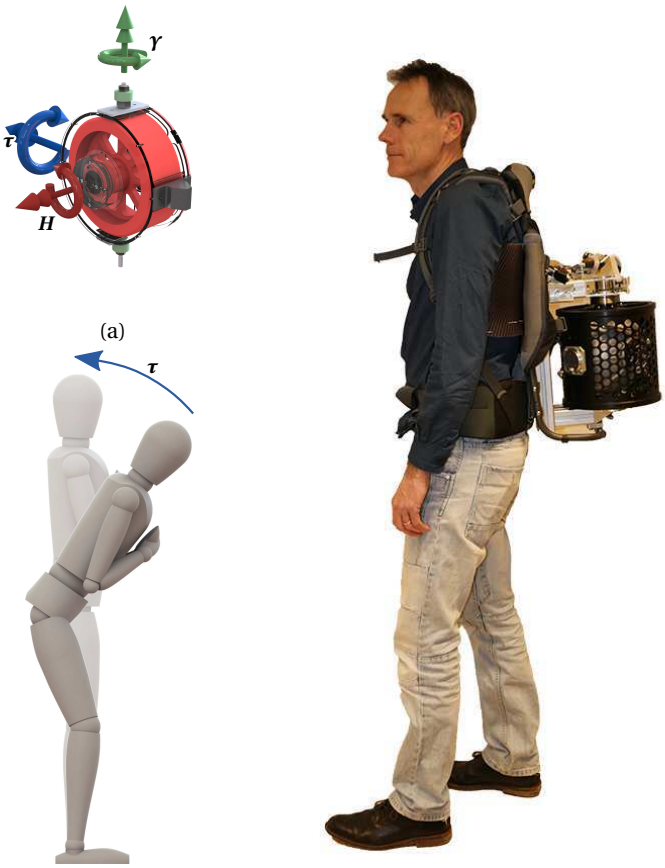

Figure 4.1: GyBAR prototype wearable gyroscopic actuator. (a): Assistive torque, τ, is proportional to the angular momentum, H, of a spinning mass and the rate at which it is gimballed, $\dot{\gamma}$, in a motorized frame. (b): Example use of a torque to restore upright posture. (c): Subject wearing the new version of the GyBAR.

could ultimately provide a compact wearable device that has the potential to translate to real life, unlike the systems above. So far, only technical designs of wearable gyroscopic actuators have been reported [35, 114].

This primary investigation inquires into the effect of gyroscopic assistance on standing and walking in a sample of able-bodied individuals and individuals with chronic stroke. Subjects performed these balance activities with and without the prototype wearable gyroscopic actuator called *the GyBAR* [114], which imparted the gyroscopic assistance (Fig. 4.1).

We implemented several simple controllers, specifically including a virtual rotary spring and a virtual rotary damper, which have an effect as if the person were connected in a compliant manner to a fixed frame in the sky or slowed by a viscous fluid, such

as when moving in a swimming pool. This virtual connection to an inertial frame, resembling overhead support systems, is only possible in this wearable system because it imparts free moments.

Outcome metrics used in clinical rehabilitation to assess balance were used to obtain clinically meaningful measures of performance of the GyBAR for balance assistance. These metrics included (i) distance walked on a narrow beam, (ii) time stood on a narrow support surface, both done with and without the GyBAR assistance. Further insights were derived from secondary measures, quantifying aspects such as the magnitude and frequency of angular motion of the trunk or the torque exerted by the actuator.

We hypothesized that such continuous gyroscopic postural assistance applied to the upper body would enable subjects to balance better than when unassisted. This derives from the assumptions that standing and walking dynamics can be approximated by inverted pendulum models [222], and that a free torque either opposing gravity-induced rotation about the ankle or dissipating kinetic energy will complement the wearer's own postural control strategy. To investigate this, we conducted a first experiment with healthy subjects in order to identify the most promising candidate controller; this was found to be the virtual rotary damper, which, despite not explicitly enforcing an upright posture as did the other controllers, yielded the greatest increase in task performance and was perceived most positively. In a subsequent investigation of this controller, we demonstrate that similar improvements to balance function are achievable for individuals with chronic stroke, among the intended beneficiaries of this technology.

4.2 | Methods

4.2.1 | GyBAR as a wearable balance aid

The GyBAR is a type of momentum exchange device that exploits conservation of angular momentum. This technology has been primarily used in attitude control of spacecrafts due to its ability to exert a reactionless torque (i.e. torque transmission that does not require an inertial frame) and torque amplification, with a relative compact and light unit. This technology is thus appealing for balance assistance. Generally, it comprises a fast-spinning rotor fixed to a motorized gimbal structure. The reactionless torque is thus generated by changes in angular momentum of its spinning rotor (Fig. 4.1a) through controlled movements of the gimbaled structure. In principle, the reactionless torque, τ, is linearly proportional to the angular momentum of the rotor, H, and the angular velocity of the actuated gimbal frame that couples the rotor to the wearer, $\dot{\gamma}$, but scales nonlinearly with the angle of the gimbal, γ creating additional off-axis components (Supplementary Section 4.A.1).

To limit off-axis components of the generated torque, a constraint was imposed on the range of motion of the GyBAR prototype used in this study (Supplementary Fig. 4.A2a). The gyroscopic torque was thus projected in approximately the intended direction during nominal operation. However, when these limits were approached, the gimbal was arrested and the generated torque ceased, at which point the actuator was said to be *geometrically saturated* (See Supplementary Section 4.A.2). For further reference, the GyBAR prototype used in this study is documented in greater detail by Lemus *et al.* [114].

4.2.2 | Balance-assisting controllers

Based on the assumption that people implicitly build internal models of the world with which they interact (e.g. prior experiences affect the selection of postural control strategies in response to external influences that both aid and perturb balance [86, 227] and humans are able to deduce complex quantities from ambiguous sensory input [128]), simple continuous controllers were designed such that interaction with the GyBAR prototype would be intuitive and the exerted torques would be quickly integrated with the user's own balancing function with little familiarization time. Given findings that proportional or proportional-derivative controllers can be used to model human postural control [97, 129, 155, 221] and that such controllers have been successful with other gait training interfaces [227], controllers with linear proportional and derivative terms were considered for the GyBAR.

Although relatively sophisticated estimation of the state of balance can be performed using minimal instrumentation [145], the current study used only angular orientation and velocity of the trunk for feedback, estimated from an inertial measurement unit (IMU) located at shoulder height in the GyBAR [138]. The selected proportional, derivative, and proportional-derivative controllers were thus equivalent to a virtual rotational spring (S), damper (D), and parallel spring-damper (S-D) acting on the trunk: the rotational spring elements exert a torque on the trunk that guides the wearer to a nominal erect posture (calibrated at the start of each test), whereas the rotational damper element does not enforce a specific posture, but rather exerts a torque proportional to the angular velocity of the trunk and opposes rotational motion, somewhat analogous to balancing in a viscous medium such as water or honey. Controller gains (Supplementary Table 4.AII) were selected through experimentation with a healthy volunteer such that the gains were a maximum yet did not lead to geometric saturation of the actuators during balance activities representative of the experimental protocol; note that these gains were consistent throughout both experiments and not adapted per subject or task.

We initially expected that the rotational spring (S) controller would be most effective due to its ability to guide to a reference posture and limit the deviation of the centre of mass from a nominal position above the base of support.

4.2.3 | Subjects

For Experiment 1, 10 healthy subjects (7 males, 3 females) aged 26 to 60 years (mean age 35) volunteered to participate (Supplementary Table 4.AI). All participants were free from neurological, orthopedic, vestibular, and visual impairment and had no recent history of skeletal or muscular injury. Ethical approval was received from the Human Research Ethics Committee, TU Delft (HREC Letter of approval 236, August, 2017).

For Experiment 2, 5 healthy controls, aged 26 to 32 years (mean age 29), and 5 individuals with chronic stroke, aged 35 to 62 years (mean age 52), were recruited (Supplementary Table 4.AI). Ethical approval was received from the Institutional Review Board Office Northwestern University (IRB NU, Study STU00205256, October, 2017).

Both experiments were conducted in accordance with the recommendations of the respective review boards. Informed signed consent was obtained from all participants.

4.2.4 | Experimental Protocol

With a single gyroscopic actuator, as in the GyBAR, it is possible to assist balance in only a single axis at a time. Consequently, the protocol consisted of tasks intended to challenge AP and ML balancing independently. These tasks induced postural instability by reducing the BoS, a strategy used in a number of validated clinical tests and studies [86, 177]; an advantage of this is that it naturally suggests an unambiguous and quantifiable functional outcome measure (distance travelled or duration remained within the BoS). Reducing the BoS has the effect of constraining the efficacy or availability of primary balancing strategies, such as stepping responses or the exertion of ankle torques, and therefore emphasizes other, secondary strategies, such as those involving motion of the trunk or upper limbs; this is not the intended focus of the study, but a consequence of such a method of challenging balance.

In Experiment 1, subjects were asked to walk, with feet in tandem (laterally aligned and with heel touching toes) and with their arms crossed, over a 3 cm wide by 4 m long wooden beam (see Fig. 4.2) both with and without the GyBAR. During the experiment, 7 different conditions (Supplementary Table 4.AII), including both assistive and non-assistive controllers, were tested 3 times each. To diminish learning effects, conditions in which the GyBAR was active were block-randomized.

In Experiment 2, subjects performed 3 sequences of tests featuring limited bases of support to challenge balance in either the anteroposterior (AP) or mediolateral (ML) directions during standing and walking (Supplementary Table 4.AV). During the experiment, conditions 'free' (FR), 'inactive' (IN), and the best-performing controller of Experiment 1 were tested. Although each sequence of tasks remained in the same order to preserve the gradient of difficulty, conditions IN and 'controller active' were block-randomized following assessment without the device. A safety system was used while using the GyBAR consisting on a spring-loaded overhead suspension system.

See Supplementary Section 4.A.2 for further detail.

4.2.5 | Data Acquisition

Traveled distance (walking tasks in Experiments 1 and 2) and standing duration (ML and AP standing tasks in Experiment 2) were recorded manually using floor markings and digital stopwatches. Absolute trunk angle and angular velocity were recorded using IMUs (MPU-6000 and MPU-9250, InvenSense Inc., San Jose, CA, USA, at 1000 Hz) contained within the GyBAR and located at shoulder height. In Experiment 2, the centre of pressure (CoP) of the ground reaction force was recorded during the standing tasks using a single force plate (Sensory Kinetics Standard, Engineering Acoustics, Inc., Casselberry, FL, USA, at 100 Hz).

4.2.6 | Balance performance metrics

Medians of 3 attempts of the distance travelled (walking tasks) and standing duration (standing tasks) for each condition were used as primary outcome measures. To account for variability across subjects, these were normalized per subject with respect to baseline condition IN, in which the GyBAR was worn but the controller turned off. Secondary

outcome measures included statistics computed from time series data such as root mean square (RMS) and peak values of the trunk pitch (θ) and roll (ϕ) angles measured with respect to an inertially-fixed vertical axis, trunk angular velocity ($\dot{\theta}$, $\dot{\phi}$), externally-applied torque (τ), and angular momentum exchanged with the GyBAR (ΔH, Supplementary Section 4.A.1). The relative perceived 'helpfulness' of each controller was recorded in Experiment 1 and ranked using the Analytic Hierarchy Process [40, 174]

4.2.7 | Statistical Analysis

Given the low sample size in both experiments (n=10 in Experiment 1 and n=5 in Experiment 2), a non-parametric test was preferred over a standard parametric one. Non-normality of the data was assessed using the signed rank Shapiro-Wilk test before the non-parametric Friedman matched samples test was performed. Subsequently a two-tailed Wilcoxon signed rank post-hoc test was performed to check for pairwise significance between tested conditions in both experiments, with a critical value of α=0.05.

In order to accommodate for multiple comparisons (i) a global statistical test across all conditions was performed before any pairwise comparison was applied [159, 181], (ii) a single primary outcome measure was analyzed in each experiment [181, 193], and (iii) statistical results from additional (secondary) outcome measures were reported and interpreted in the context of the core findings inferred from the primary one [154, 171, 172, 181, 193, 193].

4.3 | Results

To ultimately investigate the feasibility of using the GyBAR to enhance the capabilities of individuals with impaired balance, a multi-site investigation was performed, comprising two experiments. Experiment 1 was designed to elucidate two questions, namely (i) whether balance augmentation of healthy individuals with the GyBAR is feasible, and (ii) whether any of the proposed controllers are particularly (un)suitable for this aim; healthy subjects were requested to walk as far as possible along a narrow (3 cm) wooden beam with their arms crossed and feet in tandem (Fig. 4.2c), while perception, predictability and performance of multiple assistive ('spring-damper', 'damper' and 'spring') and non-assistive ('gimbal locked' and 'negative damper') balance controllers were evaluated. Experiment 1 led to identifying the most successful controller. This controller was used to perform Experiment 2, in a clinical setting, investigating whether the findings are transferable to (i) other fixed- and changing-base-of-support balancing tasks with various axes of instability, and (ii) subjects with balance impairments in the chronic phase of recovery from stroke. In Experiment 2, both healthy controls and individuals with chronic stroke performed tasks such as standing or walking with a reduced mediolateral (ML) base of support (BoS) and standing with a reduced anteroposterior (AP) BoS (Fig. 4.3c), challenging primarily ML and AP postural control respectively.

In the following subsections, the results of each experiment are reported. Symbols and descriptions of the tested conditions can be found in Supplementary Table 4.AII and details of the protocol can be found in Section 4.2 and Supplementary Section 4.A.2.

4.3.1 | Experiment 1: Effect of multiple assistive and perturbative controllers

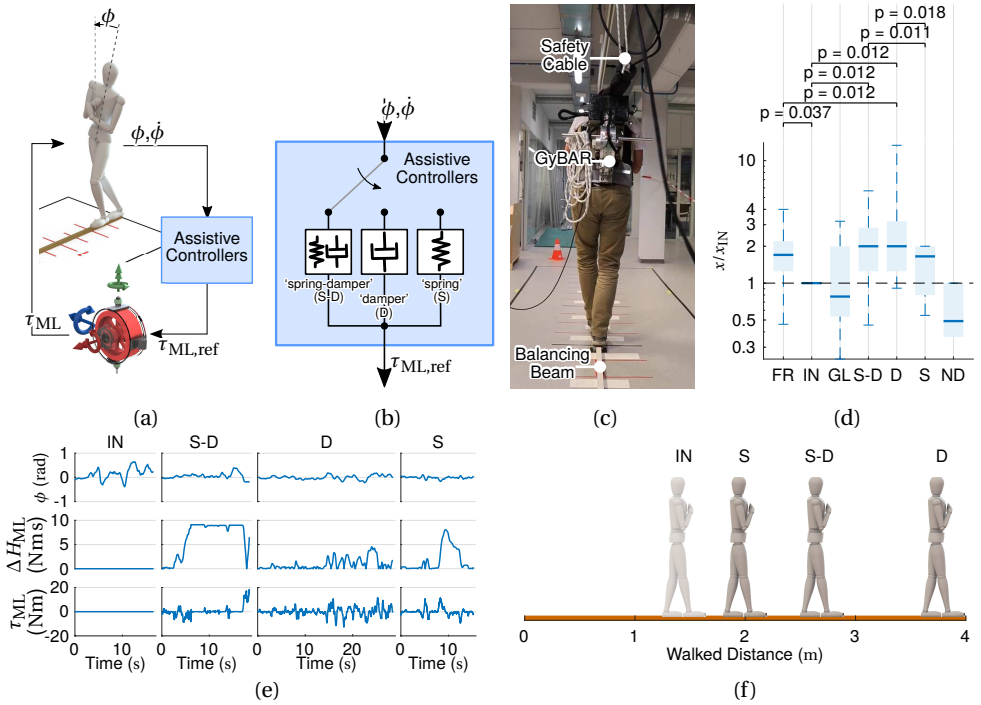

Figure 4.2: Description and main results of Experiment 1. (a) Schematic of balance control feedback loop. (b) Schematic of assistive controllers 'spring-damper' (S-D), 'damper' (D) and, 'spring' (S). (c) Subject wearing the GyBAR while traversing the beam of width 3 cm and length 4 m. (d) Distance walked under all testing conditions, normalized to condition 'inactive' (IN) and displayed in logarithmic scale. For clarity, pairwise significance brackets (p<0.05) are shown only for comparisons of controllers S-D, S, and D and conditions FR ('free', no device) and IN. Fig. 4.2e Example time series of trunk leaning angle ϕ, exchanged angular momentum ΔH, and exerted gyroscopic torque τ for baseline condition IN and assistive conditions S-D, D, and S for subject C13. (f) Example primary outcome measures (distance walked) for subject C13.

Primary outcome measures

All three assistive controllers, 'spring-damper' (S-D), 'damper' (D), and 'spring' (S), increased the median distance subjects (n=10) could walk along a 3-cm-wide (4-m-long) beam with respect to the baseline condition 'inactive' (IN, device worn but powered off), by factors of 2.0, 2.0, and 1.6, respectively (Fig. 4.2d and Supplementary Table 4.AIII). In addition, controllers S-D and D enabled one and three subjects, respectively, to reach the end of the beam.

Pairwise statistical significances (p<0.05) between assistive controllers S-D, D, and S and baseline conditions 'free' (FR, no device worn) and IN are shown in Fig. 4.2d (see Supplementary Fig. 4.A4 for all other pairs). Only controllers D (p=0.012) and S-D (p=0.012)

significantly enhanced task performance (distance walked) with respect to condition IN. Most notably, despite the detriment of bearing the 16 kg mass of the prototype GyBAR (evidenced by the significant difference, p=0.037, between FR and IN), controller D showed significant improvement against even FR (p=0.012).

Perturbations from self-induced gyroscopic torques during condition 'gimbal locked' (GL) did not alter performance with respect to IN (p=0.674), but intentional error augmentation with controller 'negative damper' (ND) did visibly hinder balance and significantly decrease the distance subjects walked (p=0.017).

The absence of learning effects, per design, was verified by performing conditions FR and IN at both the start and end of each (block-randomized) session. Indeed there was no improvement in IN, and the small improvement in the FR condition (Supplementary Table 4.AIV) was not statistically significant (p=0.123).

Secondary outcome measures

To aid interpretation of the differences in task performance, the controllers were also compared by their impact on the kinematics of the wearer, user perception, and actuator performance (Supplementary Table 4.AIII).

Absolute trunk roll angle ϕ_{RMS} and angular velocity $\dot{\phi}_{\mathrm{RMS}}$ were not significantly affected by any of the assistive controllers. However, a significant decrease in trunk sway centroidal frequency $\bar{f}(\phi)$ (Supplementary Fig. 4.A5a) was found for controller D (p=0.013).

After each trial, subjects rated the perceived 'helpfulness' of the random controller as either better or worse (binary) than the preceding trial; the Analytic Hierarchy Process [40, 174] was used to convert these pairwise comparisons into a ranking of controllers. Controller D was perceived as best, followed by S-D (Supplementary Table 4.AIII); notably, controller S was perceived as worse than condition GL, although this was contradicted by the task performance results (Fig. 4.2d).

Actuator performance was measured in terms of the magnitude of the torques exerted on the wearer τ, the amount of angular momentum exchanged between device and user ΔH (i.e. the time integral of τ), and the frequency at which the angular momentum limits ΔH_{max} were encountered (referred to as *geometric saturation*, Supplementary Fig. 4.A2). The generated torques τ were found to be well below the designed maximum (30-50 N m, depending on the gimbal range of motion) and similar for all controllers (Supplementary Fig. 4.A5b), but the angular momentum exchange was considerably less conservative (Supplementary Fig. 4.A5c). At least 60 % of subjects encountered geometric saturation while using posture-dependent controllers S and S-D, of whom more than 70 % immediately terminated the task as the assistive torque was interrupted (Supplementary Table 4.AIII); such saturations were observed to often follow low-frequent postural drift (e.g. prolonged leaning of the trunk), which resulted in sustained torques and a mostly monotonic exchange of angular momentum until ΔH_{max} was reached (Supplementary Fig. 4.A2b). In contrast, controller D is unaffected by postural orientation; only one subject encountered geometric saturation with controller D, and continued the task without direct failure.

Clinical observations

During walking and tandem stance with an unconstrained BoS, lateral balance is controlled primarily by lateral foot placement [119, 222] and torques generated by ankle eversion/inversion [220, 222], respectively. For the constrained lateral BoS in the beam-walking task, it was observed that (by design) these strategies were insufficient to maintain postural stability and hence were supplemented by the greater use of a secondary strategy: dynamic manipulation of the trunk by the hip abductors/adductors to exert horizontal shear forces at the foot [78, 86, 119]. In conditions IN and ND, in which no support and perturbations were applied, respectively, this secondary 'dynamic hip' strategy was particularly prominent. During baseline conditions FR and IN, 8 out of 10 participants actively abducted/adducted their swing leg to augment balance in an apparent extension of this strategy. Some subjects additionally rotated their trunk in the sagittal and longitudinal planes in complex and seemingly arbitrary patterns, which we do not interpret as useful. Remarkably, all such secondary strategies appeared to diminish considerably while using the assistive controllers S, D, and S-D.

To investigate differences in the responses of individuals to each controller, task performance in each condition was compared to subject-specific factors such as body mass, initial performance, and characteristics of balancing strategies. No clear relationship was found.

4.3.2 | Experiment 2: Effect of damper controller in multiple balancing tasks for healthy subjects and individuals with chronic stroke

Primary outcome measures

In the standing task with a reduced anteroposterior (AP) BoS, the size of the support surface was determined per person (Supplementary Section 4.A.2 and Supplementary Table 4.AV) and task performance was measured as the duration of fixed-stance standing on this surface. Baseline conditions 'free' (FR) and 'inactive' (IN) and controller 'damper' (D) were compared. In the latter two conditions, the safety system also provided some unloading (not used in Experiment 1), which was fixed to the GyBAR and reduced the borne weight from 16 kg to 7.5 kg.

The assistive controller (D) was found to significantly (p<0.05) improve task performance both for healthy individuals (n=5, p=0.043) and for individuals with chronic stroke (n=5, p=0.043) with respect to IN (Fig. 4.3d and Supplementary Table 4.AVI). In condition D, one individual with chronic stroke (S4 ▽) and two healthy subjects (H1 +, H4 ○) were even able to complete (i.e. achieve score ceiling) the same task that they had failed in conditions FR and IN; those who still could not, improved their primary outcome by a median[1] factor of 2.0 (stroke) and 3.1 (healthy). One individual with chronic stroke (S4 ▽) exhibited a substantially greater degree of improvement (23.3) than any other subject. In general, no participant exhibited a decrease in performance when the controller was turned on, although one individual subject (S3 △) was found to exhibit

[1] When an even number of samples exists, the mean of the two middle samples was used.

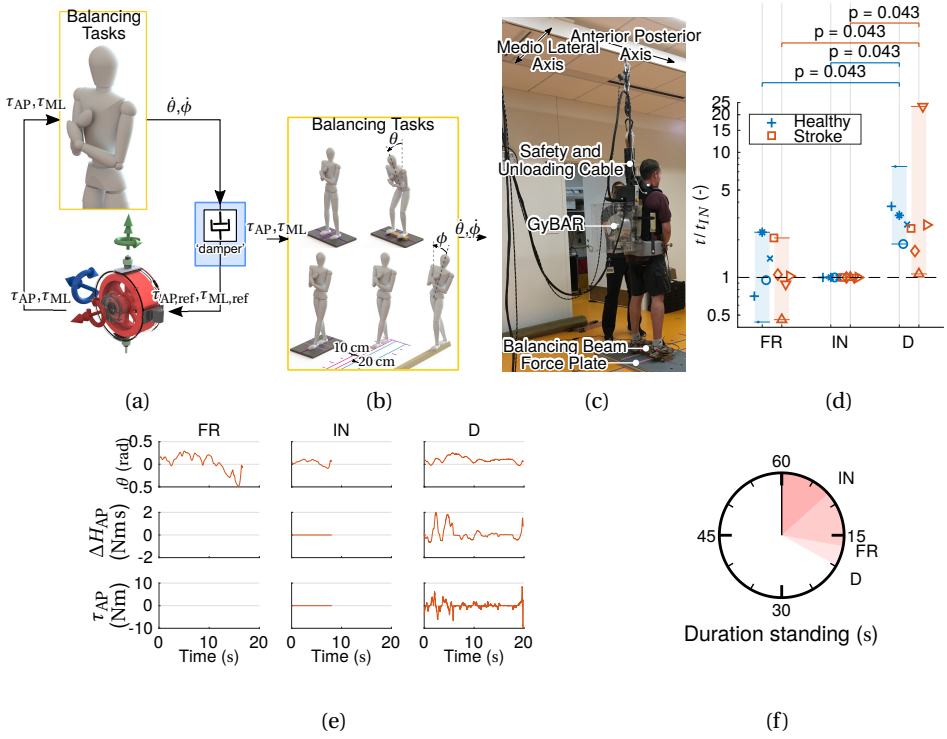

Figure 4.3: Description and main results of Experiment 2. (a) Illustration of 'damper' (D) balance controller. (b) Balancing tasks with reduced AP or ML bases of support. (c) Individual with chronic stroke wearing the GyBAR during anteroposterior (AP) balancing task over reduced BoS (10 cm). (d) Duration standing for both healthy controls and individuals with chronic stroke, normalized to condition 'inactive' (IN) and displayed in logarithmic scale; shown are condition 'free' (FR) and 'inactive' (IN) and assistive controller 'damper' (D). Subjects H1 (+), H4 (○), and S4 (▽) all reached the maximum score in condition D. (e) Example time series data of the leaning angle θ, exchanged angular momentum ΔH, and exerted gyroscopic torque τ for the individual with chronic stroke who exhibited the median degree of improvement with controller D, subject S1 (□).

only marginal improvement (1.1); this subject already had the best within-group performance at baseline (Supplementary Table 4.AV).

All subjects performed better in condition D than in IN. The degrees to which they did seemed influenced by the order in which the conditions were performed (Supplementary Table 4.AVII), likely due to the use of block-randomization to reduce testing time (Supplementary Section 4.A.2). Although the low sample size precludes statistical analysis, healthy subjects typically had greater relative task improvement of condition D when it was performed last, while individuals with chronic stroke exhibited the opposite trend, suggesting that these groups may have been susceptible to slight learning and fatigue effects, respectively.

The results of the mediolateral (ML) walking and standing tasks (Supplementary Fig. 4.A6) are not analyzed here due to (i) the prevalence of ceiling effects due to insufficient pos-

tural challenge for the participants and (ii) directional variability of the unloading force.

Secondary outcome measures

For the AP balancing task, the range and variability of the centre of pressure (CoP) excursion and its velocity were computed. Although these measures have been validated as sensitive to factors such as age and the presence/absence of visual feedback (e.g. [162]), no significant differences were found between conditions FR, IN, and D, nor were significant differences found when the same statistics were computed using the trunk pitch angle θ (relevant because $\dot{\theta}$ was used for controller feedback). Peak trunk angular excursion and angular velocity are shown in Supplementary Fig. 4.A7a. Nevertheless, the combination of small changes in both motion range and velocity resulted in a statistically significant decrease of the centroidal frequency of both CoP (p=0.043) and trunk pitch angle θ (p=0.043) amongst the individuals with chronic stroke when controller D was active (Supplementary Fig. 4.A7b), similar to findings in Experiment 1 for the trunk roll angle ϕ in frontal-plane balancing. This decrease brought the stroke group closer to the expected frequency of a healthy person in quiet, full-BoS stance (dashed line in Supplementary Fig. 4.A7b), and coincided with an increase in task performance.

Despite the different axis of instability and user groups than in Experiment 1, the gyroscopic actuator retained similar performance characteristics. The peak and RMS gyroscopic torques τ were not substantially different between members of the healthy and chronic stroke groups (Supplementary Fig. 4.A7c), and were again considerably lower than the designed maximum. Because of an additional mechanical constraint in the gimbal of the GyBAR when assisting balance in the AP direction (Supplementary Fig. 4.A2a), the angular momentum exchange limits became more stringent (dashed lines in Supplementary Fig. 4.A7c); three subjects (H2 •, H3 ✳, and S5 ▷) encountered geometric saturation, indicating that the device was unable to sustain the requested torque long enough. These three subjects saturated four times collectively, of which three immediately preceded task failure; despite this loss of assistance, these subjects were among those who exhibited the greatest improvement in task performance when the controller was active (Fig. 4.3d). The actuator capabilities were sufficient for the remaining majority of users.

Clinical observations

AP balancing during normal standing is maintained primarily by torques exerted by the ankle plantarflexors/dorsiflexors [135], but a secondary dynamic hip flexion/extension strategy similar in function to that described for lateral balancing is known to occur in the case that ankle torques are insufficient or their efficacy is inhibited by a small or soft support surface [86, 135]. With a reduced AP BoS, a mixture of primary and secondary balancing strategies was observed in both subject groups in this experiment. During condition IN, the healthy subjects exhibited persistent and high-frequent primary ankle plantarflexion/dorsiflexion and varying degrees of secondary hip motion; most performed the task with little or no motion of the upper body and with only minor motion of the knee joints, which are known to control primarily vertical displacement of the centre of mass (CoM) and are only rarely used in balance [135]. When the controller (D) was activated, little change in overall balancing modality was observed amongst this

group, but the frequency, and in some cases also the amplitude, of joint motions appeared to decrease. In comparison, during all conditions, the individuals with chronic stroke exhibited clear asymmetry in the joint motions of the lower extremities (postural corrections originated almost exclusively in the non-paretic side) and a compensatory shifting of activity upwards, resulting in an increase of secondary hip flexion/extension and arm motion; in addition, these secondary strategies appeared to be generally more exaggerated, less coordinated with other body segments, and less consistent within and between subjects than in the healthy group. When the controller (D) was activated, a general reduction of the frequency of all joint motions was visible amongst the individuals with stroke, with compensatory secondary activity of the knees and upper extremities most noticeably reduced; in addition, the balance corrections at all sites appeared to be generally less random and more coordinated.

Although the small sample size limits analysis, the balancing strategy of a user may determine the degree to which they benefit from the GyBAR or a particular controller. When the controller (D) was active, the smallest and largest improvements in task performance amongst the individuals with chronic stroke were by S3 (△) and S4 (▽), respectively; subject S3 exhibited particularly low-frequent postural adjustments and each test terminated when the centre of mass slowly drifted outside of the base of support, while subject S4, in contrast, was characterized as having excessive and high-frequent balance reactions.

4.4 | Discussion

The two experiments investigated the feasibility of using wearable gyroscopic actuators for balance augmentation, collectively examining balancing in both the frontal and sagittal planes and subject groups representing both healthy and chronic stroke demographics. This is discussed in the contexts of (i) differences in task performance and the consequences for controller and actuator design, (ii) the impact on postural control characteristics and relevance for clinical application, and (iii) technical guidelines for future actuator development.

4.4.1 | Task Performance

The GyBAR improves balance

When active, the GyBAR was demonstrated to significantly improve balance function in both healthy individuals and individuals with chronic stroke, with primary performance measures improving by median factors of 2-3 in tasks that challenged balance in both anteroposterior (AP) and mediolateral (ML) directions and in both standing and walking (Figs. 4.2d and 4.3d). In both experiments, the 'damper' (D) controller enabled subjects to complete tasks in which they were previously unsuccessful either with the controller inactive or without the burden of the weight of the GyBAR (Experiment 1).

The prescribed reduced-BoS tasks challenged balance in the AP direction during standing and in the ML direction during walking. During standing, the ground projection of the CoM is regulated within the BoS primarily by ankle and weight-shifting hip strategies [135, 220, 222], while balance during walking relies primarily on a syn-

ergy of the hip abductors/adductors and foot placement of the swing leg to keep the upper body stable [119, 222]. However, these balance strategies change when the BoS is reduced, in which an increased use of the dynamic hip strategy compensates for the reduced efficacy of the ankle plantarflexors/dorsiflexors and invertors/evertors during standing [86, 90, 135] and greater precision of the hip abductors/adductors compensates for the limited ability of foot placement to correct for lateral motion of the CoM during the single-support phase of tandem walking [222]. Similarly, individuals with stroke use the dynamic hip strategy to compensate for weakness and impaired muscle control of the affected lower limb [44].

Despite the fact that the GyBAR does not directly influence the motion of these joints (i.e. it is uncollocated and underactuated), it successfully complements existing balancing strategies to lead to an overall functional improvement. We presume that the effectiveness of the simple controllers investigated can be attributed in part due to the use of upper body sensory feedback, which results in torques that mimic the hip strategies normally exhibited by healthy individuals during both standing and walking tasks and thereby contributes to better regulation of the motion of the CoM. It is also possible that the use of simple proportional-derivative feedback terms in the GyBAR controllers mirrors the structure of the neuromotor postural controller (e.g. several validated models have the same or similar structure [97, 129, 155, 221]), thereby simplifying how, with minimal familiarization, users of the GyBAR might integrate its controller with their own postural control system to quickly and successfully exploit these external torques. Deeper investigation is necessary to assess these explanations.

Effective assistance does not require reference posture

We expected that a controller regulating the trunk angle would perform best, motivated by a connection between angle and CoM position if inverted pendulum behaviour of postural control is assumed [221]. However, our results showed that both controllers designed to regulate posture, S-D and S, were outperformed by posture-independent controller D and, in the case of S, did not significantly improve task performance over baseline condition IN (p=0.09). Although this apparently contradicts our expectation, a caveat is that both controllers S-D and S were particularly prone to discontinuous (and therefore unpredictable) behavior due to frequent limitations on the exchange of angular momentum (i.e. geometric saturations); since this is greatly influenced by the selection of the controller gains, performed *a priori* and not adapted or 'optimized' per subject or task, we cannot confirm nor reject this hypothesis without further investigation. We can conclude, however, that it is feasible to assist balance without specifically accounting for postural orientation, as demonstrated with the presented implementation of controller D in both experiments.

Interestingly, the two robotic devices found to most similarly assist postural control via the upper body also used posture-independent controllers. For a walking task similar to Experiment 1 and with a wearable reaction wheel fixed to the back, Wojtara *et al.* implemented a non-smooth and potentially discontinuous damping controller to generate a velocity-dependent torque opposing motion of the trunk *only when moving away from upright posture* [225]; the selection of the viscous controller was justified with the anecdote that while 'standing in shoulder-deep water, it is easy to keep balance'. In the

second instance, Wu *et al.* used a cable robot attached to a hip harness where lateral forces proportional to the CoM velocity were applied to either assist or perturb subjects as they follow a straight line on a treadmill [227]; here the selection of the viscous field was made due to avoid imparting position constraints on the subject. Both cited studies also reported a significant improvement in task performance and positive perception when assistance was applied in this manner; it should be noted, however, that in the study of Wojtara *et al.* this comparison was made against a perturbation condition and not a neutral baseline. Although neither study discussed the selection of a damper-like controller in great detail, a separate study on performance enhancement in teleoperation has reported that interaction with a viscous field generates particularly rich haptic information of body dynamics, thereby augmenting perception and improving task performance [170].

Virtual viscous fields also have practical benefits over their elastic and viscoelastic counterparts. Controller D does not depend on posture and is thus robust to postural biases, asymmetries, and low-frequent drift or weight-shifting, as is common amongst individuals with stroke [44, 202]; despite physiological differences between the post-stroke and healthy groups tested in Experiment 2, the degrees of improvement were not drastically different. Because of this independence from posture, we presume that a controller of this form may be applicable to balance assistance in a wider range of tasks, both in clinical and real-world settings; it is thus of interest to further investigate the benefits of the GyBAR with such a controller in other clinically-validated balance tests or in Activities of Daily Living (ADLs).

Finally, arguments also exist for the suitability of certain types of controllers for this particular actuation concept. Due to a finite ability to exchange angular momentum (i.e. the phenomenon of *geometric saturation*), gyroscopic actuators are physically incapable of sustaining indefinite or prolonged support to overcome postural bias [13], but are rather better suited to providing dynamic assistance in response to rapid, transient motions, in which the angular momentum exchange is not monotonic but ideally varying over time such that the net exchange is small. It is worth noting that a posture-dependent controller, could, in theory be adapted to mitigate low-frequent biases, but the behaviour and perception of such a controller has not yet been studied.

Subjects interact better with predictable controllers

It is presumed that controller D performed relatively well and was perceived better than controllers S and S-D due, in part, to a lower incidence of geometric saturations and therefore more continuous and predictable behavior. In the event of geometric saturation, the supporting torque would abruptly withdraw (Supplementary Fig. 4.A2b) and, in some cases, re-engage equally abruptly, resulting in washout or a destabilizing perturbation of varying severity. In Experiment 1, more than 70 % of instances in which such a situation occurred were, as a direct consequence, followed by loss of balance and task failure. Due to the high virtual stiffness of controllers S and S-D and low frequency content of human motions, controllers S and S-D resulted in a much higher exchange of angular momentum than controller D, and the angular momentum limits were encountered by an additional 50-60 % of the subject group (n=10, healthy).

Although the ranked perception of each controller (Supplementary Table 4.AIII) was

influenced also by other (nominal) qualities of the controllers, the prevalence of geometric saturation often had negative consequences. This is perhaps why controller D was perceived best and controller S was perceived worse than even non-assistive condition 'gimbal locked' (GL) despite better task performance than GL; although GL was not found to improve balance, the stationary gimbal means that the dynamics vary less and are directly coupled to the motion of the user (i.e. no control delays or nonlinear scaling) and are therefore more predictable.

The GyBAR may be stronger than is needed

Our results showed that the GyBAR, while enhancing balance with the presented realization of a virtual damping field, was capable of generating the required assistive torque within the available angular momentum limits for the majority of operation. The median peak torques were 13.8 Nm during Experiment 1 and 13 Nm and 7 Nm during Experiment 2 for healthy controls and stroke survivors, respectively. These values are significantly lower than our initial design target of 90 Nm [114] and realized maximum of over 50 Nm. This suggests that a subsequent design iteration could result in the realization of a lighter and smaller device capable of fulfilling a similar degree of support in situations of comparable balancing challenge. In the current GyBAR prototype, it is possible to implement higher gains to potentially further increase balance performance and to better utilize the device capabilities in other tasks or target groups.

4.4.2 | Clinical Relevance

The 'damper' controller decreases the frequency of postural control

When controller D was activated, a decrease in the centroidal frequency of the trunk angle was observed with respect to condition IN in both experiments and for both healthy subjects and individuals with chronic stroke (Supplementary Figs. 4.A5a and 4.A7b). Although significant differences between IN and D were not observed in the RMS or peak trunk angles or angular velocities (e.g. Supplementary Fig. 4.A7a), small increases in the former quantity and decreases in the latter explain the comparatively larger change in frequency: the controller opposed fast rotations and the user adapted by increasing their excursion amplitude, although it is unclear to what degree this response was an attempt to counter or to exploit the controller actions. Observations confirmed that, although the rate of postural corrections did appear to decrease, the influence of the controller did not lead to a fundamental change in balancing strategy.

There are several possible contributing factors to the decrease in centroidal frequency of the CoP and trunk motions observed between conditions IN and D. Using models of the neuromuscular postural control system [97, 129, 155, 221], a decrease in frequency can be associated with an increase in sway amplitude and decrease in the stiffness of the postural control loop; this may be indicative of either decreased muscle activation in the lower limbs [28] or decreased reflex gains [155]. A decrease in stiffness is presumed to occur when the level of postural threat is low and the high energetic cost of maintaining high stability margins is no longer justified [120, 221]. Since it is unmistakable when the GyBAR is active (due to e.g. sounds and vibrations from the motors), it is conceivable that a psychological element is present: for example, a decrease in anxiety due to a robotic

placebo effect may reduce neuromotor stiffness [1, 27, 120] – in fact, several of the individuals with stroke remarked that they felt an increase in confidence, although we did not quantify this, unlike others [3]. However, in our experiments the decrease in the frequency of postural corrections did not coincide with an increase in sway amplitude as in published observations [1, 27], hence we infer that the neuromotor control loop does not simply relax with controller D, but, rather, another mechanism exists whereby regulation of the motion of the CoM is improved such that less motor activity is required to maintain the same stability margins.

It is also possible that the GyBAR may improve stability through enhanced proprioceptive feedback, as similar differential effects have been observed between conditions of sensory deprivation and normal function (e.g. [56, 165]) and between conditions of normal function and sensory augmentation (e.g. the 'light touch' effect [94] and vibratory stimulation [163, 211]); however, while this may contribute, it is unlikely to be the dominant reason for the improvement of task performance or reduction of sway frequency, as relatively large torques were exerted by the GyBAR on the wearer (Supplementary Figs. 4.A5b and 4.A7c).

We conclude, therefore, that our observations are primarily due to mechanical stabilization by the GyBAR, whereby the GyBAR decreased the burden on the neuromotor postural control system such that less frequent postural adjustments were necessary to maintain balance.

The 'damper' controller scales down balance activity

The balancing activities performed in this study intentionally constrained the use of primary balancing strategies to induce postural instability. In both experiments, the reduced BoS resulted in a decreased ability to exert ankle torques and was compensated by a greater use of secondary strategies, such as the dynamic hip strategy, manipulation of the swing leg (Experiment 1), and swinging of the arms (individuals with chronic stroke[2] in Experiment 2). The smaller BoS also limited the degree to which the CoM could safely sway, thereby requiring neurologically stiffer control than with a full base of support. Compared to the healthy participants of Experiment 2, the individuals with chronic stroke were observed to exhibit greater usage of secondary balancing strategies, such as moving the hips and arms. This is in accordance with the knowledge that individuals with stroke generally have a decreased capacity to voluntarily transfer weight and hence under-utilize the full base of support and depend to a greater extent on stepping strategies to recover balance [64]. As a consequence, in the fixed-stance balancing task of Experiment 2, the individuals with stroke were observed to compensate by recruiting additional degrees of freedom (more joints were observed to move) and increasing the range of joint motion, although with the appearance of inefficient coordination between joints.

Although not manifested in the CoP or trunk angle magnitudes, visible differences in the magnitude and number of balancing strategies were observed in several subjects between conditions IN and D in both experiments. With controller D, most subjects exhibited a decrease in secondary balancing strategies, particularly usage of the hips, such

[2] Healthy participants were not permitted to use their arms for balance and participants with chronic stroke were instructed to keep the arms as close to the body as possible.

that the primary ankle and stepping (Experiment 1) strategies were again dominant and, in some cases, almost entirely sufficient. Other secondary strategies were also observed to decrease with the controller on: swing leg exploitation in Experiment 1 appeared to cease completely, and the arm motions of the individuals with stroke in Experiment 2 reduced in most cases. Subject S4 (▽), from the Experiment 2 cohort with chronic stroke, was originally characterized as using secondary strategies excessively, but exhibited a dramatic reduction of upper body motions and an increase in coordination and effectiveness of the ankle strategy when controller D was active.

The reduction of secondary balancing strategies with controller D is presumed to signify greater postural stability. It is well known that balancing strategies grow in magnitude and dimensionality with postural threat [86, 90, 135], and modelling has shown an increase in the use of the hip strategy when postural robustness is critical [4]. Based on this model, it is deduced that less hip activity when the damper controller is active is indicative of lower demand on the postural control system and greater emphasis instead on energy efficiency; however, metabolic rate was not measured in the current study, so this cannot be explored at present. In addition, it is presumed that smaller postural responses are either a consequence of smaller deviation of the CoM (however, the trunk deflection measurements, which are approximately proportional to the CoM location, do not support this) or, more likely, the CoM deviations remained somewhat consistent but postural control was shared with the GyBAR, which required less neural control. Evidence supporting the latter is the significant torque exerted by the GyBAR, as shown in Supplementary Figs. 4.A5b and 4.A7c; however, explicit quantification of muscle activity should be also studied in the future.

Potential beneficiaries of the GyBAR

Our results suggest that, at least in standing balance when stepping strategies are limited, both healthy individuals and individuals with chronic stroke can improve functional performance when wearing a gyroscopic actuator on the trunk. Although further research is needed to generalize these encouraging findings to other contexts and populations, we hypothesize that the technology demonstrated with the GyBAR prototype can, in principle, be used to develop new therapy interventions potentially treating a wide range of disorders affecting balance.

Bipedal stance is inherently unstable and relies on a number of systems for effective closed-loop control. Deterioration of the sensory system (e.g. visual, proprioceptive, and vestibular systems), nervous system (e.g. attention and coordination), or motor system (e.g. muscle weakness or paresis) can result in an inability to detect instability or correct for it sufficiently quickly and, consequently, greatly increase the risk of falling. Symptoms may be intermittent and depend on aspects such as cognitive demand during multi-tasking [19], sensory re-weighting in changing environments [15], or anxiety due to greater perceived risk of falling [121]. Groups with disorders affecting balance include the frail elderly (particularly those already with a history of falling) [11, 110, 121] or individuals with cerebellar disorders [15, 43, 109], vestibular disorders [87, 120, 155], Parkinson's disease [3, 29, 88], or psychogenic disorders such as phobic postural vertigo [106]. Even with relatively mild impairments, it has also been suggested that fear of falling may result in delayed anticipatory postural adjustments during stepping, re-

sulting in slower effective reaction times and greater risk of falling [201], and stiffening of the lower limbs [27, 121]. Compensatory stiffening can reduce the excursion of the CoM to improve robustness to unforeseen perturbations, but it has been argued that in certain cases this may even jeopardize stability by, e.g., (i) pushing the CoP to the edge of the BoS, causing loss of control authority [93], (ii) decreasing the ability to react to larger disturbances in which sudden joint motion may be beneficial, such as in hip or stepping strategies [93, 150], and (iii) increasing susceptibility to resonant sway in response to high-frequency disturbances [31, 93].

For these groups, added damping by the GyBAR may be desirable for two reasons: (i) a general, pathology-nonspecific slowing of motion, and (ii) a pathology-specific compensation for insufficient neurological damping. For individuals who are unable to react quickly enough to instability, external damping can slow motion of the trunk, which may also slow motion of the centre of mass towards the edge of the base of support if the lower extremities remain relatively rigid. This would allow longer time for the individual to generate an appropriate corrective response and is presumed to explain the improved task performance and decreased frequency of motion observed in Experiment 2 for individuals with chronic stroke, who are known to have delayed and disrupted responses to stance perturbations [64]. In postural control, neurological damping has been interpreted as having an anticipatory or predictive function [132] and is necessary to attenuate oscillatory sway that risks destabilization [31, 155]. However, in old age, neurologically-generated damping has been reported to be insufficient to avoid excessive sway [31], which may possibly be due to difficulty in modulating the time delays in muscle activity necessary to produce damping [155]. To improve robustness to sudden perturbation, the GyBAR may be able to compensate for such insufficiency. Recent research of the upper extremities has also suggested that interacting with a damping field leads to an adaptive shift of reliance from co-activation to reflex responses [206]; if this occurs also in the lower extremities, it may translate to an improved ability to react to large disturbances and execute stepping responses for persons who would otherwise rely excessively on co-activation to compensate for degraded postural control.

A continuous viscous field, as investigated with controller D in this study, may be useful for bridging the transition from body-weight-supported treadmill gait training to hands-free overground training in, e.g., individuals recovering from partial spinal cord injury or stroke, by increasing confidence and mitigating risk. Although not the focus of the present study, the GyBAR may also be used for generating perturbations, either for diagnostic [89, 130, 150] or training purposes (e.g. for the frail elderly and PD) [122]; error augmentation was successfully achieved in Experiment 1 with controller ND, and a study of discrete trunk perturbations is currently ongoing (Schumacher *et al.*, in preparation).

Some pathologies are not expected to benefit from the GyBAR. Particularly, it is not the intention that the GyBAR and tested controllers can entirely replace the ability to select an appropriate balance recovery strategy following a perturbation; rather than autonomously balancing a passive user, the GyBAR offers complementary control to temporarily delay a fall until the user can react appropriately. This device may hence be unsuitable for persons suffering severe neurological impairments that excessively prolong or entirely obstruct balance reactions, or for persons with sensory deficits that inhibit their ability to perceive instability. By design, the GyBAR is also unable to directly influ-

ence motion of the limbs, such as guide foot placement during a stepping response to a perturbation; this is in contrast to most conventional exoskeletons, which assist limb motion, but can inhibit balance. As a consequence, the GyBAR cannot independently augment the strength or weight-bearing capabilities of, e.g., persons with paraplegia, but perhaps could do so in combination with a lower-body exoskeleton, in which case the GyBAR could be worn to assist balance as the exoskeleton compensates for muscle weakness.

4.4.3 | Technical guidelines

Effective controllers can be realized with simple instrumentation

Despite the simplicity of the controllers investigated, controllers D and S-D were found to be effective for augmenting balance function. All controllers used sensors located only within the GyBAR to limit inconvenience when donning and doffing the device. Implementation of controller D is particularly simple, as the output of a gyroscopic sensor can directly be used for feedback, without the computational complexity of postural state estimation via fusion of different sensor types in an inertial measurement unit.

Peak level of assistance can be traded for mass reduction

Although the GyBAR provided sufficient assistance to improve balance, its weight is impractical for potential target groups such as recovering stroke patients or the frail elderly. The 16 kg weight of the GyBAR, corresponding to between 15-28 % of the bodyweight of the participants of both experiments (Supplementary Table 4.AI), was found to have a significant detrimental effect on the balance of even young healthy individuals, as evidenced by the significant difference between the 'free' (FR) and 'inactive' (IN) conditions in Experiment 1 (Fig. 4.2d, p=0.037), and was observed to result in increased spine flexion and neck extension during standing. Physiological studies on backpack loading suggest that, in order to avoid increased exertion or perturbed posture, backpack-type loads should not exceed 20-30 % bodyweight in young healthy individuals [5, 187]; however, other factors should also be considered, such as the duration of load carriage, construction of the backpack (including distribution of the load and concentrations of pressure), and the physical condition of the wearer [5], all of which may affect how the body is strained [84]. For impaired or frail target populations, it is expected that the maximum load should be much smaller; in Experiment 2, for example, the device when unloaded to 7-13 % bodyweight appeared to be acceptable for short durations for individuals with chronic stroke, yet specific investigation of these thresholds is required.

In the design of gyroscopic actuators, a trade-off exists between performance, size, mass, and rotor speed. Both the maximum gyroscopic torque, τ, and the angular momentum exchange, ΔH, are proportional to the (constant) angular momentum magnitude of the rotor, $H=J\Omega$, where Ω is the rotor spin-axis angular velocity and J is the rotor moment of inertia, which is itself proportional to the mass and square of the radius of the rotor. Thus, for the same rotor angular momentum (i.e. similar performance specifications), it is possible to reduce the rotor mass by increasing its speed and/or radius. For the same H=10 N m s and size of the GyBAR in this study, a new device of 7.5 kg mass (approximately 10 % body weight), as emulated in Experiment 2, could be realized by

increasing the rotor speed from 5000 to 9000 rpm (Supplementary Fig. 4.A3); this higher speed could be achieved by incorporating friction-reducing components such as specialized bearings and/or a low-pressure rotor chamber.

Our results suggest that only a fraction of the maximum capabilities of the GyBAR were exploited by median users: less than the 35 % of the maximum gyroscopic torque and less than 60 % of the exchangeable angular momentum. It would hence be possible to reduce the rotor angular momentum in proportion, meaning, for example, that a new device might have less mass even if the size and speed were to remain unchanged. However, our findings indicate that encountering geometric saturation (i.e. exchanging the maximum amount of angular momentum) is particularly detrimental to balance performance and should be avoided with a safety margin similar to that realized in this study. Finally, it is important to note that these performance specifications will, in general, depend on (i) the baseline balance function of an individual, (ii) the degree of postural challenge expected, and (iii) the controller gains and intended degree of balance improvement; further experimentation may thus be necessary to optimize the mass of the device for other groups or applications.

Handling of geometric saturations will improve performance

Despite being less problematic in posture-independent controller D, further precautions should be taken to reduce the frequency or severity of perturbations resulting from geometric saturation.

Although geometric saturations are inherent limitations of gyroscopic actuators, the frequency at which saturation occurs can be reduced by (i) increasing the angular momentum of the rotor or adding additional rotors to a similar cumulative effect, (ii) modifying the controller to exert less torque (e.g. reduce the spring or damper gains) or be less sensitive to biases or low-frequent dynamics, or (iii) increasing the degree to which the available angular momentum can be exchanged. Increasing the angular momentum as in (i) presents a trade-off with increasing the mass of the device, but is feasible to the extent discussed previously. Reducing controller sensitivity to biases as in (ii) can be accomplished by selecting different feedback signals, high-pass filtering these signals, or designing a supervisor that regulates the nominal projection of the angular momentum. Finally, (iii) is typically achieved by coordinating two or more (possibly smaller) gyroscopic actuators such that the net gyroscopic torques are projected in the desired direction, either via model-based control [13, 203] or a mechanical constraint [21, 35]; the presented GyBAR prototype was further constrained by the presence of electrical cables that prevented the gimbal from rotating freely, which can be replaced in the future with slip-rings.

To reduce abrupt perturbations occurring at saturation, safe 'singularity-robust' controllers for gyroscopic actuators have been proposed for both this specific application [13] and other generic uses and configurations [203], which improve predictability by smoothly arresting gimbal motions near geometric constraints. A simplified version of this was implemented in the GyBAR, but it is conceded that the influences of such perturbations were underestimated during selection of the parameters.

4.4.4 | Study Limitations

Sample size

Our findings showed that the GyBAR improved balance in both experiments and subject groups. However, our results in subjects with chronic stroke cannot be generalized due to the small sample size in Experiment 2 and high variability of the data [64]. From the data collected in these experiments, it is estimated that a minimum sample size of 12 subjects is required to significantly detect a normalized increased balance improvement of 100 % (i.e. twice the stance time or walked distance) with an 80 % power and a statistical significance of 0.05 %.

In addition, it was not possible to make a direct comparison between subject groups in Experiment 2 due to the lack of matching demographics.

Undesired balance artifacts

The prototype GyBAR was constructed to explore the principles of design and control of gyroscopic actuation, hence its mass was not optimized for wearability. This considerable weight (16 kg) was found to have several unintended consequences.

In addition to the aforementioned threat of physiological strain during prolonged load carriage, a heavy load is counterproductive to the aim of improving balance [77, 180]. This is illustrated in Experiment 1, where two of the three assistive controllers were found to not be statistically better than simply removing the device. From this standpoint, it is of great interest to test a lighter, optimized GyBAR that (i) does not risk potential strain or overexertion with prolonged use and (ii) does not negate a large portion of its potential benefits by its weight alone.

Whereas the healthy participants of this study were capable of bearing the full weight of the prototype GyBAR, the members of the chronic stroke group in Experiment 2, representing one of the primary target groups of this technology, were not. The safety system used in Experiment 2 served to mitigate the physiological strain experienced the individuals with chronic stroke.

However, the additional unloading provided by the safety system imparted stabilizing forces, potentially improving proprioception. It was expected that this unloading would not have a large impact due to the facts that (i) the height of the fixation point (approx. 2.5 m) was large in comparison to the expected horizontal deflections of the trunk, implying that the unloading force would remain primarily vertical and not directly influence horizontal CoM control, and (ii) the spring was relatively soft (460 N/m) to ensure minimal change in the magnitude of the unloading force with displacement of the trunk. However, the passive gantry-based safety system exhibited some direction dependence; it could translate easily along a rail in the AP direction, but was essentially fixed in the ML direction due to high inertia and friction, creating the possibility for subjects to exchange lateral forces with it. In the standing task with a reduced AP BoS, any such assistance from the safety system only offset the detriment that the remaining 7.5 kg weight may have had, and no significant difference in task performance was observed between conditions FR and IN (p=0.89, both groups). In the standing and walking tasks with a reduced ML BoS, however, the horizontal forces did significantly improve task performance (compare, e.g., condition FR and IN in Supplementary Fig. 4.A6b, p=0.043). From

the peak trunk angular deflections, it is estimated that the safety system may have imparted torques in the ML direction on the same order of magnitude as the GyBAR. We presume that this allowed subjects to rely less on the gyroscopic assistance, which explains why no significant differences were observed between conditions IN and D in the ML tasks of Experiment 2 ($p \geq 0.465$), but were observed in Experiment 1 for a comparable task ($p = 0.012$).

4.4.5 | Future work

These results, although promising, give rise to several new questions:

Effectiveness of a lighter GyBAR

Although the GyBAR prototype tested in these experiments is not intended for clinical use, we are currently testing a lighter version with similar performance and targeting clinical use (Fig. 4.4). In addition to its reduction of mass to about half of that of the current GyBAR, it includes a more ergonomic interface which improves weight bearing and comfort. Hence, we expect that this new prototype would confirm its balance assistive capabilities in a clinical setting. We are now in the planning phase of a follow-up study to investigate the impact of weight reduction in the GyBAR on balance assistance and usability in a clinical setting.

Lowest level of effective assistance

On average, the magnitude of generated torques were lower than the mechanical capabilities of the GyBAR, suggesting that a smaller/lighter device could still assist balance. A study with a new such device and *human-in-the-loop* optimal selection of controller gains [237] could help to investigate to which extent balance augmentation scales with the level of assistance and whether there is an optimal level of assistance.

Effect on metabolic cost

Although the GyBAR was able to improve balance significantly, despite its considerable mass, the impact on metabolic cost should be investigated with representative activities and different levels of assistance.

GyBAR as training or assistive device

Thus far, the GyBAR has been investigated as an assistive device, and the tests performed gave little opportunity for adaptation. However, given the versatility of its actuation capabilities, it can, in principle, also be used as training device. Previous studies on error augmentation/reduction in the rehabilitation of individuals with stroke or incomplete spinal cord injury have reported beneficial results on the implementation of active stabilizing/destabilizing force fields as training paradigms [151, 227], which can similarly be realized with the GyBAR.

(a) (b)

Figure 4.4: GyBAR prototype 2 Subject wearing the lighter GyBAR prototype 2

Performance assessment in more realistic applications

Although mostly based on validated clinical balance characterization tests, our study was limited to a constrained set of tasks and simple balance performance metrics. Future studies could include more sensitive performance metrics (e.g. CoP, CoM) and more representative tasks (e.g. ADLs and more comprehensive clinical tests). Such studies might also investigate other balance recovery strategies, such as stepping, and other means of perturbation, such as slipping or tripping.

Ultimately, the purpose of our device is to enable subjects with balance disabilities to restore balance function as close as possible to that of a healthy individual. An idealization of our device would enhance balance capabilities regardless the population, type of balance disability or balancing task. The complexity of realistic balancing tasks (e.g.

ADLs) and balance disabilities make the realization of such a device challenging.

Still, although our experiments were limited to somewhat artificial challenging balancing tasks with a narrow cross-section of a single patient group, we believe that our results represent a key advancement on the path towards effective and practical wearable balance assistance.

Acknowledgment

We wish to acknowledge the help of the the staff of the Center for Bionic Medicine in the Shirley Ryan AbilityLab and specifically the technical assistance of C.K. Mummidisetty during the preparation of the experimental setup and Lory McGee for her support during the application to the Institutional Review Board. The authors also thank Dr. Carel Meskers of the department of Rehabilitation Medicine in the VU Medical Center Amsterdam for his advice during the design of the protocol, Giel Hermans and Andries Oort of the Electronic and Mechanical Support Division (DEMO) at TU Delft for providing technical support while upgrading the GyBAR, Niek Wondergem and Joost van Leeuwen of Westland Orthopedie for their assistance modifying the GyBAR attachment interface, and Christian Schumacher for advice and fruitful discussions in the development of this manuscript. This research was supported by the U.S. Department of Education, National Institute on Disability and Rehabilitation Research, NIDRR-RERC, Grant No. H133E120010, the Marie-Curie career integration Grant No. PCIG13-GA-2013-618899, and the Innovational Research Incentives Scheme Vidi with Project No. 14865, which is (partly) financed by The Netherlands Organization for Scientific Research (NWO).

4.A | Supplementary Material

4.A.1 | GyBAR Dynamics

Gyroscopic torque

A control moment gyroscope consists of a spinning rotor fixed to a motorized gimbal frame, as shown in Supplementary Fig. 4.A1. The gyroscopic torque $\boldsymbol{\tau}(t) \in \mathbb{R}^3$ applied to the person has magnitude proportional to the gimbal angular velocity $\dot{\boldsymbol{\gamma}}(t) \in \mathbb{R}^3$, the angular velocity of the person $\dot{\boldsymbol{\theta}}(t) \in \mathbb{R}^3$, and the angular momentum of the rotor $\boldsymbol{H}(t) = \boldsymbol{H}(\boldsymbol{\gamma}(t)) \in \mathbb{R}^3 \mid H = \left\|\boldsymbol{H}(t)\right\| = J\Omega$, where J and Ω are the respective spin-axis moment of inertia and angular velocity of the rotor (assumed constant). The gyroscopic torque $\boldsymbol{\tau}$ can be decomposed into two components, one of which results from controlled motion of the gimbal and that the other is uncontrolled and induced by motion of the person:

$$\boldsymbol{\tau}(t) = -\dot{\boldsymbol{H}}(t) \tag{4.A.1}$$

$$= -(\dot{\boldsymbol{\gamma}}(t) + \dot{\boldsymbol{\theta}}(t)) \times \boldsymbol{H}(t) = -\underbrace{\dot{\boldsymbol{\gamma}}(t) \times \boldsymbol{H}(t)}_{\text{controlled}} - \underbrace{\dot{\boldsymbol{\theta}}(t) \times \boldsymbol{H}(t)}_{\text{uncontrolled}} \tag{4.A.2}$$

When $\dot{\boldsymbol{\theta}}$ is considered small in comparison to $\dot{\boldsymbol{\gamma}}$ and is neglected, $\boldsymbol{\tau}$ is stationary with respect to a gimbal-fixed frame as shown in Supplementary Fig. 4.A1. In Experiment 1, the effects of the uncontrolled term were isolated with the condition 'gimbal locked' (GL, Supplementary Table 4.AII), which was found to not significantly impact beam-walking performance compared to the condition 'inactive' (IN), in which $\|\boldsymbol{H}\|$ is zero; see Supplementary Fig. 4.A4.

The gimbal-fixed coordinates map to a human-fixed coordinate system via rotations by the gimbal angle γ. For a human-fixed frame $(\hat{\boldsymbol{x}}, \hat{\boldsymbol{y}}, \hat{\boldsymbol{z}})$ oriented as *(anterior,left,up)*, and with a vertical gimbal axis (as in this study), the generated $\boldsymbol{\tau}$ spans the axial plane:

$$\boldsymbol{\tau}(t) = \left|J\Omega\dot{\gamma}(t)\right|\left(\sin\gamma(t)\hat{\boldsymbol{x}} - \cos\gamma(t)\hat{\boldsymbol{y}}\right) = \tau_{\mathrm{ML}}(\gamma(t), \dot{\gamma}(t))\,\hat{\boldsymbol{x}} + \tau_{\mathrm{AP}}(\gamma(t), \dot{\gamma}(t))\,\hat{\boldsymbol{y}} \tag{4.A.3}$$

where non-bold symbols are scalar quantities with signs as defined in Supplementary Fig. 4.A1.

Angular momentum exchange and geometric saturation

Gyroscopic actuators cannot indefinitely exert a torque (or torque component) in a fixed direction. Since generating a gyroscopic torque requires rotation of a gimbal by angular rate $\dot{\boldsymbol{\gamma}}$, the projection of $\boldsymbol{\tau}$ onto the human frame, depending on γ, will vary with time. For a statically-oriented objective torque, the gimbal will thus ultimately rotate to a configuration in which either mechanical limitations prohibit it from moving further (as in this study) or $\boldsymbol{\tau}$ becomes orthogonal to the objective; both instances are referred to here as *geometric saturation*.

It is also possible to express proximity to geometric saturation using the angular momentum state vector as a function of the gimbal angle, $\boldsymbol{H}(\gamma(t))$. This has the advantages that (i) actuator performance can be expressed in terms of an important design variable, the angular momentum magnitude H, and (ii) a relationship to the generated torque can be found by integrating Supplementary Eq. 4.A.1. For any time t, the angular momen-

tum exchanged between the rotor and person, $\Delta \boldsymbol{H}(t)$, can be expressed as:

$$\Delta \boldsymbol{H}(t) = \boldsymbol{H}(t) - \boldsymbol{H}(0) = \int_0^t \dot{\boldsymbol{H}}(T)\mathrm{d}T = \int_0^t \boldsymbol{\tau}(T)\mathrm{d}T \tag{4.A.4}$$

The angular momentum state $\boldsymbol{H}(t) = \boldsymbol{H}(\gamma(t))$ can change only through rotation of the gimbal and hence prescribes an arc of radius H (or a circle, if γ is unconstrained). As a result, the exchanged momentum $\Delta \boldsymbol{H}(t)$ is bounded to a maximum of $[-2H, 2H]$, although this can be smaller depending on the initial state $\boldsymbol{H}(0)$ in relation to the direction of $\boldsymbol{\tau}$ and the presence of further limitations on γ. Equivalently, this acts as a constraint on the time integral of $\boldsymbol{\tau}$. It is therefore pertinent to measure the trajectory of $\Delta \boldsymbol{H}(t)$ to determine how close the actuator comes to geometric saturation and quantify overall performance.

As in Supplementary Eq. 4.A.3, $\Delta \boldsymbol{H}$ can be decomposed into human-fixed coordinates:

$$\Delta \boldsymbol{H}(t) = \underbrace{H\big(\cos\gamma(t) - \cos\gamma(0)\big)}_{\Delta H_{\mathrm{ML}}}\hat{\boldsymbol{x}} + \underbrace{H\big(\sin\gamma(t) - \sin\gamma(0)\big)}_{\Delta H_{\mathrm{AP}}}\hat{\boldsymbol{y}} \tag{4.A.5}$$

where γ is defined such that $\boldsymbol{H} || \boldsymbol{x}$ when $\gamma = 0$. For compactness of notation, the term ΔH is used to mean either one of these scalar components, depending on the context. Supplementary Fig. 4.A2 illustrates the phenomenon and consequences of geometric saturation in the context of human balance control; the angular momentum exchange reaches a maximum when the gimbal reaches its mechanical end-stop, causing the gyroscopic torque to cease.

Given the importance of the angular momentum of the rotor H for both the magnitude and duration of a gyroscopic torque (Supplementary Eq. 4.A.2 and 4.A.4, respectively), it is a fundamental design parameter for gyroscopic actuators. For a fixed $H = J\Omega$, Supplementary Fig. 4.A3 shows the tradeoff between mass and size (both relating to rotor moment of inertia J) and rotor speed Ω during GyBAR design optimization.

4.A.2 | Methods

GyBAR as a wearable balance aid

For the present study, the GyBAR gimbal motor and gearbox were replaced to reduce weight; this change reduced the mass by almost 1 kg, at the cost of a reduction of estimated peak gyroscopic torque from 70 Nm to 53 Nm.

To generate a gyroscopic torque, the gimbal is rotated, which, in turn, causes the output torque to change orientation. With a single gyroscopic actuator, as in the GyBAR prototype, it is not possible to control both the magnitude and orientation of the generated torque simultaneously; by constraining the range of motion of the gimbal (Supplementary Fig. 4.A2a), the gyroscopic torque was projected in approximately the intended direction during nominal operation. Given this constraint, in addition to further gimbal restrictions to avoid cable entanglement, the estimated maximum torque was reduced to ±43 Nm for balancing in the frontal plane (Experiment 1) and −32 to 43 Nm in sagittal plane (Experiment 2).

Experiment 1

Ten healthy adults of various age and without known balance impairment were recruited for Experiment 1 (Supplementary Table 4.AI). Subjects were asked to walk, with feet in tandem (i.e. feet aligned laterally and with the heel of the anterior foot touching the toes of the posterior foot during the double-support phase of the gait cycle) and with their arms crossed, over a 3 cm wide by 4 m long wooden beam (Fig. 4.2), both with and without wearing the GyBAR. Such beam-walking tests have previously been explored for characterizing the balance performance of amputees [177].

During each test, an overhead rail provided emergency fall prevention by means of slack ropes fixed to both a safety harness worn by the participant and the GyBAR itself; care was taken to ensure that neither rope was under tension at any time, such that they could not be exploited for mechanical stabilization.

Seven different conditions were tested, as listed in Supplementary Table 4.AII. Due to the time needed to don/doff the device and accelerate/decelerate the rotor to/from its nominal speed, the conditions were block-randomized for efficiency. Conditions 'free' and 'inactive' both preceded and succeeded a block-randomized set of the conditions in which the GyBAR was both worn and active ('gimbal locked', 'spring-damper', 'damper', 'spring', and 'negative damper', referred to here as 'device active' conditions). The experiment was thus performed as follows, with three repetitions per condition:

1. Baseline condition 'free' (x3 repetitions).
2. Baseline condition 'inactive' (x3 repetitions).
3. Randomized 'device active' conditions (x3 repetitions).
4. Baseline condition 'inactive' (x3 repetitions).
5. Baseline condition 'free' (x3 repetitions).

The task was terminated when the subject (i) reached the end of the beam, (ii) contacted the ground beneath the beam, (iii) violated the 'tandem stepping' constraint, (iv) violated the 'crossed arms' constraint, or (v) relied on either of the safety ropes for assistance; in the rare event of (iii-v), the subject was asked to repeat the condition. The primary outcome measure was the distance walked along the beam until task termination, measured as the last point of contact of the heel on the beam. In addition, task duration (recorded from the moment of first foot placement on the beam) was recorded manually, and trunk angle and angular velocity were measured using inertial measurement units (MPU-9250, InvenSense Inc., San Jose, CA, USA, at 1000 Hz) embedded in the GyBAR ('inactive' and 'device active' conditions only) and a nonlinear state estimator [138]. During the randomized 'device active' conditions, subjects were also asked after each task whether they felt the helpfulness of the controller was either 'better' or 'worse' than that in the previous task; only binary responses were accepted. The data was condensed by comparing only the results of the trial resulting in the median distance walked of the three repetitions per condition and per subject.

Experiment 2

In Experiment 2, five stroke survivors with mild balance impairments and an equal number of healthy control subjects were recruited (Supplementary Table 4.AI, note that no effort was made to match the ages of the groups). To participate in the study, both post-stroke (S) and healthy (H) participants had to meet the following inclusion and exclusion criteria:

Inclusion criteria

- (S,H) Must be able and willing to give written consent and comply with study procedures.
- (S,H) Must be between 18-85 years of age.
- (S,H) Must be able to fit in the device, with chest measurements in the range 98-132 cm and waist measurements in the range 80-150 cm.
- (S,H) Must be between 1.50 m and 2.0 m in height (flexible requirement).
- (S,H) Weigh between 50 kg to 100 kg (flexible requirement).
- (S,H) Must be able to tolerate upright standing position with device 7.5 kg for 30 min.
- (S,H) Must be able to ambulate 10 m without physical assistance or use of an assistive device (ankle orthoses and braces permitted).
- (S) Must be greater than 6 months post stroke.
- (S) Must be able to perform unsupported Romberg balance on firm surface with eyes open for a minimum of 30 s.
- (S) Must demonstrate balance deficit as measured on condition 2, 3, or 4 of the modified Clinical Test of Sensory Interaction on Balance (mCTSIB) in Romberg (feet together) or tandem (one foot directly in front of the other foot, heel touching toe) position of less than 30 s average.
- (S) Mini Mental Status Exam (MMSE) score > 17.
- (S) Medical clearance from physician.

Exclusion Criteria

- (S,H) Currently pregnant (self-reported).
- (S) Medical issues that impede the patient from carrying the full body weight and ambulation.
- (S) Cognitive and/or communicative disability (e.g. due to brain injury). Subjects must be able to follow directions and communicate their experiences to the researchers.
- (S) Untreated deep vein thrombosis (DVT).

- (H) Previously diagnosed balance impairment.

In addition to this, the post-stroke group underwent a baseline functional balance assessment consisting of the Berg Balance Scale (BBS) [12], Functional Gait Assessment (FGA) [226], and the modified Clinical Test of Sensory Interaction on Balance (mCTSIB) [37], all of which were performed without wearing the GyBAR; the results are presented in Supplementary Table 4.AI.

The experimental protocol consisted of three sequences of balancing tests with increasing difficulty that challenged either mediolateral (ML) or anteroposterior (AP) balancing by constraining the size of the support surface: (i) walking heel-toe between two lines or on a beam (similar to Experiment 1), (ii) standing with feet in tandem, (iii) standing with feet shoulder-width apart on a surface with decreased AP base of support (BoS). The ML and AP directions of instability were challenged separately because the prototype GyBAR is not currently capable of influencing balance in both axes simultaneously. Nevertheless, the chosen balancing tasks do not deviate far from validated clinical tests and peer-reviewed studies: the standing tests are similar to those used in the Romberg test [169], BBS [12], and CTSIB [37], the use of a reduced BoS in AP balance is inspired by work by Horak and Nashner [86], and walking tasks with narrow bases of support have been used in the FGA [226], Bruininks-Oseretsky Test (BOT) [24, 210], and in the works of Sawers *et al.* [176, 177]. This protocol was performed with a subset of the conditions from Experiment 1: 'free', 'inactive', and 'damper' (Supplementary Table 4.AII).

In the walking tasks, subjects were instructed to walk heel-toe 2.5 m between two lines set 20 cm or 10 cm, or along a foam gymnastics beam of the same length and 8 cm width; as in Experiment 1, subjects were instructed to keep their arms close to their bodies, and total distance walked before violation of the prescribed constraints was recorded as the primary outcome measure. In the standing task with a reduced ML base of support, subjects were instructed to stand with their feet again in a tandem heel-toe position, but refrain from shifting their feet for 120 s; the primary outcome measure was the test duration up to the point that (i) 120 s had elapsed, (ii) the feet moved from their initial configuration, (iii) the 'arms crossed' constraint was violated[3], or (iv) the cable holding the safety harness was taut and fully extended. In the standing task with a reduced AP base of support, the same procedure was followed, but with the feet parallel and shoulder-width apart (specifically, the medial edges of both feet were separated by 20 cm) and while standing on support surfaces of different AP dimension.

In order to account for differences in subject balance function and reduce the occurrence of ceiling effects, the challenge of each sequence was progressively increased by reducing the BoS or depriving the subject of vision; the exact construction of each sequence is described in Supplementary Table 4.AV. If a task could be completed (score ceiling attained) in the first attempt, the subject would progress immediately to the next task within the sequence; otherwise, they would repeat the same task three times and progress through the sequence no further than the next task. To preserve this graduated structure within each sequence and reduce the time and inconvenience of switching between active and inactive conditions, each sequence was performed uninterrupted and only the order of conditions 'inactive' and 'damper' was randomized.

[3]This constraint was only verbally enforced for the post-stroke group, who often had difficulty achieving or maintaining the specified arm configuration.

Whereas all participants in Experiment 1 were healthy and capable of bearing the mass of the prototype GyBAR (16 kg), in Experiment 2 the different load-bearing capabilities of the stroke survivors were accommodated by unloading part of the added weight. In conditions 'inactive' and 'damper', a soft spring (460 N/m) connected the GyBAR to a two-axis gantry ceiling lift system (Fig. 4.3c) and unloaded the GyBAR to an effective weight of 7.5 kg (note, however, that the inertia of the device could not be compensated for). The apparatus was arranged such that walking or anteroposterior motions occurred in the axis of the gantry system with the lowest amount of inertia; the second axis had comparably high inertia and could be considered to be approximately fixed.

As in Experiment 1, task-based performance metrics (distance walked or duration stood) were used as the primary outcome measures, and trunk angle and angular velocity were used as secondary measures. In addition, standing tests were performed on top of a single forceplate (Sensory Kinetics Standard, Engineering Acoustics, Inc., Casselberry, FL, USA, at 100 Hz). The hardest task in each sequence that was attempted in all testing conditions was selected as the basis for comparison for that subject, and, in the instance of multiple trials per condition, the trial with the median primary outcome score was selected.

4.A.3 | Supplementary Figures

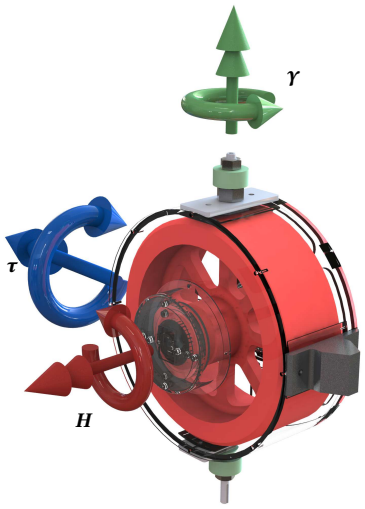

Supplementary Fig. 4.A1: GyBAR schematic showing the orientation of the angular momentum vector ($\boldsymbol{H}$), gimbal rotation ($\boldsymbol{\gamma}$), and output gyroscopic torque ($\boldsymbol{\tau}$) for the case that the trunk angular velocity ($\dot{\boldsymbol{\theta}}$) is small in comparison to $\dot{\boldsymbol{\gamma}}$.

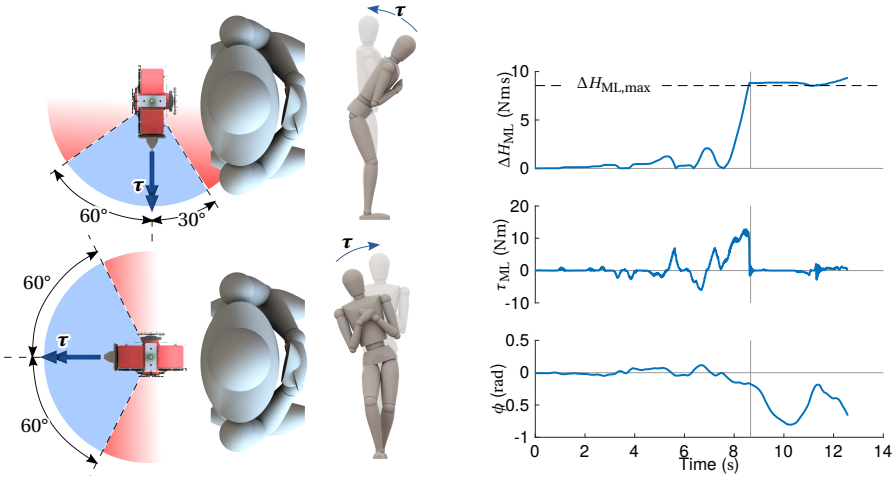

Supplementary Fig. 4.A2: Geometric saturations. (a): Overhead views showing the ranges of gimbal operation (in blue) for AP (top) and ML (bottom) torque (τ) generation. When the gimbal rotates such that τ approaches the boundary, the gimbal is arrested and torque generation ceases, referred to here as *geometric saturation* of the gyroscopic actuator. (b): Example timeseries data of subject C14 of Experiment 1, showing the occurrence of geometric saturation (vertical line) with the 'spring' (S) controller. As the subject leans (ϕ), the controller produces an opposing torque (τ); the gimbal reaches its limit when the time integral of the torque (the exchanged angular momentum in this direction, ΔH_{ML}) reaches a maximum ($\Delta H_{\mathrm{ML,max}}$), at which point τ ceases.

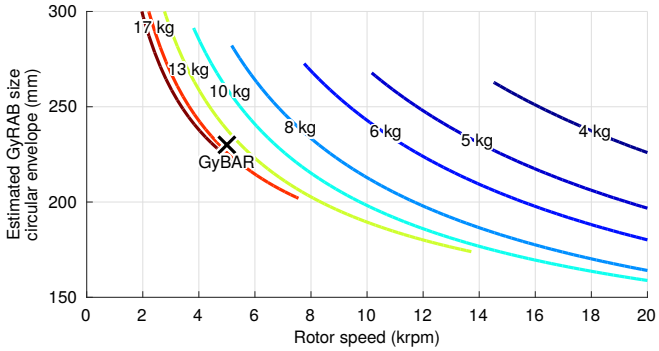

Supplementary Fig. 4.A3: Approximated GyBAR size and mass (iso-lines) as a function of rotor angular velocity Ω for the performance of the current prototype ($H = 10\,\mathrm{N\,m\,s}$).

Experiment 1

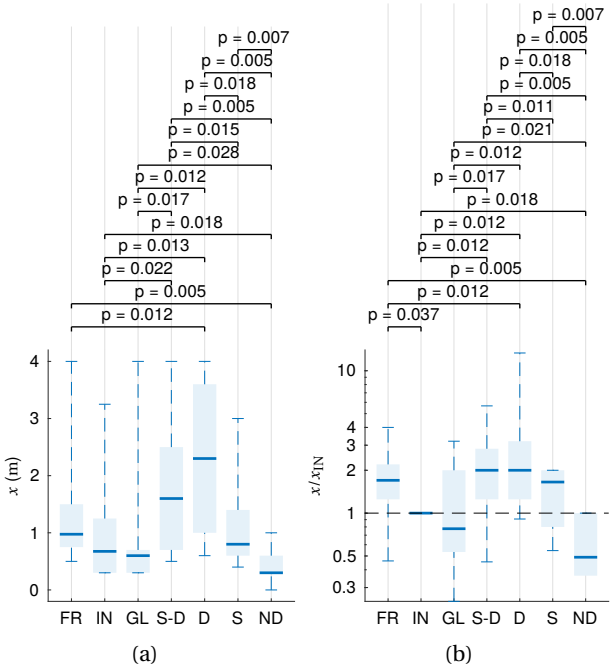

Supplementary Fig. 4.A4: Experiment 1 primary outcome measures (distance walked along a beam of width 3 cm and length 4 m) showing all statistically significant pairs ($p < 0.05$) for conditions 'free' (FR), 'inactive' (IN), 'gimbal locked' (GL), 'spring-damper' (S-D), 'damper' (D), 'spring' (S), and 'negative damper' (ND) shown (a) in original units and (b) normalized with respect to condition 'inactive' (displayed in a logarithmic scale).

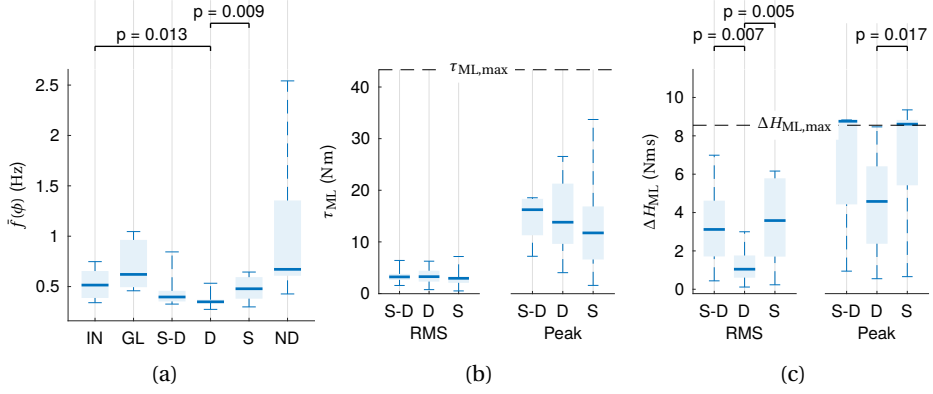

Supplementary Fig. 4.A5: Experiment 1 secondary outcome measures showing all statistically significant pairs ($p < 0.05$) for conditions 'inactive' (IN), 'gimbal locked' (GL), 'spring-damper' (S-D), 'damper' (D), 'spring' (S), and 'negative damper' (ND). (a) centroidal frequency of the trunk roll angle, (b) RMS and peak gyroscopic torque, and (c) RMS and peak exchanged angular momentum.

Experiment 2

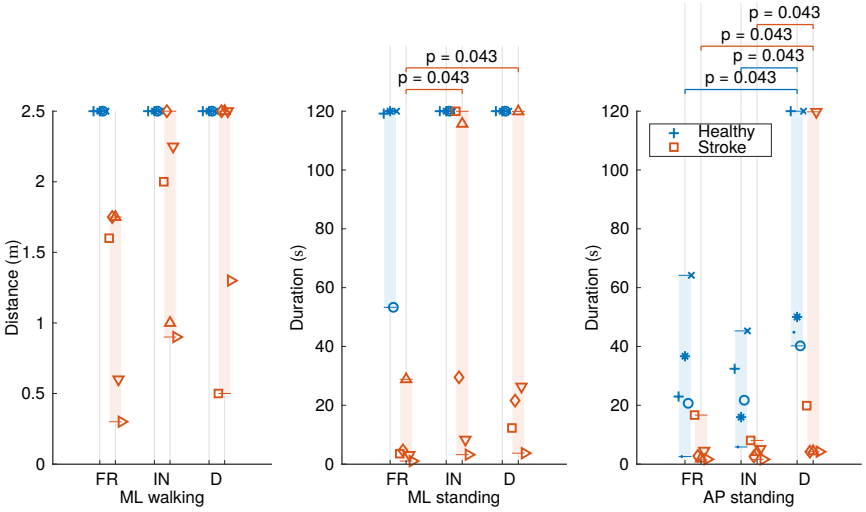

(a) (b) (c)

Supplementary Fig. 4.A6: Experiment 2 primary outcome measures for most difficult level of balancing task completed per subject, both stroke survivors (pairwise left, blue) and healthy controls (pairwise right, red), for conditions 'free' (FR), 'inactive' (IN), and 'damper' (D). Within-group significant differences ($p < 0.05$) are denoted by brackets. Note that, in contrast to Experiment 1, part of the weight of the GyBAR was unloaded in all conditions in which it was worn (IN and D) to avoid overburdening the stroke subjects. In each plot, the upper boundary represents the maximum attainable score for that task. The ML task results were not analyzed due to prevalent ceiling effects and significant improvement between conditions FR and IN, indicating that the unloading system was exploited for stabilization.

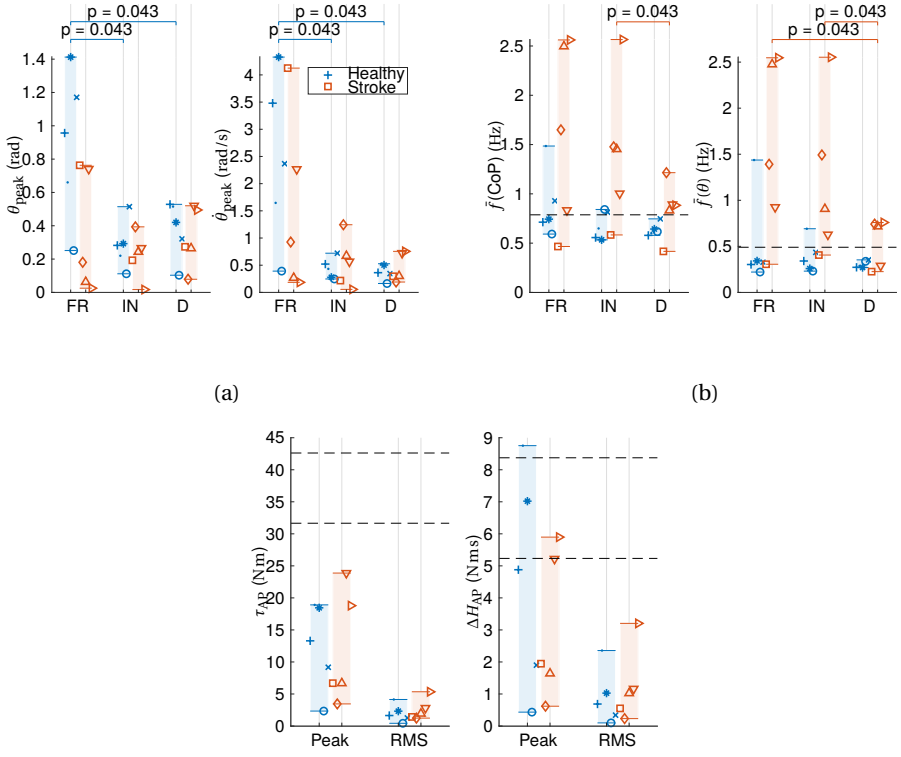

Supplementary Fig. 4.A7: Experiment 2 secondary outcome measures for the AP balancing task showing within-group significant differences ($p < 0.05$). (a): Peak trunk pitch angle (θ) and angular velocity. Significant differences in the healthy population between 'free' (FR) and 'inactive' (IN) may be due to the added mass/inertia of the GyBAR or exploitation of the accompanying unloading system (note, however, that such differences are not present in the primary outcome measures). (b): Centre of pressure (CoP) and trunk pitch angle (θ) centroidal sway frequencies. Median healthy full-BoS frequencies for the IN condition are denoted by dotted lines. (c): Gyroscopic torque τ and exchanged angular momentum ΔH. The dashed lines correspond to the angular momentum limits of the asymmetric gimbal stops. Subjects H2 (•), H3 (✱), and S5 (▷) encountered geometric saturation and subsequent loss of assistance.

4.A.4 | Supplementary Tables

Subject	Marker	Group[1]	Gender	Age	Mass (kg)	Height (m)	Stroke type[2]	Years since stroke	Dominance[3]	Hemiparesis	BBS[4]	FGA[5]	mCTSIB[6]
Experiment 1													
C05			F	26	70	1.68							
C06			M	35	91	1.82							
C07			F	26	57.5	1.66							
C08			M	60	86	1.91							
C09			M	28	82.3	1.83							
C10			M	34	73	1.79							
C12			F	51	80	1.73							
C13			M	27	70	1.83							
C14			M	30	78	1.86							
C15			M	30	95	1.94							
Experiment 2													
S1	□	B	M	49	79	1.83	IS	5.5	R	R	53	22	[30,30,9,5]
S2	◇	A	M	57	101	1.83	IS	1.3	R	L	53	22	[11,7,-,-]
S3	△	A	F	35	70	1.80	HS	1.1	R	R	52	23	[30,26,21,5]
S4	▽	B	F	62	64	1.63	IS	5.0	R	L	42	13	[30,3,16,2]
S5	▷	B	F	59	88	1.65	HS	9.4	R	R	48	16	[16,9,-,-]
H1	+	A	M	32	91	1.91							
H2	•	A	F	30	64	1.75							
H3	✳	A	M	27	73	1.83							
H4	○	B	M	26	73	1.83							
H5	×	B	M	29	70	1.70							

[1] Group testing orders. Group A: free-inactive-damper (FR-IN-D). Group B: free-damper-inactive (FR-D-IN).
[2] IS: Ischemic, HS: Hemorrhagic.
[3] Side of dominance identified as the side of preference for writing.
[4] Berg Balance Scale [12]: to a maximum of 56 points.
[5] Functional Gait Assessment [226]: to a maximum of 30 points.
[6] Modified Clinical Test of Sensory Interaction on Balance [37]: to a maximum of 30 s per item (average of three trials). Reported values are for tandem stance; values for Romberg position were 30 s for all participants for all items. Subjects S2 and S5 were unable to assume tandem stance in the last two tasks.

Supplementary Table 4.AI: Participant information for both experiments.

Experiment 1

Condition	Abbrv.	Description	Balance Controller Gains[1] K_p $\mathrm{N\,m\,rad^{-1}}$	K_d $\mathrm{N\,m\,s\,rad^{-1}}$
'free'	FR	Device is not worn. Subjects wear only a loose safety harness.	-	-
'inactive'	IN	Device is worn but power off, acting as dead weight. Here the effect of added mass on task performance is tested, serving also as baseline for the conditions in which the device is worn.	-	-
'gimbal locked'	GL	Device is worn with rotor spinning, but controller off. Gimbal position is kept in place to test the effect of self-induced, or *parasitic*, torques).	-	-
'spring-damper'	S-D	Device is worn and active with an assistive controller, consisting of a continuous visco-elastic field (rotational spring and damper). Controller is intended to maintain a user-determined reference posture, while reducing sudden torso movements.	100	30
'damper'	D	Device is worn and active with an assistive controller, consisting of a continuous viscous field (rotational damper). Controller is intended to reduce sudden torso movements without affecting subject's posture.	0	30
'spring'	S	Device is worn and active with an assistive controller, consisting of a continuous elastic field (rotational spring). Controller is intended to maintain a user-determined reference posture.	100	0
'negative damper'	ND	Device is worn and active with an error-augmenting controller, consisting of a continuous additive viscous field (negative rotational damper). Controller augments sudden torso movements.	0	-30

[1] K_p: proportional gain (rotational spring stiffness). K_d: derivative gain (rotational damper viscosity).

Supplementary Table 4.AII: Experiment 1 description of controllers and conditions.

Outcome measures	Symbol	Units	$\tilde{x}(^{P_{75}}_{P_{25}})$[1] 'free' (FR)	'inactive' (IN)	'gimbal locked' (GL)	'spring-damper' (S-D)	'damper' (D)	'spring' (S)	'negative damper' (ND)
Distance walked, x									
Raw	x	m	$0.975(^{1.500}_{0.750})$	$0.675(^{1.250}_{0.300})$	$0.600(^{0.700}_{0.300})$	$1.600(^{2.500}_{0.700})$	$2.300(^{3.600}_{1.000})$	$0.800(^{1.400}_{0.600})$	$0.300(^{0.600}_{0.300})$
Normalized [2]	x/x_{IN}	-	$1.7(^{2.2}_{1.25})$	1	$0.777(^{2}_{0.533})$	$2(^{2.83}_{1.25})$	$2(^{3.2}_{1.25})$	$1.65(^{2}_{0.8})$	$0.49(^{1}_{0.364})$
Trunk roll angle, ϕ									
RMS	ϕ_{RMS}	deg	-	$3.499(^{6.655}_{2.792})$	$3.563(^{4.838}_{2.376})$	$3.636(^{4.439}_{2.164})$	$5.613(^{6.421}_{3.924})$	$3.650(^{9.982}_{2.763})$	$3.478(^{4.527}_{1.492})$
Peak	ϕ_{peak}	deg	-	$7.933(^{15.916}_{5.646})$	$9.674(^{11.997}_{4.807})$	$9.285(^{18.738}_{5.984})$	$13.083(^{15.409}_{12.335})$	$11.495(^{22.993}_{6.726})$	$7.654(^{14.297}_{3.165})$
Excursion	$\Delta(\phi)$	deg	-	$10.562(^{28.449}_{7.628})$	$12.646(^{18.055}_{4.586})$	$12.108(^{25.461}_{9.414})$	$22.073(^{24.184}_{15.945})$	$18.220(^{30.779}_{10.520})$	$9.351(^{18.001}_{3.017})$
Centroidal Frequency	$\bar{f}(\phi)$	Hz	-	$0.515(^{0.654}_{0.387})$	$0.621(^{0.963}_{0.494})$	$0.397(^{0.458}_{0.352})$	$0.349(^{0.370}_{0.343})$	$0.478(^{0.594}_{0.380})$	$0.671(^{1.355}_{0.607})$
Trunk roll angular velocity, $\dot{\phi}$									
RMS	$\dot{\phi}_{\mathrm{RMS}}$	deg/s	-	$5.519(^{10.554}_{3.848})$	$8.370(^{10.414}_{7.393})$	$6.008(^{7.893}_{4.774})$	$8.892(^{10.699}_{7.339})$	$10.220(^{13.830}_{7.182})$	$7.529(^{14.149}_{4.953})$
Peak	$\dot{\phi}_{\mathrm{peak}}$	deg/s	-	$17.398(^{47.522}_{14.357})$	$28.691(^{35.520}_{16.726})$	$24.357(^{32.730}_{17.240})$	$28.972(^{34.741}_{21.406})$	$36.099(^{65.669}_{20.872})$	$23.460(^{51.215}_{14.788})$
Gyroscopic torque, τ									
RMS	τ_{RMS}	Nm	-	-	$0.136(^{0.201}_{0.019})$	$3.219(^{3.797}_{2.645})$	$3.263(^{4.413}_{2.307})$	$2.947(^{3.026}_{2.065})$	$1.456(^{2.439}_{0.756})$
Percentage of Max		%	-	-	$0.314(^{0.463}_{0.0435})$	$7.43(^{8.76}_{6.1})$	$7.53(^{10.2}_{5.32})$	$6.8(^{6.98}_{4.76})$	$3.36(^{5.63}_{1.74})$
Peak	τ_{peak}	Nm	-	-	$0.993(^{1.196}_{0.177})$	$16.234(^{18.337}_{11.288})$	$13.809(^{21.282}_{9.616})$	$11.740(^{16.864}_{6.590})$	$7.341(^{9.341}_{2.740})$
Percentage of Max		%	-	-	$2.29(^{2.76}_{0.408})$	$37.5(^{42.3}_{26})$	$31.9(^{49.1}_{22.2})$	$27.1(^{38.9}_{15.2})$	$16.9(^{21.6}_{6.32})$
Exchanged angular momentum, ΔH									
RMS	ΔH_{RMS}	Nms	-	-	$0.032(^{0.039}_{0.019})$	$3.119(^{4.620}_{1.712})$	$1.046(^{1.761}_{0.605})$	$3.583(^{5.785}_{1.702})$	$0.284(^{0.819}_{0.126})$
Percentage of Max		%	-	-	$0.337(^{0.478}_{0.0243})$	$34.7(^{54.1}_{18.9})$	$12.2(^{20.7}_{7.07})$	$41.5(^{64.3}_{20.5})$	$3.34(^{9.39}_{1.69})$
Peak	ΔH_{peak}	Nms	-	-	$0.106(^{0.135}_{0.022})$	$8.760(^{8.819}_{4.425})$	$4.579(^{6.410}_{2.374})$	$8.609(^{8.828}_{5.421})$	$1.098(^{2.717}_{0.384})$
Percentage of Max		%	-	-	$1.1(^{1.61}_{0.0546})$	$102(^{102}_{44.2})$	$53.4(^{75.3}_{27.6})$	$98.1(^{99.5}_{64.1})$	$11.3(^{30.9}_{4.7})$
Geometric Saturation									
Ocurrences[3]		% (n)	-	-	-	70 (7)	10 (1)	60 (6)	0 (0)
Lead to failure		% (n)	-	-	-	71.4 (5)	0 (0)	83.3 (5)	0 (0)
Exchanged mean power $\bar{P}$		W	-	-	$-0.011(^{-0.001}_{-0.020})$	$-0.249(^{-0.163}_{-0.319})$	$-0.416(^{-0.225}_{-0.734})$	$-0.152(^{-0.107}_{-0.229})$	$0.164(^{0.462}_{0.057})$
Perception AHP ranking[4]			-	-	⋆⋆⋆	⋆⋆⋆⋆	⋆⋆⋆⋆⋆	⋆⋆	⋆

[1] Median of the recorded data with its 25^{th} and 75^{th} percentiles showed in parentheses.
[2] With respect to baseline condition 'inactive' (IN).
[3] Percentage of subjects who experienced geometric saturation (number of subjects in parentheses).
[4] Ranking from worst (⋆) to best (⋆⋆⋆⋆⋆) using the Analytic Hierarchy Process (AHP).

Supplementary Table 4.AIII: Experiment 1 group metrics.

		$\tilde{x}(^{P_{75}}_{P_{25}})$	
Condition	Trial	Distance walked (m)	Learning Rate [1]
'free' (FR)	Initial	$0.775(^{1.600}_{0.600})$	$1.267(^{1.667}_{1.000})$
	Final	$1.050(^{2.100}_{0.750})$	
'inactive' (IN)	Initial	$0.600(^{1.250}_{0.300})$	$0.860(^{1.833}_{0.500})$
	Final	$0.675(^{1.000}_{0.300})$	

[1] Computed as the median of 'Final'/'Initial' for each subject. Values > 1 indicate possible learning.

Supplementary Table 4.AIV: Experiment 1 learning effects.

Experiment 2

Task	BoS[1] cm	Eyes	Basis for Comparison[2]
Walking (constrained ML BoS)[3]			
Virtual beam	20	Open	
Virtual beam	10	Open	S4
Foam beam	8	Open	S1-3, S5, H1-5
Standing (constrained ML BoS)[4]			
Static stance	full	Open	
Static stance	full	Closed	S1-5, H1-5
Standing (constrained AP BoS)[5]			
Flat surface	full	Open	
Flat surface	full	Closed	
Wooden block	10	Open	
Wooden block	10	Closed	
Wooden block	6	Open	S1-2, S4-5
Wooden block	6	Closed	S3
Wooden block	4	Open	H1, H3-5
Wooden block	4	Closed	H2

[1] Base of Support size in constrained direction.
[2] The test selected for comparison for each subject was the most difficult in which all three conditions were attempted. After failing to achieve the maximum score on a test, subjects were permitted to attempt only one level of difficulty higher.
[3] Tandem walking over a 2.5 m beam. BoS is width of delineated virtual beam or foam gymnastics beam.
[4] Tandem stance on a flat surface with no BoS restriction.
[5] Feet placed hip-width apart. BoS is standing on either flat ground or a wooden block with toes and heels overhanging.

Supplementary Table 4.AV: Experiment 2 tasks description.

			$\tilde{x}(^{P_{75}}_{P_{25}})$[1]					
			Healthy			Stroke		
Metric	Symbol	Units	'free' (FR)	'inactive' (IN)	'damper' (D)	'free' (FR)	'inactive' (IN)	'damper' (D)
Duration								
Raw	t	s	$22.964(^{43.546}_{16.141})$	$21.727(^{35.637}_{13.420})$	$50.024(^{120.000}_{43.674})$	$2.735(^{7.581}_{1.810})$	$4.061(^{5.869}_{2.346})$	$4.334(^{44.843}_{4.216})$
Normalized[2]	t/t_{IN}	-	$0.951(^{1.637}_{0.641})$	$1.000(^{1.000}_{1.000})$	$3.135(^{4.705}_{2.450})$	$1.025(^{1.308}_{0.779})$	$1.000(^{1.000}_{1.000})$	$2.466(^{7.798}_{1.487})$
Trunk pitch angle, θ								
RMS	θ_{RMS}	rad	$0.195(^{0.386}_{0.158})$	$0.084(^{0.096}_{0.066})$	$0.069(^{0.147}_{0.065})$	$0.182(^{0.226}_{0.077})$	$0.075(^{0.141}_{0.055})$	$0.214(^{0.242}_{0.122})$
Peak	θ_{peak}	rad	$0.738(^{0.861}_{0.631})$	$0.194(^{0.233}_{0.149})$	$0.265(^{0.288}_{0.174})$	$0.352(^{0.500}_{0.142})$	$0.158(^{0.262}_{0.090})$	$0.338(^{0.353}_{0.259})$
RMS vel	$\dot{\theta}_{\mathrm{RMS}}$	rad/s	$0.292(^{0.524}_{0.237})$	$0.129(^{0.186}_{0.078})$	$0.085(^{0.121}_{0.068})$	$0.240(^{0.486}_{0.093})$	$0.287(^{0.358}_{0.066})$	$0.119(^{0.169}_{0.091})$
Peak vel	$\dot{\theta}_{\mathrm{peak}}$	rad/s	$2.367(^{3.692}_{1.333})$	$0.433(^{0.571}_{0.270})$	$0.363(^{0.509}_{0.300})$	$0.926(^{2.730}_{0.247})$	$0.566(^{0.814}_{0.177})$	$0.301(^{0.731}_{0.270})$
Centroidal frequency	$\bar{f}(\theta)$	Hz	$0.329(^{0.616}_{0.283})$	$0.341(^{0.499}_{0.252})$	$0.288(^{0.342}_{0.272})$	$1.391(^{2.493}_{0.770})$	$0.906(^{1.757}_{0.572})$	$0.717(^{0.746}_{0.273})$
Centre of pressure, CoP								
RMS	$\mathrm{CoP}_{\mathrm{RMS}}$	mm	$7.194(^{8.140}_{6.396})$	$6.758(^{7.214}_{4.724})$	$5.867(^{6.804}_{4.461})$	$7.718(^{13.299}_{3.758})$	$6.305(^{8.045}_{3.309})$	$5.669(^{11.299}_{4.876})$
Peak	$\mathrm{CoP}_{\mathrm{peak}}$	mm	$17.077(^{20.814}_{13.394})$	$14.100(^{17.288}_{11.778})$	$15.950(^{19.205}_{12.008})$	$13.667(^{24.617}_{8.347})$	$15.828(^{18.351}_{7.822})$	$16.211(^{23.487}_{9.340})$
RMS vel	$\frac{\mathrm{d}}{\mathrm{d}t}\mathrm{CoP}_{\mathrm{RMS}}$	mm/s	$54.077(^{60.904}_{49.637})$	$50.609(^{54.296}_{36.142})$	$39.837(^{44.032}_{37.024})$	$51.004(^{113.281}_{49.753})$	$76.940(^{80.634}_{34.782})$	$51.867(^{64.415}_{44.326})$
Peak vel	$\frac{\mathrm{d}}{\mathrm{d}t}\mathrm{CoP}_{\mathrm{peak}}$	mm/s	$215.225(^{252.978}_{182.600})$	$167.883(^{212.468}_{139.032})$	$172.109(^{211.995}_{143.182})$	$214.822(^{302.070}_{174.384})$	$220.309(^{253.768}_{120.204})$	$199.492(^{326.645}_{168.328})$
Centroidal frequency	$\bar{f}(\mathrm{CoP})$	Hz	$0.814(^{1.101}_{0.746})$	$0.689(^{0.790}_{0.609})$	$0.768(^{0.803}_{0.597})$	$1.696(^{4.063}_{0.716})$	$1.475(^{2.071}_{0.929})$	$0.878(^{1.008}_{0.718})$
Gyroscopic moment, τ								
RMS	τ_{RMS}	Nm	-	-	$1.636(^{2.774}_{1.049})$	-	-	$1.934(^{3.445}_{1.373})$
Peak	τ_{peak}	Nm	-	-	$13.296(^{18.565}_{7.463})$	-	-	$6.687(^{20.061}_{5.870})$
Exchanged angular momentum, ΔH								
RMS	ΔH_{RMS}	Nms	-	-	$0.687(^{1.359}_{0.279})$	-	-	$1.024(^{1.672}_{0.471})$
Peak	ΔH_{peak}	Nms	-	-	$4.879(^{7.453}_{1.533})$	-	-	$1.946(^{5.387}_{1.385})$

[1] Median value with 25^{th} and 75^{th} percentiles shown in parentheses. For vector quantities, only the AP component is reported.

[2] With respect to baseline condition 'inactive' (IN).

Note that in Experiment 2 the weight of the GyBAR was partially unloaded in conditions 'inactive' (IN) and 'damper' (D) for both groups, whereas in Experiment 1 the full weight was borne in all conditions but 'free' (FR).

Supplementary Table 4.AVI: Experiment 2 group metrics (AP standing task only).

Subject	Group[1]	t_D / t_{IN}	$\dot{\theta}_{peak,D} / \dot{\theta}_{peak,IN}$	RPE_D-RPE_{IN}[2]
H1	A	3.70	0.70	+0
H2	A	7.71	1.22	+1
H3	A	3.14	1.81	-1
H4	B	1.85	0.66	+0
H5	B	2.65	0.48	+1
S1	B	2.47	1.36	+2
S2	A	1.63	0.15	+0
S3	A	1.07	0.45	+2
S4	B	23.30	1.28	+0
S5	B	2.63	13.61	-1

[1] Group testing orders. Group A: FR-IN-D. Group B: FR-D-IN.
[2] An increase in Borg rating (RPE) indicates greater perceived exertion [16].

Supplementary Table 4.AVII: Experiment 2 investigation of temporal effects for the AP standing task.

5

General Conclusions, Discussion and Future Directions

5.1 | General Conclusions

The goal of this thesis was to assess the feasibility of a control moment gyroscope based (CMG) upper-body actuator as balance assistance device in individuals with balance disorders. Based on the findings presented in this thesis I conclude:

- Wearable upper-body CMGs effectively augment balance.
- Only 32 % of the output torque capacity of the GyBAR was used to assist balance.
- Feedback based on inertial upper body sensors is sufficient for effective balance assistance.

5.2 | Discussion

5.2.1 | Wearable upper-body CMGs effectively augment balance

I have shown, for the first time, that wearable CMGs in the upper-body, such as the GyBAR, are capable of improving balance performance of able-bodied and post-stroke individuals. Our results showed that balance was augmented by median factors of 2-3, based on simple and reliable outcome measures for a series of challenging standing and walking balance tasks, as documented in Chapter 4. In addition to the proven feasibility of the GyBAR as balance assistive device, I further conclude

- Attenuating torso oscillations with the GyBAR effectively augments balance.
- Unintended parasitic and off-axis torques do not influence GyBAR balance assistance.
- Potential GyBAR beneficiaries are expected to have sufficient muscle strength to ambulate without physical assistance.
- The GyBAR can be adapted to home and/or clinical settings.

Attenuating torso oscillations with the GyBAR effectively augments balance

To assess the GyBAR's feasibility as balance assistive device, I implemented a set of simple continuous controllers based on trunk angular position and velocity to regulate posture with a virtual spring and spring-damper (posture dependent controllers) and attenuate velocity with a virtual damper (posture-independent controller). Experiments with healthy individuals presented in Chapter 4 showed that, from these set of tested continuous controllers, the damping controller resulted in better task performance compared to the posture-dependent controllers. In addition, only the damper controller consistently improved balance across all subjects, opposed to the posture dependent controllers where some individuals exhibited lower performance compared to their baseline. This was surprising as I expected that a controller regulating trunk angular position would perform best, given its close relation with the center of mass (CoM) as the behavior of an inverted pendulum was assumed. However, data from these low-performance

individuals suggested that postural changes present during the balance task, such as postural biases, asymmetries and low frequent drift trough weight shifting, resulted in constant bias torques for the posture-dependent controllers. As a consequence, the GyBAR constantly reached its limit in the exchange of angular momentum (i.e. geometric saturations) generating a non-continuous (and thus unpredictable) assistance, explaining the low performance.

In contrast, the damper controller showed to be robust to these postural changes as trunk angular velocity does not depend on angular position biases. Here its response to only rapid changes in posture resulted in lower exchange of angular momentum, not being affected by the geometric saturations and therefore exhibiting better performance (Chapter 4). This was particularly advantageous for the GyBAR given its limited ability of continuous torque generation. Although these results did not present sufficient evidence to confirm or reject the hypothesis of the best performing posture-dependent controllers, they indicate that balance can be effectively assisted by damping trunk excursions in both able-bodied and post-stroke individuals.

Unintended parasitic and off-axis torques do not influence GyBAR balance assistance

Both off-axis and parasitic torques are effects inherent to the GyBAR's single CMG dynamics. These torques, however, did not have a significant incidence in the overall performance of the GyBAR, given that balance was effectively augmented for both able-bodied and post-stroke individuals. In fact, they only accounted for a small fraction of the peak assisted torque (15 % for off-axis and 12.5 % for parasitic torques) about the axis orthogonal to the desired output torque in the transverse plane as found in the results from the experiments in Chapter 4. This is also supported by the results of condition 'gimbal locked' in the experiments in Chapter 4, where the effect of parasitic torques was tested fixing the gimbal rotation while the flywheel was spinning. Here balance performance did not show any significant difference with that of the baseline condition 'inactive', in which participants were wearing the GyBAR as a dead weight.

Despite their insignificant influence on balance performance, reducing the effects of these unintended torques have several advantages. This can be achieved, for example, by adding a synchronized second CMG to counteract off-axis torques and diminish the effect of parasitic torques. Counteracting off-axis torques enable wider gimbal excursions diminishing the effect of geometric saturations and increasing actuation time. In consequence, not only higher peak torques and longer actuation torques can be achieved, but better performance can be expected from the implementation of posture-dependent controllers (spring and spring-damper). In turn, smaller parasitic torques result in the reduction of potentially undesired balance artifacts such as weight shifting, trunk flexion/extension and trunk rotation due to parasitic torques projected into the sagittal, frontal and longitudinal axes respectively.

Finally, it is worth noting that although the results showed evidence of insignificant influence of these unintended torques on balance performance, they were limited to very specific balancing tasks. Further research in normal gait and activities of daily living (ADLs) is required to generalize these claims.

Potential GyBAR beneficiaries are expected to have sufficient muscle strength to ambulate without physical assistance

The experimental results presented in Chapter 4 suggest that both able-bodied and post-stroke individuals benefited from augmented balance while wearing the GyBAR. Although further research is required to generalize these findings, there are indications that the GyBAR can be used to develop new therapy interventions for a wide variety of balance disorders. In particular, disorders caused by neurological conditions that can benefit from the GyBAR include stroke, spinal cord injury, Parkinson's disease, vestibular dysfunction, and cerebral palsy, or the elderly with a history of falling. Not only the GyBAR would enable a higher balance response time by temporarily delaying sudden trunk motions, but could effectively compensate degraded postural control caused by increased trunk stiffness [166] through active damping.

Given that the GyBAR is not intended to (i) replace the wearer's ability of balance recovery or (ii) augment strength or weight-bearing capabilities, individuals exhibiting severely reduced muscle strength, such as those affected by severe neurological impairments, would not benefit from the GyBAR. Beneficiaries are therefore expected to have sufficient muscle strength and postural control to ambulate without physical assistance, such that the complementary balance control from the GyBAR enables self-generation of appropriate corrective responses.

The GyBAR can be adapted to home and/or clinical settings

Given the GyBAR capabilities of assisting balance and the findings about lower performance requirements, its adaptation to clinical and home settings seems possible. Compared to currently implemented robotic solutions, such as exoskeletons and mobile body-weight support systems (mobile BWS), the realization of a compact and light GyBAR exhibits interesting benefits that would make it more appealing for clinical and home settings. First the GyBAR free-torque exertion allows a direct and flexible collocation along the upper-body or any other body segment: it does not require structures connected to the ground or subsequent bodies. As a consequence it exhibit significant advantages over exoskeletons and BWS, (i) minimal device fitting and preparation: joint alignment is not required (ii) simpler device-user interface: it only requires to be attached to a single body segment (iii) greater unrestricted movement: suitable for ambulation in curves, uneven terrain and stairs. Second the GyBAR torque amplification principle enables more compact realizations with higher torque-to-weight ratios compared to exoskeletons. As an example, the simplest commercial exoskeleton, the HONDA Stride Management Assist system (SMA), has a peak actuation torque in the thigh of 4 N m with a mass of 2.7 kg. Comparatively, a GyBAR attached to the thigh with similar peak torque as the SMA could be realized with less weight and a small footprint(4 N m, 2 kg and 6 cm^3).

It is important noting that a GyBAR in the thigh (or any other body segment) would be comparatively bulkier than an exoskeleton given its spherical footprint. However, the use of multiple smaller CMGs can further reduce bulkiness while maintaining the same desired output torque. Thanks to its unique actuation capabilities and its simpler and versatile use, the GyBAR has a big potential in clinical and home settings.

5.2.2 | Only 32 % of the output torque capacity of the GyBAR was used to assist balance

Experimental results presented in Chapter 4 showed that only a third of the GyBAR maximum torque capacity was used to assist balance. Based on these results and the design methodology presented on Chapter 3, I further conclude:

- The GyBAR was overdimensioned
- Lighter and smaller CMGs for effective balance assistance can be realized
- Multiple CMGs could enable better GyBAR actuation and collocation

The GyBAR was overdimensioned

The GyBAR was initially designed based on an overly conservative simplification of a falling human as an inverted pendulum as described in Chapter 3. Based on this simplification, a target actuation torque of around 90 Nm was set for a single CMG which resulted in the subsequent design and realization of the current GyBAR. Interestingly, the experimental results presented in Chapter 4 showed, for the first time, that a lower torque in the upper body was required for effective balance assistance; only 32 % of the maximum output torque was exploited with only 53 % of the available angular momentum. As a result, I concluded that the current GyBAR was overdimensioned given that only a fraction of its maximum capabilities were used. As a consequence, lighter and more compact CMGs can be realized which, in turn enable their implementation in better configurations aiming for an overall lighter and more compact GyBAR.

Lighter and smaller CMGs for effective balance assistance can be realized

Being momentum exchange devices, CMGs require high angular momenta to generate usable output torques implying a trade-off between flywheel size, weight and angular speed, as described in Chapter 3. This trade off can be exemplified by analyzing different possible realizations of our current GyBAR as shown in Fig. 5.1. Here different flywheel materials are used to show the effect of size and weight on gyroscopic performance (angular momentum and maximum output torque), based on the characteristics of our current GyBAR flywheel and gimbal motors. Points A and B, for example, show alternative flywheel realizations for the current GyBAR performance. Here, a size reduction of 26 % (Point B) and 41 % (Point A) is possible with an increase of mass of 14 % and 26 % for steel and densimet respectively. Points C, D and E in Fig. 5.1 show different flywheel realizations based on the new target performance of 5 N m (Chapter 4). Compared to the current GyBAR, size and weight are reduced respectively by 52 % and 33 % for densimet, 42 % and 41 % for steel and 20 % and 50 % for aluminum. Densimet is therefore the most favorable flywheel material as it has the highest size reduction. As a consequence, much more compact and therefore lighter gimbal structures can be realized, compensating the previously mentioned lower mass reduction compared to steel and aluminum flywheels.

It is important to mention that additional improvements in weight and size are possible if friction sources are diminished. Alternatives such as the use of magnetic bearings and/or a vacuumized flywheel chamber will increase flywheel speeds and therefore

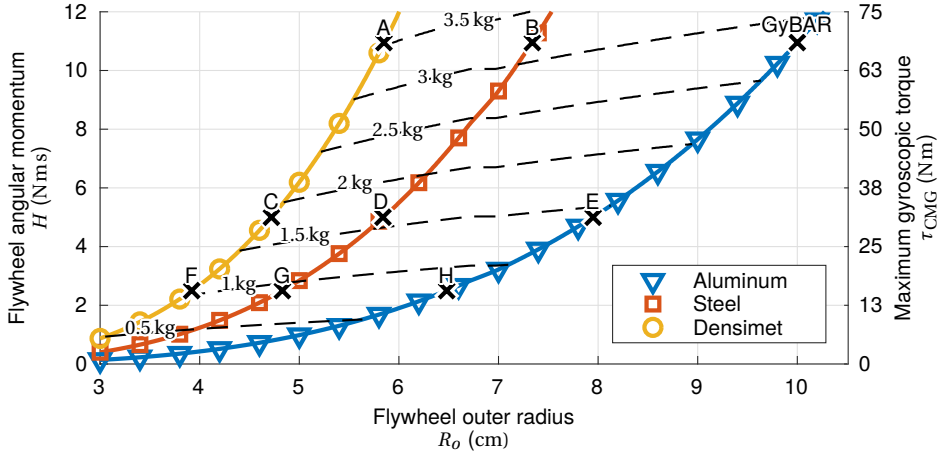

Figure 5.1: Effect of different flywheel materials and outer radii in actuation performance for the current GyBAR (Maximum angular momentum and gyroscopic torque). Actuation performance was calculated based on the current GyBAR input power for both gimbal and flywheel motors. Corresponding flywheel mass is found as the intersection of the dashed iso-lines with any of the depicted materials. Note that flywheel-size reduction results in an increase of mass for a fixed actuation performance, which in turn causes a reduction in flywheel torque-to-weight ratio. Points A and B show alternative realizations of the current GyBAR (point GyBAR) with densimet and steel, maintaining the current actuation performance. Points C, D and E depict flywheel realizations for the new target performance found from experiments presented in Chapter 4. Points F, G and H show smaller flywheels with half the target performance of points C, D and E.

decrease size and weight. With all these improvements in denser flywheel materials, smoother flywheel suspensions and reduced air pressure in the flywheel chamber, reduction in size and weight will have a positive impact in usability as a more compact GyBAR can be realized.

Multiple CMGs could enable better GyBAR actuation and collocation

Aiming for a very compact GyBAR, the use of multiple small CMGs is appealing for various reasons: (i) unlike big CMGs, small ones can be located in unobtrusive places. (ii) parasitic and off-axis torques compensation (iii) longer sustained torque generation in a single axis. First argument exploits even more the advantage of CMG's free-torque actuation. Given that an inertial frame is not needed to transmit the generated torque, smaller CMGs can be better collocated anywhere in the desired body segment. For instance, an alternative to our current GyBAR could be a less obtrusive arrange of small CMGs distributed around the waist. Second, configurations of multiple CMGs in which the gimbals are electrically or mechanically synchronized can cancel out off-axis torques and diminish the effect of parasitic torques [21, 35]. Third, longer sustained single axis actuation is possible as a consequence of off-axis torques compensation. Given that limits on gimbal excursions are not longer needed to diminish the effect of off-axis torques,

actuating torques can be held longer being limited only by singular configurations[1].

Despite the mentioned benefits of an assembly of multiple CMGs, it is worth noting that overall torque-to-weight ratio of such assembly is inherently lower than that of a single bigger unit with similar output torque. This can be seen in points F, G and H in Fig. 5.1 where using 2 CMGs with half the new target performance result in an overall heavier configuration. Moreover, this reduction of torque-to-weight ratio is worsened as multiple stand-alone CMGs require individual gimbal motors with their respective structures. A clever design where structural components are shared between CMGs can mitigate this increase in weight. Despite the inherent reduction in torque-to-weight ratio, a GyBAR with multiple small CMGs is a viable choice given the greater benefits of better actuation and versatile collocation.

5.2.3 | Feedback based on inertial upper body sensors is sufficient for effective balance assistance.

Results from this thesis not only have shown that the use of a single upper body inertial sensor (IMU) is sufficient to accurately estimate center of mass velocity (Chapter 2), but also that simple torso angular velocity sensing proved to be sufficient for effective balance assistance (Chapter 4). From these findings I further conclude:

- Simple trunk angular velocity sensing suffices effective continuous controllers.
- Single upper body IMU enables the implementation of CoM-velocity based controllers.

Simple trunk angular velocity sensing suffices effective continuous controllers

The simple and effective continuous controllers presented in Chapter 4 relied on rather simple information of the trunk's angular position and velocity. This resulted advantageous aiming for portability of the GyBAR, as a single IMU could be embedded in the GyBAR embodiment. Interestingly, the damper controller being the best performer also showed to be the easiest to implement. Given that only feedback from the trunk angular velocity was required, the raw output of the gyroscopic sensor from the IMU was sufficient. Conversely, the posture-dependent controllers (spring and spring damper) required state estimation from the fusion of the different sensor types as trunk angular position cannot be directly measured. In practice, however, this is not an issue as this state estimation is a feature that most commercially available IMUs have already implemented. Therefore, single upper-body IMU are suitable for the implementation of simple continuous controllers.

Single upper body IMU enables the implementation of CoM-velocity based controllers

From the developments of this thesis in Chapter 4, it is clear that simple and effective continuous controllers can be easily implemented by readily available IMU sensors. However, many other balance control approaches for both humans and biped robots

[1] Configuration in which the flywheel spin axis is aligned with the desired torque axis

are based on CoM-based stability measures, particularly CoM-velocity [22, 52, 133, 143, 204]. The implementation of CoM metrics enable control paradigms that, for example, provide just the necessary support to recover balance once loss-of-balance is detected [204] or assist balance by regulating the body linear and angular momenta [113]. Unlike the simple controllers implemented in this thesis, CoM-velocity based controllers require additional information that cannot be directly measured by the GyBAR embedded IMU. Although this was particularly challenging for the GyBAR, the method presented in Chapter 2 showed that based on a single upper-body IMU, CoM velocity and position can be estimated. These results not only enable the implementation of CoM velocity-based controllers in the GyBAR, but also the assessment of stability measures (e.g. extrapolated CoM, foot placement estimator, stabilizing and destabilizing forces, etc. [23]).

It is worth noting that many limitations have to be addressed prior the implementation of the method presented in Chapter 2 with CoM velocity-based assistive controllers. First, the proposed observer was most sensitive to input model parameters, such as spring stiffness and leg length. Although leg length can be measured relatively accurately, the spring stiffness used in the model is very difficult to measure as there is no clear physiological correspondence with actual leg stiffness. Here a simpler model such as the linear inverted pendulum (LIP) could prove to be more robust, given that its parameters can be more accurately calculated. Second, the dynamic model was limited to estimations in 2D for anterior-posterior walking. Here a similar decoupled 2D model could be used for the frontal plane, although its estimation accuracy still remains to be investigated.

5.3 | Future directions

This thesis presented the feasibility of CMG-based actuators as balance assistive devices in human beings, particularly those with balance disorders. However, there are still many open questions to be addressed regarding its use in rehabilitation and other future applications.

5.3.1 | The GyBAR in rehabilitation.

Based on the promising results presented in this thesis and its actuation uniqueness, I believe that a lighter and more compact GyBAR can be a very useful tool in rehabilitation. Pursuant to this, the following issues should be addressed:

Minimum effective amount of assistance Aiming for lighter and more compact devices, the question of the minimum amount of effective assistance arises. Results presented in this thesis only quantified the torque necessary to effectively assist balance in very specific balance tasks. It is important to note that this minimum amount of assistance might be subject-dependent, based not only on physiological characteristics (weight, height, etc.) but also on balance capabilities. This could be seen partially in the results presented in Chapter 4, where big variability was exhibited during the assistive conditions despite the overall balance improvement. However, it is still unclear what this minimum level of assistance is and its relation to physiological characteristics or balance capabilities. The realization of a study involving subjects grouped by physiological and patho-

logical characteristics with decreasing assisting torques could help to identify the lower limit in required assistance and its relationship with the individual's characteristics, if any. These results could enable the realization of lighter and more compact CMGs improving usability.

GyBAR as training device: Although the GyBAR presented in this thesis targeted primarily continuous balance assistance, it can be potentially used in training. Thanks to its versatile actuation, the GyBAR is suitable for the implementation of training paradigms such as: (i) assist-as-needed, where only the necessary assistance is provided and (ii) error augmentation force fields. These paradigms not only encourage patients to actively participate during training, but also provide sufficient challenge and progressive adaptation which can increase motor learning [51, 107]. This is supported by evidence of improvement in clinical measures with post-stroke individuals using active treadmill-based BWS systems [107, 192].

Effectiveness in representative tasks: Results presented in this thesis were based on a rather constrained set of tasks. Although they were based on validated clinical balance characterization tests, the effectiveness of the GyBAR in more representative tasks still remains to be evaluated. Therefore, further studies with ADL's and more extensive clinical tests are required.

Metabolic cost: Although the GyBAR was able to improve balance significantly respect to the doffed condition, its impact in energy expenditure is unclear. Particularly, the GyBAR considerable mass might have had an impact in the metabolic cost as the added mass accounted for more than 15 % of the subjects body weight [72]. Thus, the impact of a lighter GyBAR remains to be investigated.

5.3.2 | Future applications

The findings presented in this thesis open the way for further implementation of the GyBAR in different settings and applications. As first step home use of the GyBAR and its implementation as actuator in other body segments are here introduced.

GyBAR in home use: The GyBAR prototype presented in this thesis was primarily designed assess its balance assistance capabilities and it was not optimized for mass, size or usability. Targeting home use several issues need to be addressed. (i) Weight and size: A compact and light wearable device not only improves usability but also comfort and aesthetics. (ii) Wearability and ergonomics: Although the GyBAR currently does not restrict movements while using it during balance tasks, it should not interfere significantly with the user's regular activities (Sitting down, tying a shoe, going to the toilet, amongst other ADLs). In addition users should be able to easily don and doff the GyBAR without any assistance. (iii) Battery life: Ideally the GyBAR should be able to operate autonomously during a whole day. Still, this would require a very heavy battery arrange making it impractical. Moreover, alternative commercial robotic wearable devices, such as the HONDA SMA [85] guarantee only 1 hour of battery autonomy.

Gyroscopic assistance in other body segments Thanks to its wearability and versatile collocation, different realizations of the GyBAR can be used to assist movements in body

segments other than the torso. Current reasearch include applications such as hand tremor supression for individuals with Parkinson's disease [157] and foot placement assistance thanks to lower limb prostheses/orthoses. The later research is currently being developed at the TUD where one of the main features exploited is CMGs reactionless actuation compared to joint torques generated by traditional powered orthoses-prostheses.

Acknowledgements

It has been a long journey over the past five years and this dissertation shows an important part of it. The words captured in this dissertation not only represent my contribution to science, but are the result of the interaction with wonderful people that helped me throughout the years. This small chapter is dedicated to them.

I would like to start by thanking my promotor Heike Vallery who not only has been an incredible mentor, both academically and personally, but also a person who I particularly admire. Thanks to her I have grown intellectually and personally. I have enjoyed our deep discussions about dynamics, and even more our talks about equality and science. Thank you Heike for showing me how good research is made. I would also like to thank my promotor Frans van der Helm, who shared with me a tiny part of his valuable experience and knowledge. Thank you for our deep conversations about science and our bike rides in the Groene Hart, the Ardennes and the Eifel.

I would also like to thank the guys at the Delft BioRobotics Lab. To Andy, Wouter, Mukunda, Michiel, Carlos, Joost, Gijs, Saher and Patricia, thank you for all the deep and no so deep lunch conversations, the outings, and most importantly the lab clean-ups!. Thanks to Michiel for getting me into chess, which became an obsession. Thanks to Wouter and Mukunda for the nice chess games. To Joost, Patricia, Saher and Carlos thank you for the laughs and nice lunch conversations. To the support engineers at 3ME and DEMO, Jan, Nisse, Simon, Cor, Giel, Lars and Andries, thank you for all your effort in the realization and maintenance of the prototypes. Without you guys this work would have not been possible.

To Andy Berry, who was a fundamental part of the project, thank you for putting your expertise and valuable knowledge to help me during the development and execution of the experiments. It was a pleasure sharing with you all the nice experiences during our trips to Chicago, from cooking to our home-sick trip to Holland, Michigan.

Special thanks to Arun Jayaraman and his staff at the Shirley Ryan Ability Lab. To Kristen, Lori and Chandra, thank you for all your support during the experiments. Thanks to you guys we manage to pull them out in only three weeks.

To my family who were there every step of the way, since I put my feet on a plane in 2012 pursuing a dream. Thank you for showing me the path and set me free to fly. Thank you for all the unconditional love. Thank you mom and dad for your prayers and unconditional support. Thank you for pushing me and letting me pursuit my dreams. To my little sister Mildred and my beloved brother Dario, thank you for being my role models.

To my grandparents Agustin, Ninfa María, Joaquin and Marina, who are not here anymore. I would have liked you to see me graduate, just as my beloved grandma Ninfa María wanted.

To my best friend Javier, thank you man for being there since I arrived to Delft. I enjoyed the lousy cooking, the picking, the beers, the bike rides and the chocolate cakes!. To my friend Oliver Lee. Thank you bro for showing me how fun a race bike is. Thank you for all the geeky conversations and all the computer lessons. Thank you for the company, the bike rides, the beers, the laughs and the tears. To my cycling friends Eliana, Lucas, German and Jelle, thank you for all the rides and the suffering.

Finally I would like to thank my beloved girlfriend Patricia who has been a very important part of my life in the past two years. You have been my strength during these final years. Thank you baby for all the deep conversations, the patience while I was away, and the push in the right direction when I needed it. A ti mi amor, mis Ojitos bonitos, gracias. Te amo con el alma y con el corazón. To your friends Carlos, Tim, Irene and Marieke, who I feel like my own, thank you for the company and the good times. To Mercedes, Salus, Cesar, Carmen, Victor and Boss, thank you for making me feel part of your family.

Thank you all for what has been the most rewarding journey of my life.

A mis padres, Imelda y Edgar, quiero decirles que estoy y estaré eternamente agradecido por su apoyo incondicional desde el día que puse un pie en un avión hacia Madrid hace 7 años. Gracias ma y pa por enseñarme a volar, gracias por mostrarme el camino y gracias por dejarme recorrerlo. A mis hermanos, gracias por ser mis modelos a seguir. Gracias por cuidarme e inculcarme el deseo de aprender. A mi hermana Mildred, tuga, gracias por ser ese ser maravilloso que siempre ha estado ahi para apoyarme, en las cosas buenas y en las malas. Siempre la veré como un ejemplo a seguir de integridad y perseverancia. A mi hermano Dario, gracias por su cariño y sus enseñanzas. Usted inculco en mi el gusanito de la ingeniería.

A mis tíos Andres, Pedro y Hector gracias por enseñarme, sin saberlo, perseverancia y tenacidad. A mis queridas tías, Mariana, Erlinda y Emperatriz gracias por su inmenso amor y sus cuidados que siempre me hicieron sentir como un hijo. Siempre las veré como mi figura materna. A mis queridos abuelos Ninfa María, Agustin, Marina y Joaquin que ya no estan con nosotros, gracias por su compañía durante mis primeros años de doctorado.

Finalmente, a mi amada abuelita Ninfa María, a la que extraño mucho, quisiera decirle que me hubiera gustado darle la felicidad de verme convertido en un "gran doctor".

Daniel Lemus
Delft, February 2019

References

[1] A. L. Adkin, J. S. Frank, M. G. Carpenter, and G. W. Peysar, *Postural control is scaled to level of postural threat,* Gait & Posture **12**, 87 (2000).

[2] A. L. Adkin, J. S. Frank, M. G. Carpenter, and G. W. Peysar, *Fear of falling modifies anticipatory postural control,* Experimental Brain Research **143**, 160 (2002).

[3] A. L. Adkin, J. S. Frank, and M. S. Jog, *Fear of falling and postural control in Parkinson's disease,* Movement Disorders **18**, 496 (2003).

[4] M. Afschrift, I. Jonkers, J. De Schutter, and F. De Groote, *Mechanical effort predicts the selection of ankle over hip strategies in nonstepping postural responses,* Journal of Neurophysiology **116**, 1937 (2016).

[5] Y. S. Al-Khabbaz, T. Shimada, and M. Hasegawa, *The effect of backpack heaviness on trunk-lower extremity muscle activities and trunk posture,* Gait & Posture **28**, 297 (2008).

[6] F. C. Anderson and M. G. Pandy, *Dynamic optimization of human walking,* Journal of biomechanical engineering **123**, 381 (2001).

[7] E. Aoki, H. Konosu, H. Kimura, T. Wojtara, and S. Shimoda, *Balance device,* (2012), u.S. Classification 601/112; International Classification A61H1/00; Cooperative Classification A63B21/15, A63B21/151, A63B21/153, A63B21/4009, A63B21/4043, A63B21/4025, A61H2201/5069, A61H2201/165, A63B26/003, A63B2220/24, A63B2220/16, A63B21/00178, A63B21/0058, A61H2201/5079, A63B21/225, A61H2201/5007, A61H2230/625, A63B21/0004, A61H3/00, A63B21/00181; European Classification A61H3/00.

[8] A. T. Asbeck, S. M. De Rossi, K. G. Holt, and C. J. Walsh, *A biologically inspired soft exosuit for walking assistance,* The International Journal of Robotics Research **34**, 744 (2015).

[9] N. S. BEDROSSIAN, J. PARADISO, E. V. BERGMANN, and D. ROWELL, *Steering law design for redundant single-gimbal control moment gyroscopes,* Journal of Guidance, Control, and Dynamics **13**, 1083 (1990).

[10] M. Benedetti, R. Piperno, L. Simoncini, P. Bonato, A. Tonini, and S. Giannini, *Gait abnormalities in minimally impaired multiple sclerosis patients,* Multiple Sclerosis **5**, pp. 363 (1999).

[11] N. Benjuya, I. Melzer, and J. Kaplanski, *Aging-Induced Shifts From a Reliance on Sensory Input to Muscle Cocontraction During Balanced Standing,* The Journals of Gerontology Series A: Biological Sciences and Medical Sciences **59**, M166 (2004).

[12] K. Berg, S. Wood-Dauphine, J. I. Williams, and D. Gayton, *Measuring balance in the elderly: Preliminary development of an instrument,* Physiotherapy Canada (2009), 10.3138/ptc.41.6.304.

[13] A. Berry, D. Lemus, R. Babuška, and H. Vallery, *Directional Singularity-Robust Torque Control for Gyroscopic Actuators,* IEEE/ASME Transactions on Mechatronics **21**, 2755 (2016).

[14] E. Bilgen and R. Boulos, *Functional Dependence of Torque Coefficient of Coaxial Cylinders on Gap Width and Reynolds Numbers,* Journal of Fluids Engineering **95**, 122 (1973).

[15] I. V. Bonan, F. M. Colle, J. P. Guichard, E. Vicaut, M. Eisenfisz, P. Tran Ba Huy, and A. P. Yelnik, *Reliance on visual information after stroke. Part I: Balance on dynamic posturography 1 1No commercial party having a direct financial interest in the results of the research supporting this article has or will confer a benefit upon the author(s) or upon any organization with which the author(s) is/are associated.* Archives of Physical Medicine and Rehabilitation **85**, 268 (2004).

[16] G. A. Borg, *Pyschophysical bases of physical exertion,* Medicine and Science in Sports and Exercise **14**, 377 (1982).

[17] A. K. Bourke and G. M. Lyons, *A threshold-based fall-detection algorithm using a bi-axial gyroscope sensor,* Medical engineering & physics **30**, 84 (2008).

[18] A. Bourke, K. O'donovan, and G. Olaighin, *The identification of vertical velocity profiles using an inertial sensor to investigate pre-impact detection of falls,* Medical engineering & physics **30**, 937 (2008).

[19] S. G. Brauer, M. Woollacott, and A. Shumway-Cook, *The Interacting Effects of Cognitive Demand and Recovery of Postural Stability in Balance-Impaired Elderly Persons,* The Journals of Gerontology Series A: Biological Sciences and Medical Sciences **56**, M489 (2001).

[20] L. Brennan, *Means for imparting stability to unstable bodies,* (1905).

[21] D. Brown and M. A. Peck, *Scissored-Pair Control-Moment Gyros: A Mechanical Constraint Saves Power,* Journal of Guidance, Control, and Dynamics **31**, 1823 (2008).

[22] S. M. Bruijn and J. H. van Dieën, *Control of human gait stability through foot placement,* Journal of The Royal Society Interface **15**, 20170816 (2018).

[23] S. M. Bruijn, O. G. Meijer, P. J. Beek, and J. H. van Dieën, *Assessing the stability of human locomotion: A review of current measures,* Journal of The Royal Society Interface **10**, 20120999 (2013).

[24] R. Bruininks, *Bruininks-Oseretsky Test of Motor Proficiency: Examiner's Manual* (American Guidance Service, 1978).

[25] C. Buesing, G. Fisch, M. O'Donnell, I. Shahidi, L. Thomas, C. K. Mummidisetty, K. J. Williams, H. Takahashi, W. Z. Rymer, and A. Jayaraman, *Effects of a wearable exoskeleton stride management assist system (SMA®) on spatiotemporal gait characteristics in individuals after stroke: A randomized controlled trial,* Journal of NeuroEngineering and Rehabilitation **12**, 69 (2015).

[26] A. J. Campbell, M. J. Borrie, and G. F. Spears, *Risk factors for falls in a community-based prospective study of people 70 years and older.* Journal of gerontology **44**, M112 (1989).

[27] M. G. Carpenter, J. S. Frank, and C. P. Silcher, *Surface height effects on postural control: A hypothesis for a stiffness strategy for stance*$_*$, , 10 (1999).

[28] M. G. Carpenter, J. S. Frank, A. L. Adkin, A. Paton, and J. Allum, *Influence of Postural Anxiety on Postural Reactions to Multi-Directional Surface Rotations,* Journal of Neurophysiology **92**, 3255 (2004).

[29] M. G. Carpenter, *Postural abnormalities to multidirectional stance perturbations in Parkinson's disease,* Journal of Neurology, Neurosurgery & Psychiatry **75**, 1245 (2004).

[30] M. Cempini, D. Marconi, M. Muscolo, M. Moisè, M. Fantozzi, M. Cortese, A. Parri, T. Yan, S. Crea, F. Giovacchini, F. Posteraro, M. C. Carrozza, and N. Vitiello, *Relevance of Series-Elastic actuation in rehabilitation and assistance robotic: Two cases of study,* in *2015 IEEE 1st International Forum on Research and Technologies for Society and Industry Leveraging a Better Tomorrow (RTSI)* (2015) pp. 76–81.

[31] M. Cenciarini, P. J. Loughlin, P. J. Sparto, and M. S. Redfern, *Stiffness and Damping in Postural Control Increase With Age,* IEEE Transactions on Biomedical Engineering **57**, 267 (2010).

[32] P.-T. Cheng, S.-H. Wu, M.-Y. Liaw, A. M. K. Wong, and F.-T. Tang, *Symmetrical body-weight distribution training in stroke patients and its effect on fall prevention,* Archives of Physical Medicine and Rehabilitation **82**, 1650 (2001).

[33] P. Cherelle, V. Grosu, P. Beyl, A. Mathys, R. V. Ham, M. V. Damme, B. Vanderborght, and D. Lefeber, *The MACCEPA actuation system as torque actuator in the gait rehabilitation robot ALTACRO,* in *2010 3rd IEEE RAS EMBS International Conference on Biomedical Robotics and Biomechatronics* (2010) pp. 27–32.

[34] P. R. N. Childs, *Rotating Flow* (Elsevier, 2010).

[35] J. Chiu and A. Goswami, *Design of a Wearable Scissored-Pair Control Moment Gyroscope (SP-CMG) for Human Balance Assist,* , V05AT08A023 (2014).

[36] T. Chyou, G. Liddell, and M. Paulin, *An upper-body can improve the stability and efficiency of passive dynamic walking,* Journal of theoretical biology **285**, 126 (2011).

[37] H. Cohen, C. A. Blatchly, and L. L. Gombash, *A Study of the Clinical Test of Sensory Interaction and Balance,* Physical Therapy **73**, 346 (1993).

[38] B. R. Connell and S. L. Wolf, *Environmental and behavioral circumstances associated with falls at home among healthy elderly individuals,* Archives of Physical Medicine and Rehabilitation **78**, 179 (1997).

[39] H. Crabtree, *An Elementary Treatment of the Theory of Spinning Tops and Gyroscopic Motion* (Longmans, Green, 1914).

[40] L. Csató, *Ranking by pairwise comparisons for Swiss-system tournaments,* Central European Journal of Operations Research **21**, 783 (2013).

[41] S. Czarnetzki, S. Kerner, and O. Urbann, *Observer-based dynamic walking control for biped robots,* Robotics and Autonomous Systems **57**, 839 (2009).

[42] J. W. Daily and R. E. Nece, *Chamber Dimension Effects on Induced Flow and Frictional Resistance of Enclosed Rotating Disks,* Journal of Basic Engineering **82**, 217 (1960).

[43] M. de Haart, A. C. Geurts, S. C. Huidekoper, L. Fasotti, and J. van Limbeek, *Recovery of standing balance in postacute stroke patients: A rehabilitation cohort study1,* Archives of Physical Medicine and Rehabilitation **85**, 886 (2004).

[44] C. De Oliveira, I. De Medeiros, N. A. Frota, M. E. Greters, and A. B. Conforto, *Balance control in hemiparetic stroke patients: Main tools for evaluation.* Journal of rehabilitation research and development **45**, 1215 (2008).

[45] K. Delbaere, J. C. T. Close, H. Brodaty, P. Sachdev, and S. R. Lord, *Determinants of disparities between perceived and physiological risk of falling among elderly people: Cohort study,* **341**, c4165 (2010).

[46] K. Delbaere, C. Sherrington, and S. R. Lord, *Chapter 70 - Falls Prevention Interventions A2 - Marcus, Robert,* in *Osteoporosis (Fourth Edition),* edited by D. Feldman, D. W. Dempster, M. Luckey, and J. A. Cauley (Academic Press, San Diego, 2013) pp. 1649–1666.

[47] R. Denman, *System for improving the balance of a person,* (2006), u.S. Classification 135/66; International Classification A45B3/00; Cooperative Classification A45F3/14, A61H3/02, A45F2003/144, A45B9/00, A45F2003/146, A45B3/00, A61H2003/0205; European Classification A61H3/02, A45B3/00, A45B9/00, A45F3/14.

[48] C. Duclos, P. Desjardins, S. Nadeau, A. Delisle, D. Gravel, B. Brouwer, and H. Corriveau, *Destabilizing and stabilizing forces to assess equilibrium during everyday activities,* Journal of biomechanics **42**, 379 (2009).

[49] K. R. Duda and D. J. Newman, *Variable Vector Countermeasure Suit (V2Suit) for Space Exploration,* in *2013 IEEE Aerospace Conference* (2013) pp. 1–8.

[50] K. R. Duda, R. A. Vasquez, A. J. Middleton, M. L. Hansberry, D. J. Newman, S. E. Jacobs, and J. J. West, *The Variable Vector Countermeasure Suit (V2Suit) for space habitation and exploration,* Frontiers in Systems Neuroscience **9**, 55 (2015).

[51] A. Duschau-Wicke, A. Caprez, and R. Riener, *Patient-cooperative control increases active participation of individuals with SCI during robot-aided gait training,* Journal of NeuroEngineering and Rehabilitation **7**, 43 (2010).

[52] J. Englsberger, C. Ott, M. A. Roa, A. Albu-Schäffer, and G. Hirzinger, *Bipedal walking control based on Capture Point dynamics,* in *2011 IEEE/RSJ International Conference on Intelligent Robots and Systems* (2011) pp. 4420–4427.

[53] A. Esquenazi, M. Talaty, A. Packel, and M. Saulino, *The ReWalk Powered Exoskeleton to Restore Ambulatory Function to Individuals with Thoracic-Level Motor-Complete Spinal Cord Injury,* American Journal of Physical Medicine & Rehabilitation **91**, 911 (2012).

[54] T. Exell, M. Gittoes, G. Irwin, and D. Kerwinb, *Gait asymmetry: Composite scores for mechanical analyses of sprint running,* Journal of Biomechanics **45**, 1108 (2012).

[55] F. Feldman and H. Chaudhury, *Falls and the Physical Environment: A Review and a New Multifactorial Falls-Risk Conceptual Framework , Falls and the Physical Environment: A Review and a New Multifactorial Falls-Risk Conceptual Framework,* Canadian Journal of Occupational Therapy **75**, 82 (2008).

[56] R. Fitzpatrick, D. Burke, and S. C. Gandevia, *Task-dependent reflex responses and movement illusions evoked by galvanic vestibular stimulation in standing humans.* The Journal of Physiology **478**, 363 (1994).

[57] K. A. Ford and C. D. Hall, *Singular Direction Avoidance Steering for Control-Moment Gyros,* Journal of Guidance, Control, and Dynamics **23**, 648 (2000).

[58] M. Frey, G. Colombo, M. Vaglio, R. Bucher, M. Jorg, and R. Riener, *A Novel Mechatronic Body Weight Support System,* IEEE Transactions on Neural Systems and Rehabilitation Engineering **14**, 311 (2006).

[59] G. F. Fuller, *Falls in the Elderly,* American Family Physician **61**, 2159 (2000).

[60] D. A. Ganz, Y. Bao, P. G. Shekelle, and L. Z. Rubenstein, *Will My Patient Fall?* **297**, 77 (2007).

[61] M. M. Gardner, M. C. Robertson, and A. J. Campbell, *Exercise in preventing falls and fall related injuries in older people: A review of randomised controlled trials,* British Journal of Sports Medicine **34**, 7 (2000).

[62] A. D. Gardner, J. Potgieter, and F. K. Noble, *A review of commercially available exoskeletons' capabilities,* in *2017 24th International Conference on Mechatronics and Machine Vision in Practice (M2VIP)* (2017) pp. 1–5.

[63] G. Genta, *Kinetic Energy Storage: Theory and Practice of Advanced Flywheel Systems* (Butterworth-Heinemann, 2014).

[64] A. C. Geurts, M. de Haart, I. J. van Nes, and J. Duysens, *A review of standing balance recovery from stroke,* Gait & Posture **22**, 267 (2005).

[65] H. Geyer and H. Herr, *A muscle-reflex model that encodes principles of legged mechanics produces human walking dynamics and muscle activities,* Neural Systems and Rehabilitation Engineering, IEEE Transactions on **18**, 263 (2010).

[66] H. Geyer, A. Seyfarth, and R. Blickhan, *Compliant leg behaviour explains basic dynamics of walking and running,* Proceedings of the Royal Society B: Biological Sciences **273**, 2861 (2006).

[67] F. Giovacchini, F. Vannetti, M. Fantozzi, M. Cempini, M. Cortese, A. Parri, T. Yan, D. Lefeber, and N. Vitiello, *A light-weight active orthosis for hip movement assistance,* Robotics and Autonomous Systems Wearable Robotics, **73**, 123 (2015).

[68] R. C. González, A. M. López, J. Rodriguez-Uría, D. Álvarez, and J. C. Alvarez, *Real-time gait event detection for normal subjects from lower trunk accelerations,* Gait & Posture **31**, 322 (2010).

[69] M. Goršič, R. Kamnik, L. Ambrožič, N. Vitiello, D. Lefeber, G. Pasquini, and M. Munih, *Phase Detection Using Wearable Sensors for Walking with a Robotic Prosthesis,* **2**, 2776 (2014).

[70] A. Goswami and V. Kallem, *Rate of change of angular momentum and balance maintenance of biped robots,* in *2004 IEEE International Conference on Robotics and Automation, 2004. Proceedings. ICRA '04*, Vol. 4 (2004) pp. 3785–3790 Vol.4.

[71] M. D. Grabiner, S. Donovan, M. L. Bareither, J. R. Marone, K. Hamstra-Wright, S. Gatts, and K. L. Troy, *Trunk kinematics and fall risk of older adults: Translating biomechanical results to the clinic,* Journal of Electromyography and Kinesiology **18**, 197 (2008).

[72] A. Grabowski, C. T. Farley, and R. Kram, *Independent metabolic costs of supporting body weight and accelerating body mass during walking,* Journal of Applied Physiology **98**, 579 (2005).

[73] K. G. Gruben and W. L. Boehm, *Force direction pattern stabilizes sagittal plane mechanics of human walking,* Human Movement Science **31(3)**, 649 (2012).

[74] P. Gwynne, *Technology: Mobility machines,* https://www.nature.com/articles/503S16a (2013).

[75] J. E. Harris, J. J. Eng, D. S. Marigold, C. D. Tokuno, and C. L. Louis, *Relationship of Balance and Mobility to Fall Incidence in People With Chronic Stroke,* Physical Therapy **85**, 150 (2005).

[76] J. M. Hausdorff, D. A. Rios, and H. K. Edelberg, *Gait variability and fall risk in community-living older adults: A 1-year prospective study,* Archives of Physical Medicine and Rehabilitation **82**, 1050 (2001).

[77] M. F. Heller, J. H. Challis, and N. A. Sharkey, *Changes in postural sway as a consequence of wearing a military backpack,* Gait & Posture **30**, 115 (2009).

[78] H. Herr and M. Popovic, *Angular momentum in human walking,* Journal of Experimental Biology **211**, 467 (2008).

[79] J. Hidler, D. Nichols, M. Pelliccio, K. Brady, D. D. Campbell, J. H. Kahn, and T. G. Hornby, *Multicenter Randomized Clinical Trial Evaluating the Effectiveness of the Lokomat in Subacute Stroke , Multicenter Randomized Clinical Trial Evaluating the Effectiveness of the Lokomat in Subacute Stroke,* Neurorehabilitation and Neural Repair **23**, 5 (2009).

[80] J. Hidler, D. Brennan, I. Black, D. Nichols, K. Brady, and T. Nef, *ZeroG: Overground gait and balance training system.* Journal of rehabilitation research and development **48**, 287 (2011).

[81] K. Hirai, M. Hirose, Y. Haikawa, and T. Takenaka, *The development of Honda humanoid robot,* in *Robotics and Automation, 1998. Proceedings. 1998 IEEE International Conference On*, Vol. 2 (IEEE, 1998) pp. 1321–1326.

[82] A. L. Hof, M. G. J. Gazendam, and W. E. Sinke, *The condition for dynamic stability,* Journal of Biomechanics **38**, 1 (2005).

[83] A. L. Hof, *The 'extrapolated center of mass' concept suggests a simple control of balance in walking,* Human Movement Science **27**, 112 (2008).

[84] M. Holewijn, *Physiological strain due to load carrying,* European Journal of Applied Physiology and Occupational Physiology **61**, 237 (1990).

[85] Honda, *SMA| Walking Assist | Features,* https://world.honda.com/Walking-Assist/features/index.html (2018).

[86] F. B. Horak and L. M. Nashner, *Central programming of postural movements: Adaptation to altered support-surface configurations,* Journal of Neurophysiology **55**, 1369 (1986).

[87] F. Horak, L. Nashner, and H. Diener, *Postural strategies associated with somatosensory and vestibular loss,* Experimental Brain Research **82** (1990), 10.1007/BF00230848.

[88] F. B. Horak, J. Frank, and J. Nutt, *Effects of dopamine on postural control in parkinsonian subjects: Scaling, set, and tone,* Journal of Neurophysiology **75**, 2380 (1996).

[89] F. B. Horak, S. M. Henry, and A. Shumway-Cook, *Postural Perturbations: New Insights for Treatment of Balance Disorders,* Physical Therapy **77**, 517 (1997).

[90] F. B. Horak, *Clinical Measurement of Postural Control in Adults,* Physical Therapy **67**, 1881 (1987).

[91] B. Husemann, F. Müller, C. Krewer, S. Heller, and E. Koenig, *Effects of locomotion training with assistance of a robot-driven gait orthosis in hemiparetic patients after stroke. A randomized controlled pilot study,* (2007).

[92] International Electrotechnical Commission, *IEC 60601-1-11:2010 - Medical electrical equipment Part 1-11: General requirements for basic safety and essential performance – Collateral standard: Requirements for medical electrical equipment and medical electrical systems used in the home healthcare environment,* (2010).

[93] A. Ishida, T. Masuda, H. Inaoka, and Y. Fukuoka, *Stability of the human upright stance depending on the frequency of external disturbances,* Medical & Biological Engineering & Computing **46**, 213 (2008).

[94] J. J. Jeka and J. R. Lackner, *Fingertip contact influences human postural control,* , 8 (1994).

[95] S. Jezernik, G. Colombo, T. Keller, H. Frueh, and M. Morari, *Robotic Orthosis Lokomat: A Rehabilitation and Research Tool,* Neuromodulation: Technology at the Neural Interface **6**, 108 (2003).

[96] S. Jo, *A neurobiological model of the recovery strategies from perturbed walking,* **90**, 750 (2007).

[97] R. Johansson, M. Magnusson, and M. Akesson, *Identification of human postural dynamics,* IEEE Transactions on Biomedical Engineering **35**, 858 (1988).

[98] C. K. Jung and S. Park, *Compliant bipedal model with the center of pressure excursion associated with oscillatory behavior of the center of mass reproduces the human gait dynamics,* Journal of Biomechanics **47**, 223 (2014).

[99] S. Kajita, F. Kanehiro, K. Kaneko, K. Yokoi, and H. Hirukawa, *The 3D Linear Inverted Pendulum Mode: A simple modeling for a biped walking pattern generation,* in *Intelligent Robots and Systems, 2001. Proceedings. 2001 IEEE/RSJ International Conference On*, Vol. 1 (IEEE, 2001) pp. 239–246.

[100] S. Kajita, F. Kanehiro, K. Kaneko, K. Fujiwara, K. Harada, K. Yokoi, and H. Hirukawa, *Biped walking pattern generation by using preview control of zero-moment point,* in *Robotics and Automation, 2003. Proceedings. ICRA'03. IEEE International Conference On*, Vol. 2 (IEEE, 2003) pp. 1620–1626.

[101] M. Kangas, A. Konttila, I. Winblad, and T. Jamsa, *Determination of simple thresholds for accelerometry-based parameters for fall detection,* in *Engineering in Medicine and Biology Society, 2007. EMBS 2007. 29th Annual International Conference of the IEEE* (IEEE, 2007) pp. 1367–1370.

[102] M. Kangas, A. Konttila, P. Lindgren, I. Winblad, and T. Jämsä, *Comparison of low-complexity fall detection algorithms for body attached accelerometers,* Gait & posture **28**, 285 (2008).

[103] B. Kenwright, R. Davison, and G. Morgan, *Dynamic balancing and walking for real-time 3d characters,* in *Motion in Games* (Springer, 2011) pp. 63–73.

[104] K.-I. Kim, H.-K. Jung, C. O. Kim, S.-K. Kim, H.-H. Cho, D. Y. Kim, Y.-C. Ha, S.-H. Hwang, C. W. Won, J.-Y. Lim, H. J. Kim, and J. G. Kim, *Evidence-based guidelines for fall prevention in Korea,* The Korean Journal of Internal Medicine **32**, 199 (2017).

[105] T. Koolen, T. De Boer, J. Rebula, A. Goswami, and J. Pratt, *Capturability-based analysis and control of legged locomotion, Part 1: Theory and application to three simple gait models,* The International Journal of Robotics Research **31**, 1094 (2012).

[106] S. Krafczyk, V. Schlamp, M. Dieterich, P. Haberhauer, and T. Brandt, *Increased body sway at 3.5–8 Hz in patients with phobic postural vertigo,* Neuroscience Letters **259**, 149 (1999).

[107] C. Krishnan, D. Kotsapouikis, Y. Y. Dhaher, and W. Z. Rymer, *Reducing Robotic Guidance During Robot-Assisted Gait Training Improves Gait Function: A Case Report on a Stroke Survivor,* Archives of Physical Medicine and Rehabilitation **94**, 1202 (2013).

[108] H. K. Kwa, J. H. Noorden, M. Missel, T. Craig, J. E. Pratt, and P. D. Neuhaus, *Development of the IHMC Mobility Assist Exoskeleton,* in *2009 IEEE International Conference on Robotics and Automation* (2009) pp. 2556–2562.

[109] Y. Laufer, D. Sivan, R. Schwarzmann, and E. Sprecher, *Standing Balance and Functional Recovery of Patients with Right and Left Hemiparesis in the Early Stages of Rehabilitation,* Neurorehabilitation and Neural Repair **17**, 207 (2003).

[110] C. A. Laughton, M. Slavin, K. Katdare, L. Nolan, J. F. Bean, D. Kerrigan, E. Phillips, L. A. Lipsitz, and J. J. Collins, *Aging, muscle activity, and balance control: Physiologic changes associated with balance impairment,* Gait & Posture **18**, 101 (2003).

[111] V. Lebastard, Y. Aoustin, and F. Plestan, *Observer-based control of a biped robot,* in *Robot Motion and Control, 2004. RoMoCo'04. Proceedings of the Fourth International Workshop On* (IEEE, 2004) pp. 67–72.

[112] S.-H. Lee and A. Goswami, *Reaction Mass Pendulum (RMP): An explicit model for centroidal angular momentum of humanoid robots,* IEEE Internation Conference on Robotics and Automation , 4667 (2007).

[113] S. Lee and A. Goswami, *Ground reaction force control at each foot: A momentum-based humanoid balance controller for non-level and non-stationary ground,* in *2010 IEEE/RSJ International Conference on Intelligent Robots and Systems* (2010) pp. 3157–3162.

[114] D. Lemus, J. van Frankenhuyzen, and H. Vallery, *Design and Evaluation of a Balance Assistance Control Moment Gyroscope,* Journal of Mechanisms and Robotics **9**, 051007 (2017).

[115] F. A. Leve, B. J. Hamilton, and M. A. Peck, *Spacecraft Momentum Control Systems,* Vol. 1010 (Springer, 2015).

[116] D. Li and H. Vallery, *Gyroscopic assistance for human balance,* in *2012 12th IEEE International Workshop on Advanced Motion Control (AMC)* (2012) pp. 1–6.

[117] S. R. Lord, J. A. Ward, P. Williams, and K. J. Anstey, *An epidemiological study of falls in older community-dwelling women: The Randwick falls and fractures study,* Australian Journal of Public Health **17**, 240 (1993).

[118] V. Lugade, V. Lin, and L.-S. Chou, *Center of mass and base of support interaction during gait,* Gait & Posture **33**, 406 (2011).

[119] C. D. MacKinnon and D. A. Winter, *Control of whole body balance in the frontal plane during human walking,* Journal of Biomechanics **26**, 633 (1993).

[120] B. E. Maki, P. J. Holliday, and G. R. Fernie, *A Posture Control Model and Balance Test for the Prediction of Relative Postural Stability,* IEEE Transactions on Biomedical Engineering **BME-34**, 797 (1987).

[121] B. E. Maki, P. J. Holliday, and A. K. Topper, *Fear of Falling and Postural Performance in the Elderly,* Journal of Gerontology **46**, M123 (1991).

[122] A. Mansfield, J. S. Wong, J. Bryce, S. Knorr, and K. K. Patterson, *Does Perturbation-Based Balance Training Prevent Falls? Systematic Review and Meta-Analysis of Preliminary Randomized Controlled Trials,* Physical Therapy **95**, 700 (2015).

[123] C. Martin, B. Phillips, T. Kilpatrick, H. Butzkueven, T. N, E. McDonald, and M. Galeg, *Gait and balance impairment in early multiple sclerosis in the absence of clinical disability,* Multiple Sclerosis **12**, pp. 620 (2006).

[124] H.-M. Maus, J. Rummel, and A. Seyfarth, *Stable upright walking and running using a simple pendulum based control scheme,* in *Advances in Mobile Robotics: Proc. 11th Int. Conf. Climbing and Walking Robots. Coimbra, Portugal: World Scientific* (2008) pp. 623–629.

[125] H.-M. Maus, S. W. Lipfert, M. Gross, J. Rummel, and A. Seyfarth, *Upright human gait did not provide a major mechanical challenge for our ancestors,* Nature Communications **1**, 70 (2010).

[126] A. Mayr, M. Kofler, E. Quirbach, H. Matzak, K. Fröhlich, and L. Saltuari, *Prospective, Blinded, Randomized Crossover Study of Gait Rehabilitation in Stroke Patients Using the Lokomat Gait Orthosis , Prospective, Blinded, Randomized Crossover Study of Gait Rehabilitation in Stroke Patients Using the Lokomat Gait Orthosis,* Neurorehabilitation and Neural Repair **21**, 307 (2007).

[127] T. McGeer, *Passive dynamic walking,* the international journal of robotics research **9**, 62 (1990).

[128] D. M. Merfeld, L. Zupan, and R. J. Peterka, *Humans use internal models to estimate gravity and linear acceleration,* Nature **398**, 615 (1999).

[129] T. Mergner, *A neurological view on reactive human stance control,* Annual Reviews in Control **34**, 177 (2010).

[130] C. G. M. Meskers, J. H. de Groot, E. de Vlugt, and A. C. Schouten, *NeuroControl of movement: System identification approach for clinical benefit,* Frontiers in Integrative Neuroscience **9** (2015), 10.3389/fnint.2015.00048.

[131] J.-B. Mignardot, C. G. L. Goff, R. van den Brand, M. Capogrosso, N. Fumeaux, H. Vallery, S. Anil, J. Lanini, I. Fodor, G. Eberle, A. Ijspeert, B. Schurch, A. Curt, S. Carda, J. Bloch, J. von Zitzewitz, and G. Courtine, *A multidirectional gravity-assist algorithm that enhances locomotor control in patients with stroke or spinal cord injury,* Science Translational Medicine **9**, eaah3621 (2017).

[132] P. G. Morasso and M. Schieppati, *Can Muscle Stiffness Alone Stabilize Upright Standing?* Journal of Neurophysiology **82**, 1622 (1999).

[133] M. Morisawa, S. Kajita, F. Kanehiro, K. Kaneko, K. Miura, and K. Yokoi, *Balance control based on Capture Point error compensation for biped walking on uneven terrain,* in *2012 12th IEEE-RAS International Conference on Humanoid Robots (Humanoids 2012)* (2012) pp. 734–740.

[134] S. A. Murray, K. H. Ha, and M. Goldfarb, *An Assistive Controller for a Lower-Limb Exoskeleton for Rehabilitation after Stroke, and Preliminary Assessment Thereof,* Conference proceedings : ... Annual International Conference of the IEEE Engineering in Medicine and Biology Society. IEEE Engineering in Medicine and Biology Society. Annual Conference **2014**, 4083 (2014).

[135] L. M. Nashner and G. McCollum, *The organization of human postural movements: A formal basis and experimental synthesis,* Behavioral and Brain Sciences **8**, 135 (1985).

[136] NICE, *Falls in older people: Assessing risk and prevention | Guidance and guidelines | NICE,* https://www.nice.org.uk/guidance/cg161 (2013).

[137] A. A. Nobles and N. A. Baladi, *Device and method for assisting end-to-side anastomosis,* (1999), u.S. Classification 606/151, 606/158, 606/198; International Classification A61B17/02, A61B17/11, A61B17/00; Cooperative Classification A61B2017/00243, A61B2017/1107, A61B2017/1135, A61B2017/0243, A61B17/11; European Classification A61B17/11.

[138] H. Nøkland, *Nonlinear Observer Design for GNSS and IMU Integration,* , 111 (2011).

[139] R. L. Norton, *Design of Machinery: An Introduction to the Synthesis and Analysis of Mechanisms and Machines* (McGraw-Hill Professional, 2004).

[140] M. Nyan, F. Tay, and M. Mah, *Application of motion analysis system in pre-impact fall detection,* Journal of Biomechanics **41**, pp. 2297 (2008).

[141] M. Nyan, F. Tay, and E. Murugasu, *A wearable system for pre-impact fall detection,* Journal of Biomechanics **41**, pp. 3475 (2008).

[142] N. Ogihara and N. Yamazaki, *Generation of human bipedal locomotion by a bio-mimetic neuro-musculoskeletal model,* Biological cybernetics **84**, 1 (2001).

[143] C. Ott, M. A. Roa, and G. Hirzinger, *Posture and balance control for biped robots based on contact force optimization,* in *2011 11th IEEE-RAS International Conference on Humanoid Robots* (2011) pp. 26–33.

[144] P. W. Overstall, *Falls after strokes.* BMJ : British Medical Journal **311**, 74 (1995).

[145] C. Paiman, D. Lemus, D. Short, and H. Vallery, *Observing the State of Balance with a Single Upper-Body Sensor,* Frontiers in Robotics and AI **3** (2016), 10.3389/frobt.2016.00011.

[146] E. Palermo, S. Rossi, F. Marini, F. PatanÃ¨, and P. Cappa, *Experimental evaluation of accuracy and repeatability of a novel body-to-sensor calibration procedure for inertial sensor-based gait analysis,* **52**, 145 (2014).

[147] E. Palermo, S. Rossi, F. Patanè, and P. Cappa, *Experimental evaluation of indoor magnetic distortion effects on gait analysis performed with wearable inertial sensors.* Physiol Meas **35**, 399 (2014).

[148] J. H. Park, *Impedance control for biped robot locomotion,* Robotics and Automation, IEEE Transactions on **17**, 870 (2001).

[149] A. Parri, T. Yan, N. d'Elia, F. Vannetti, G. Pasquini, F. Giovacchini, M. Fantozzi, M. Cortese, R. M. Lova, and N. Vitiello, *Control of an active pelvis orthosis for gait assistance in the elderly,* in *Gruppo Nazionale Bioingegneria GNB2014* (2014).

[150] J. Pasma, D. Engelhart, A. Schouten, H. van der Kooij, A. Maier, and C. Meskers, *Impaired standing balance: The clinical need for closing the loop,* **267**, 157 (2014).

[151] J. L. Patton, M. E. Stoykov, M. Kovic, and F. A. Mussa-Ivaldi, *Evaluation of robotic training forces that either enhance or reduce error in chronic hemiparetic stroke survivors,* Experimental Brain Research **168**, 368 (2006).

[152] J. Patton, D. A. Brown, M. Peshkin, J. J. Santos-Munné, A. Makhlin, E. Lewis, E. J. Colgate, and D. Schwandt, *KineAssist: Design and Development of a Robotic Overground Gait and Balance Therapy Device,* Topics in Stroke Rehabilitation **15**, 131 (2008).

[153] A. Pennycott, D. Wyss, H. Vallery, and R. Riener, *Effects of added inertia and body weight support on lateral balance control during walking,* in *2011 IEEE International Conference on Rehabilitation Robotics* (2011) pp. 1–5.

[154] T. V. Perneger, *What's wrong with Bonferroni adjustments,* **316**, 1236 (1998).

[155] R. J. Peterka, *Sensorimotor Integration in Human Postural Control,* Journal of Neurophysiology **88**, 1097 (2002).

[156] R. M. Pickering, Y. A. M. Grimbergen, U. Rigney, A. Ashburn, G. Mazibrada, B. Wood, P. Gray, G. Kerr, and B. R. Bloem, *A meta-analysis of six prospective studies of falling in Parkinson's disease,* Movement Disorders: Official Journal of the Movement Disorder Society **22**, 1892 (2007).

[157] W. C. Pinheiro, B. E. Bittencourt, L. B. Luiz, L. A. Marcello, V. F. Antonio, P. H. A. de Lira, R. G. Stolf, and M. C. F. Castro, *Parkinson's Disease Tremor Suppression,* (2017).

[158] M. Plooij, U. Keller, B. Sterke, S. Komi, H. Vallery, and J. von Zitzewitz, *Design of RYSEN: An Intrinsically Safe and Low-Power Three-Dimensional Overground Body Weight Support,* IEEE Robotics and Automation Letters **3**, 2253 (2018).

[159] S. J. Pocock, *Clinical Trials: A Practical Approach* (John Wiley & Sons, 2013).

[160] M. B. Popovic and H. Herr, *Ground reference points in legged locomotion: Definitions, biological trajectories and control implications,* International Journal of Robotics Research **24**, 2005 (2005).

[161] J. E. Pratt and R. Tedrake, *Velocity-based stability margins for fast bipedal walking,* in *Fast Motions in Biomechanics and Robotics* (Springer, 2006) pp. 299–324.

[162] T. E. Prieto, J. B. Myklebust, R. G. Hoffmann, E. G. Lovett, and B. M. Myklebust, *Measures of postural steadiness: Differences between healthy young and elderly adults,* IEEE Transactions on Biomedical Engineering **43**, 956 (1996).

[163] A. Priplata, J. Niemi, M. Salen, J. Harry, L. A. Lipsitz, and J. J. Collins, *Noise-Enhanced Human Balance Control,* Physical Review Letters **89** (2002), 10.1103/PhysRevLett.89.238101.

[164] A. Randel, *AGS Releases Guideline for Prevention of Falls in Older Persons,* American Family Physician **82**, 81 (2010).

[165] M. S. Redfern, L. Yardley, and A. M. Bronstein, *Visual influences on balance,* Journal of Anxiety Disorders **15**, 81 (2001).

[166] N. P. Reeves, V. Q. Everding, J. Cholewicki, and D. C. Morrisette, *The effects of trunk stiffness on postural control during unstable seated balance,* Experimental Brain Research **174**, 694 (2006).

[167] R. Riener, L. Lünenburger, I. C. Maier, G. Colombo, and V. Dietz, *Locomotor Training in Subjects with Sensori-Motor Deficits: An Overview of the Robotic Gait Orthosis Lokomat,* https://www.hindawi.com/journals/jhe/2010/517674/abs/ (2010).

[168] S. N. Robinovitch, F. Feldman, Y. Yang, R. Schonnop, P. M. Leung, T. Sarraf, J. Sims-Gould, and M. Loughin, *Video capture of the circumstances of falls in elderly people residing in long-term care: An observational study,* **381**, 47 (2013).

[169] M. H. Romberg, *A Manual of the Nervous Diseases of Man*, Vol. 2 (Sydenham Society, 1853).

[170] L. B. Rosenberg, *Virtual haptic overlays enhance performance in telepresence tasks,* in *Telemanipulator and Telepresence Technologies*, Vol. 2351 (International Society for Optics and Photonics, 1995) pp. 99–109.

[171] K. J. Rothman, *No Adjustments Are Needed for Multiple Comparisons,* **1**, 43 (1990).

[172] K. J. Rothman, *Six Persistent Research Misconceptions,* Journal of General Internal Medicine **29**, 1060 (2014).

[173] L. Z. Rubenstein, *Falls in older people: Epidemiology, risk factors and strategies for prevention,* Age and ageing **35**, ii37 (2006).

[174] T. L. Saaty, *How to make a decision: The analytic hierarchy process,* European Journal of Operational Research Decision Making by the Analytic Hierarchy Process: Theory and Applications, **48**, 9 (1990).

[175] U. Saranlı, O. Arslan, M. M. Ankaralı, and O. Morgül, *Approximate analytic solutions to non-symmetric stance trajectories of the passive spring-loaded inverted pendulum with damping,* Nonlinear Dynamics **62**, 729 (2010).

[176] A. Sawers and B. J. Hafner, *A study to assess whether fixed-width beam walking provides sufficient challenge to assess balance ability across lower limb prosthesis users,* Clinical Rehabilitation **32**, 483 (2018).

[177] A. Sawers and L. H. Ting, *Beam walking can detect differences in walking balance proficiency across a range of sensorimotor abilities,* Gait & Posture **41**, 619 (2015).

[178] H. Schaub and J. Junkins, *Analytical Mechanics of Space Systems*, 2nd ed. (AIAA, Reston, VA, 2009).

[179] H. Schaub, S. R. Vadali, and J. L. Junkins, *Feedback control law for variable speed control moment gyros,* Journal of the Astronautical Sciences **46**, 307 (1998).

[180] J. M. Schiffman, C. K. Bensel, L. Hasselquist, K. N. Gregorczyk, and L. Piscitelle, *Effects of carried weight on random motion and traditional measures of postural sway,* Applied Ergonomics **37**, 607 (2006).

[181] K. F. Schulz and D. A. Grimes, *Multiplicity in randomised trials I: Endpoints and treatments,* The Lancet **365**, 1591 (2005).

[182] I. Schwartz, A. Sajin, I. Fisher, M. Neeb, M. Shochina, M. Katz-Leurer, and Z. Meiner, *The Effectiveness of Locomotor Therapy Using Robotic-Assisted Gait Training in Subacute Stroke Patients: A Randomized Controlled Trial,* PM&R **1**, 516 (2009).

[183] V. Scott, M. Pearce, and C. Pengelly, *Deaths due to falls among Canadians age 65 and over,* Public Health Agency of Canada, Tech. Rep (2005).

[184] T. Seel, J. Raisch, and T. Schauer, *IMU-Based Joint Angle Measurement for Gait Analysis,* **14**, pp.6891 (2014).

[185] J. E. Seipel and P. Holmes, *Running in three dimensions: Analysis of a point-mass sprung-leg model,* The International Journal of Robotics Research **24**, 657 (2005).

[186] A. Shumway-Cook, W. Gruber, M. Baldwin, and S. Liao, *The Effect of Multidimensional Exercises on Balance, Mobility, and Fall Risk in Community-Dwelling Older Adults,* Physical Therapy **77**, 46 (1997).

[187] K. M. Simpson, B. J. Munro, and J. R. Steele, *Effect of load mass on posture, heart rate and subjective responses of recreational female hikers to prolonged load carriage,* Applied Ergonomics **42**, 403 (2011).

[188] L. A. Simpson, W. C. Miller, and J. J. Eng, *Effect of Stroke on Fall Rate, Location and Predictors: A Prospective Comparison of Older Adults with and without Stroke,* PLOS ONE **6**, e19431 (2011).

[189] D. Skelton, S. Dinan, M. Campbell, and O. Rutherford, *Tailored group exercise (Falls Management Exercise — FaME) reduces falls in community-dwelling older frequent fallers (an RCT),* Age and Ageing **34**, 636 (2005).

[190] D. A. Skelton, *Effects of physical activity on postural stability,* Age and Ageing **30**, 33 (2001).

[191] SKF, *Bearing friction, power loss and starting torque,* http://www.skf.com/group/products/bearings-units-housings/principles/bearing-selection-process/operating-temperature-and-speed/friction-powerloss-startingtorque/index.html.

[192] S. Srivastava, P. Kao, S. H. Kim, P. Stegall, D. Zanotto, J. S. Higginson, S. K. Agrawal, and J. P. Scholz, *Assist-as-Needed Robot-Aided Gait Training Improves Walking Function in Individuals Following Stroke,* IEEE Transactions on Neural Systems and Rehabilitation Engineering **23**, 956 (2015).

[193] D. L. Streiner, *Best (but oft-forgotten) practices: The multiple problems of multiplicity—whether and how to correct for many statistical tests,* The American Journal of Clinical Nutrition **102**, 721 (2015).

[194] A. Stroke, *Balance problems after stroke,* https://www.stroke.org.uk/resources/balance-problems-after-stroke (2018).

[195] J. Taborri, S. Rossi, E. Palermo, Patanè, and P. F.; Cappa, *A Novel HMM Distributed Classifier for the Detection of Gait Phases by Means of a Wearable Inertial Sensor Network,* **9**, 16212 (2014).

[196] T. Tamura, T. Yoshimura, M. Sekine, M. Uchida, and O. Tanaka, *A Wearable Airbag to Prevent Fall Injuries,* IEEE Transactions on Information Technology in Biomedicine **13**, 910 (2009).

[197] C. Tefertiller, K. Hays, J. Jones, A. Jayaraman, C. Hartigan, T. Bushnik, and G. F. Forrest, *Initial Outcomes from a Multicenter Study Utilizing the Indego Powered Exoskeleton in Spinal Cord Injury,* Topics in Spinal Cord Injury Rehabilitation **24**, 78 (2018).

[198] B. Thornton, T. Ura, Y. Nose, and S. Turnock, *Internal actuation of underwater robots using Control Moment Gyros,* in *Europe Oceans 2005*, Vol. 1 (2005) pp. 591–598 Vol. 1.

[199] B. Thornton, T. Ura, Y. Nose, and S. Turnock, *Zero-G Class Underwater Robots and Unrestricted Attitude Control using Control Moment Gyros,* in *OCEANS 2006 - Asia Pacific* (2006) pp. 1–5.

[200] M. E. Tinetti, *Performance-Oriented Assessment of Mobility Problems in Elderly Patients,* Journal of the American Geriatrics Society **34**, 119 (1986).

[201] R. Tisserand, T. Robert, P. Chabaud, M. Bonnefoy, and L. Chèze, *Elderly Fallers Enhance Dynamic Stability Through Anticipatory Postural Adjustments during a Choice Stepping Reaction Time,* Frontiers in Human Neuroscience **10** (2016), 10.3389/fnhum.2016.00613.

[202] S. F. Tyson, M. Hanley, J. Chillala, A. Selley, and R. C. Tallis, *Balance Disability After Stroke,* Physical Therapy **86**, 30 (2006).

[203] L. Valk, A. Berry, and H. Vallery, *Directional Singularity Escape and Avoidance for Single-Gimbal Control Moment Gyroscopes,* Journal of Guidance, Control, and Dynamics **0**, 1 (2018).

[204] H. Vallery, A. Bögel, C. O´Brien, and R. Riener, *Cooperative Control Design for Robot-Assisted Balance During Gait,* at - Automatisierungstechnik Methoden und Anwendungen der Steuerungs-, Regelungs- und Informationstechnik **60**, 715 (2012).

[205] H. Vallery, P. Lutz, J. von Zitzewitz, G. Rauter, M. Fritschi, C. Everarts, R. Ronsse, A. Curt, and M. Bolliger, *Multidirectional transparent support for overground gait training,* in *2013 IEEE 13th International Conference on Rehabilitation Robotics (ICORR)* (2013) pp. 1–7.

[206] M. van de Ruit, J. Lataire, F. C. T. van der Helm, W. Mugge, and A. C. Schouten, *Adaptation rate in joint dynamics depends on the time-varying properties of the environment,* 2018 7th IEEE International Conference on Biomedical Robotics and Biomechatronics (BioRob) , 273 (2018).

[207] S. Van der Geld, *Step Location Control to Overstep Obstacles for Running Robots,* Ph.D. thesis, TU Delft, Delft University of Technology (2012).

[208] R. A. Vasquez, M. L. Hansberry, K. R. Duda, A. J. Middleton, and D. J. Newman, *Wearable CMG design for the Variable Vector Countermeasure Suit,* in *2015 IEEE Aerospace Conference* (2015) pp. 1–13.

[209] G. S. Verheyden, V. Weerdesteyn, R. M. Pickering, D. Kunkel, S. Lennon, A. C. Geurts, and A. Ashburn, *Interventions for preventing falls in people after stroke,* in *The Cochrane Library* (John Wiley & Sons, Ltd, 2013).

[210] R. Villamonte, P. R. Vehrs, J. B. Feland, A. W. Johnson, M. K. Seeley, and D. Eggett, *Reliability of 16 Balance Tests in Individuals with down Syndrome,* Perceptual and Motor Skills **111**, 530 (2010).

[211] C. Wall III and E. Kentala, *Control of sway using vibrotactile feedback of body tilt in patients with moderate and severe postural control deficits,* Journal of Vestibular Research **15**, 313 (2005).

[212] B. Wang, K. Gong, D. Yang, and J. Li, *Fine attitude control by reaction wheels using variable-structure controller,* Acta Astronautica **52**, 613 (2003).

[213] S. Wang, L. Wang, C. Meijneke, E. van Asseldonk, T. Hoellinger, G. Cheron, Y. Ivanenko, V. L. Scaleia, F. Sylos-Labini, M. Molinari, F. Tamburella, I. Pisotta, F. Thorsteinsson, M. Ilzkovitz, J. Gancet, Y. Nevatia, R. Hauffe, F. Zanow, and H. van der Kooij, *Design and Control of the MINDWALKER Exoskeleton,* IEEE Transactions on Neural Systems and Rehabilitation Engineering **23**, 277 (2015).

[214] V. Weerdesteyn, M. Niet, H. Duijnhoven, and A. Geurts, *Falls in individuals with stroke,* **45** (2008), 10.1682/JRRD.2007.09.0145.

[215] K. P. Westlake and C. Patten, *Pilot study of Lokomat versus manual-assisted treadmill training for locomotor recovery post-stroke,* Journal of NeuroEngineering and Rehabilitation **6**, 18 (2009).

[216] B. R. Whittington and D. G. Thelen, *A Simple Mass-Spring Model With Roller Feet Can Induce the Ground Reactions Observed in Human Walking,* Journal of Biomechanical Engineering **131** (2009).

[217] B. Wie, D. Bailey, and C. Heiberg, *Singularity Robust Steering Logic for Redundant Single-Gimbal Control Moment Gyros,* Journal of Guidance, Control, and Dynamics **24**, 865 (2001).

[218] D. L. Wight, E. G. Kubica, and D. W. Wang, *Introduction of the Foot Placement Estimator: A Dynamic Measure of Balance for Bipedal Robots,* J. Comput. Nonlinear Dynam. **3** (2007).

[219] K. N. Winfree, J. Gewirtz, T. Mather, J. Fiene, and K. J. Kuchenbecker, *A high fidelity ungrounded torque feedback device: The iTorqU 2.0,* in *World Haptics 2009 - Third Joint EuroHaptics Conference and Symposium on Haptic Interfaces for Virtual Environment and Teleoperator Systems* (2009) pp. 261–266.

[220] D. A. Winter, F. Prince, J. S. Frank, C. Powell, and K. F. Zabjek, *Unified theory regarding A/P and M/L balance in quiet stance,* Journal of Neurophysiology **75**, 2334 (1996).

[221] D. A. Winter, A. E. Patla, F. Prince, M. Ishac, and K. Gielo-Perczak, *Stiffness control of balance in quiet standing,* Journal of Neurophysiology **80**, 1211 (1998).

[222] D. A. Winter, *Human balance and posture control during standing and walking,* Gait & Posture **3**, 193 (1995).

[223] M. Wirz, D. H. Zemon, R. Rupp, A. Scheel, G. Colombo, V. Dietz, and T. G. Hornby, *Effectiveness of automated locomotor training in patients with chronic incomplete spinal cord injury: A multicenter trial,* Archives of Physical Medicine and Rehabilitation **86**, 672 (2005).

[224] M. Wisse, A. Schwab, and F. C. T. van der Helm, *Passive dynamic walking model with upper body,* **22**, 681 (2004).

[225] T. Wojtara, M. Sasaki, H. Konosu, M. Yamashita, S. Shimoda, F. Alnajjar, and H. Kimura, *Artificial balancer – Supporting device for postural reflex,* Gait & Posture **35**, 316 (2012).

[226] D. M. Wrisley, G. F. Marchetti, D. K. Kuharsky, and S. L. Whitney, *Reliability, Internal Consistency, and Validity of Data Obtained With the Functional Gait Assessment,* Physical Therapy **84**, 906 (2004).

[227] M. Wu, G. Brown, and K. E. Gordon, *Control of locomotor stability in stabilizing and destabilizing environments,* Gait & Posture **55**, 191 (2017).

[228] G. Wu, *Distinguishing fall activities from normal activities by velocity characteristics,* Journal of Biomechanics **33**, pp. 1497 (2000).

[229] D. Wyss, V. Bartenbach, A. Pennycott, R. Riener, and H. Vallery, *A body weight support system extension to control lateral forces: Realization and validation,* in *2014 IEEE International Conference on Robotics and Automation (ICRA)* (2014) pp. 328–332.

[230] D. Wyss, A. Pennycott, P. Bartenbach, R. Riener, and H. Vallery, *An Under-Actuated Multidimensional Compliant Manipulator for Pelvic Support during Gait,* IEEE Transactions on Mechatronics (in minor revision).

[231] C.-C. Yang and Y.-L. Hsu, *A Review of Accelerometry-Based Wearable Motion Detectors for Physical Activity Monitoring,* **10**, pp. 7772 (2010).

[232] K. Yasuhara, K. Shimada, T. Koyama, T. Ido, K. Kikuchi, and Y. Endo, *Walking assist device with stride management system,* Honda R&D technical review **21**, 54 (2009).

[233] P. M. M. Young, J. M. Wilken, and J. B. Dingwell, *Dynamic margins of stability during human walking in destabilizing environments,* Journal of Biomechanics **46**, 1053 (2012).

[234] X. Yun and E. R. Bachmann, *Design, Implementation, and Experimental Results of a Quaternion-Based Kalman Filter for Human Body Motion Tracking,* IEEE Transactions on Robotics **22**, 1216 (2006).

[235] R. E. Zee, S. C. Grocott, and J. Matthews, *The MOST microsatellite mission: All systems go for launch,* in *12th CASI (Canadian Aeronautics and Space Institute) Conference on Astronautics* (2002).

[236] L. Zhang, D. Xu, M. Makhsous, and F. Lin, *Stiffness and viscous damping of the human leg,* in *Proc. of the 24th Ann. Meeting of the Am. Soc. of Biomech., Chicago, IL* (2000).

[237] J. Zhang, P. Fiers, K. A. Witte, R. W. Jackson, K. L. Poggensee, C. G. Atkeson, and S. H. Collins, *Human-in-the-loop optimization of exoskeleton assistance during walking,* Science **356**, 1280 (2017).

[238] *World Health Organization Global Report on Falls Prevention in Older Age*, Tech. Rep. (World Health Organization, 2007).

About the author

August 03, 1986
Born in Bogotá, Colombia.

1996–2002
Secondary School, Colegio Cafam, Bogotá, Colombia

2003–2008
Bachelor degree in Mechanical Engineering, Universidad Nacional de Colombia, Bogotá, Colombia.

2009–2011
Master of Science in Engineering at Universidad de los Andes in Bogotá, Colombia. Master Thesis: *Development of a dynamic workspace controller for a Stewart-Gough platform* which was awarded the Best Master Thesis in Mechanical Engineering during the second semester of 2011.

2012–2013
Internship at Toyota Motor Europe NV/SA, Zaventem, Belgium. Internship topic: *Development of test algorithms for automated testing on engine test benches.*

2013–2018
PhD candidate at Delft University of Technology, of which this thesis presents the final results. The topic of the research was *Gyroscopic assistance for human balance.*

2018-present
Scientific researcher at Delft University of Technology, with a focus on the development of second and third generation gyroscopic actuators for trunk stabilization and foot placement assistance.

List of Publications

Journal Publications

5. C. Schumacher, A Berry, **D. Lemus**, C. Rode, A. Seyfarth, and H. Vallery, *Biarticular muscles are most responsive to upper-body pitch perturbations in human standing.* Submitted to Nature Scientific Reports (2019).

4. **D. Lemus** & A. Berry, S. Jabeen, C. Jayaraman, K. Hohl, F. C. T. van der Helm, A. Jayaraman and H. Vallery, *Gyroscopic Actuators on the Upper Body Effectively Assist Human Balance.* Submitted to Nature Scientific Reports (2019).

3. **D. Lemus**, J. van Frankenhuyzen, and H. Vallery, *Design and Evaluation of a Balance Assistance Control Moment Gyroscope*, Journal of Mechanisms and Robotics 9, 051007 (2017).

2. A. Berry , **D. Lemus**, R. Babuška and H. Vallery, *Directional Singularity-Robust Torque Control for Gyroscopic Actuators*, IEEE/ASME Transactions on Mechatronics (2016)

1. C. Paiman, **D. Lemus**, D. Short, and H. Vallery, *Observing the State of Balance with a Single Upper-Body Sensor*, Frontiers in Robotics and AI, Volume 3, (2016).

Conference Abstracts

1. **D. Lemus** and H. Vallery, *Towards gyroscopic balance assistance: Proof of concept,* Proceedings of the 36th Annual International Conference of the IEEE Engineering in Medicine and Biology Society (EMBC14), Chicago, IL, USA (2014)